Università degli Studi dell'Insubria

Structural Studies of Active Pharmaceutical Ingredients: Polymorphism and Solid-State Reactivity

by Chiara Vladiskovic

Dipartimento di Scienza e Alta Tecnologia

Dipharma Francis S.r.l.

Tutor: Prof. Norberto MASCIOCCHI

Dottorato di Ricerca in Scienze Chimiche

XXVI^{o} Ciclo – 2009-2014

To Viola and Simone,

because I love you.

Acknowledgements

Summary

Polymorphism, the ability of a substance to crystallize in two or more different structures, is a fundamental issue in the Pharmaceutical Industry because API's can indeed afford multiple solid phases. As different crystalline forms can have different properties, polymorphic identity can have influence on processability, handling, formulability and also the physico-chemical and pharmacological properties of the finished drug product. Characterizing the various crystalline forms of API's is therefore crucial.

Structural studies can help interpreting the origin, and the consequences, of polymorphism, yielding important information on phase transitions or thermal and chemical stability. As the classical technique for structural analysis, single crystal X-ray diffraction, is not always applicable to solid forms of API's, structure solution from powder diffraction data is an ideal solution.

Here, structure determination from laboratory X-ray powder diffraction (XRPD) data is successfully carried out on different API's, illustrating the potential and usefulness of the technique. Three different species are studied (bupropion hydrohalide salts, nortriptyline hydrochloride and ibuprofen lysine salt), exploring different aspects (conformational and packing polymorphism, solvation/desolvation processes, thermodynamic relations and thermally-induced phase transitions).

Finally, a new approach to Quantitative Phase Analysis, implemented in a publicly available software, has been tested on an API, particularly relevant when accessibility to the complete structural model is hampered by the complexity of the molecular/crystal form, not amenable to ab-initio XRPD characterization.

Table of Contents

12

1. Polymorphism of Active Pharmaceutical Ingredients

Polymorphism, the ability of a substance to exist in different crystalline forms, has been steadily gaining importance in the pharmaceutical industry over the last few years. The mounting attention given to the solid state of pharmaceutical ingredients is due to the fact that solid state properties can have a deep influence on many aspects of the manufacturing, handling, formulation and ultimately efficacy and safety of a drug product.

Different polymorphs can have very different properties, including but not limited to solubility, hygroscopicity, melting point, stickiness, bulk density, stability (both chemical and crystallographic), flowability, color, compactability and crystal habit. These properties can therefore have influence not only on safety and efficacy reproducibility of a drug, but also on industrial handling and processability. Moreover, polymorphs of active pharmaceutical ingredients are patentable in many of the major patent systems (including the European Patent Office, EPO, and the United States Patent and Trademark Office, USPTO). This can offer pharmaceutical companies protection and market exclusivity on certain aspects of solid-state issues and offer advantages in the life cycle management of drug products.

The knowledge of the solid-state landscapes of active pharmaceutical ingredients, therefore, is of fundamental importance in the manufacturing and production of a drug product.

1.1 Definitions

1.1.1 Polymorphism

Polymorphism in solid-state chemistry has been defined in many different ways. The usually accepted formal definition is the ability of a substance to exist in at least two different crystalline forms having the same composition. [1] Strictly speaking, therefore, polymorphs must have the same chemical formula and must differ only in the organization of molecules in the solid state. In other words, according to one of the oldest definitions of polymorphism, two solids are polymorphs if their melt and vapor phases are identical. [2]

Figure 1.1 – Polymorphs – Different crystal structures having the same composition
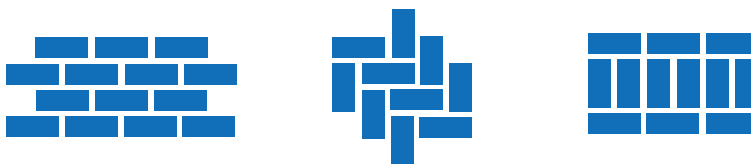
The addition of other components in the crystal structure, strictly speaking, does not lead to polymorphs, but to salts, solvates or co-crystals, depending on the nature of the added component. However, the term "polymorph" is often used loosely, especially in the pharmaceutical industry, to comprehend all the solid states of a molecule, including the amorphous state, solvates, hydrates and, occasionally, even salts and co-crystals. [3]

1.1.2 Salts

When a molecule is combined with an acid or a base and proton transfer occurs, a salt is formed. A salt, made up of two charged species, has a different composition from the neutral molecule (free base or acid) and is therefore a different chemical entity, generally with different properties like solubility and chemical stability. Obviously, a salt will also potentially exhibit polymorphism.

Figure 1.2 – Polymorphs of a salt

Acid
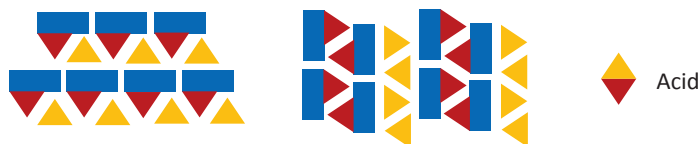
1.1.3 Solvates and co-crystals

When an additional neutral molecule is part of the crystalline structure of a substance and no proton transfer occurs, the definition of the resulting species traditionally depends on the state of the pure co-former (the neutral molecule taking part in the crystalline structure) at room temperature. When the co-former is liquid at room temperature, the resulting species is called a solvate, while when the co-former is solid at room temperature, the resulting species is called a co-crystal. Obviously, solvates and co-crystals can also exhibit polymorphism.

Figure 1.3 – Polymorphs of solvates or co-crystals

Co-former

An important subgroup of solvates is represented by hydrates, where the co-former which takes part in the crystalline structure is water. Hydrates are of particular interest in the pharmaceutical industry because water is non-toxic and acceptable in the formulated product. This considerably expands the landscape of solid forms potentially usable in formulation, as will be discussed in paragraph 1.3.

Even though the definitions are theoretically quite clear-cut and simple, in reality the boundaries between the various cases are not as simple as may seem. For example, a crystal structure can contain more than one co-former, resulting in, for example, solvates of a co-crystal, hydrates of a salt or hydrated solvates. Moreover, all of these species can obviously exhibit polymorphism and crystallize in more than one structure with the same chemical formula.

Figure 1.4 – Polymorphs of a solvate of a salt
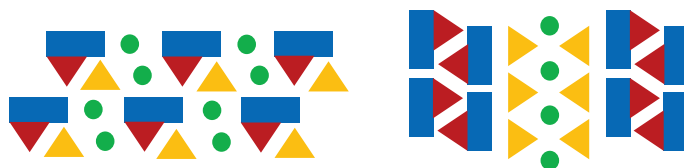
More significant in the pharmaceutical industry, the definition of salt and co-crystal often can become controversial. When an acid or a base is combined with a molecule to give a crystalline structure, the occurrence or not of proton transfer should determine whether the resulting species is a salt or a co-crystal. However, it is not always evident if proton transfer occurred. This can become a major problem especially in the pharmaceutical industry, because, form a regulatory point of view, a salt and a co-crystal will be dealt with very differently in some countries, and a solvate will generally not be considered acceptable. Generally, the pK_a difference between the API and the co-former can be used to predict whether salt formation has occurred or not. FDA Regulatory guidelines, in trying to draw a line between salts and co-crystals, suggest that proton transfer is expected when the differences in the ΔpK_a (pK_a(acid) - pK_a(base)) is greater or equal to one, while a co-crystal is expected when the ΔpK_a is less than one. [4] This said, pK_a values are not easy to determine, especially in non-aqueous solvents or when more than one acidic or basic site are present. The clarification given by the FDA therefore does not simplify matters much.

To complicate matters further, the occurrence or not of proton transfer is not only experimentally difficult to determine, but is often partial or incomplete in the solid state, and often also depends on temperature and pressure. For example, di-hydrated phases of oxalic acid (**1α** and **1β**) have been shown to exist as neutral species at ambient pressure and as being made up of ionic moieties at high pressure. [5, 6] In fact, it is usually more correct to talk about "degree of proton transfer". [7] This makes the boundary between salt and co-crystal very fuzzy indeed.

1.2 Structural Aspects of Polymorphism of Molecular Crystals

Different polymorphs of a substance therefore have the same chemical composition but a different organization in space. In the case of polymorphism of ionic crystals made up of only simple components, the differences between crystalline forms tend to be due to packing arrangements, as the packed species don't have many degrees of internal freedom. In the case of molecular crystals, as molecules can have many degrees of internal freedom, the structural differences between crystalline forms can be due not only to the packing of molecules having the same conformation (packing polymorphism), but also to differences in the conformations of molecules (conformational polymorphism). Even though it is very common to talk about conformational vs. packing polymorphism, by far the most common case is that two polymorphs will differ both in the packing and the conformation of the molecule.

Packing polymorphism can generally be found in molecules which are relatively rigid and don't have a lot of conformational flexibility. An interesting example of packing polymorphism, discussed in detail in Chapter 3 of this work, can be found in the rich solid state landscape of bupropion hydrohalides. [8] Bupropion is an atypical antidepressant formulated in different salt forms. Bupropion hydroiodide forms I and II are made up of molecules in very similar conformation, but are packed rather differently, as shown in Figure 1.5.

Conformational polymorphism without packing differences is very rare in active pharmaceutical ingredients, because differences in conformations will generally also lead to differences in the packing arrangement. An example of this are forms I and II of Venlafaxine hydrochloride. [9, 10] Venlafaxine hydrochloride is an antidepressants which exists in two anhydrous polymorphs. The two crystal forms, belonging to space groups $Pca2_1$ and $P2_1/n$, respectively, are made up of venlafaxine molecules having a different orientation of the methoxyl group on the aromatic ring, as shown in Figure 1.6. This small difference in conformation results in similar, but not identical, packing, as shown in Figure 1.7.

Figure 1.5. Bupropion hydroiodide forms a) I and b) II viewed along the short axis

a)

b)
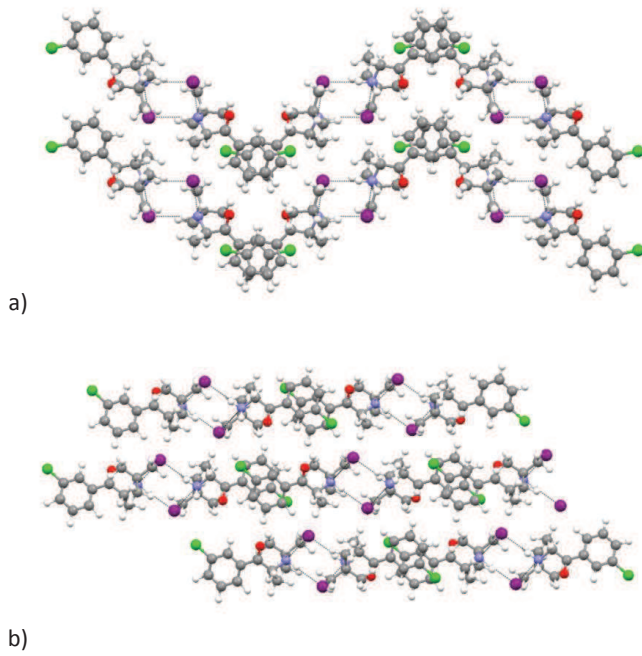
Figure 1.6. Venlafaxine HCl molecules in forms a) I and b) II

a)   b)
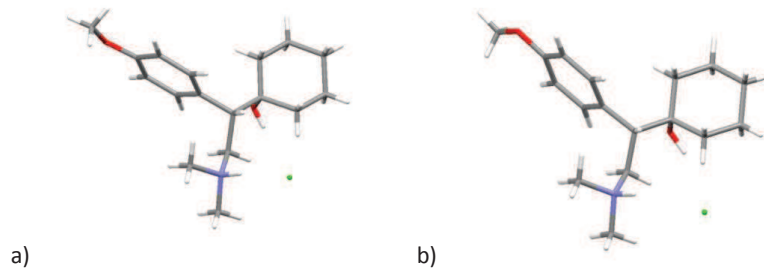
Figure 1.7. Packing of Venlafaxine HCl forms a) I and b) II viewed along the **b** axis.

a)   b)
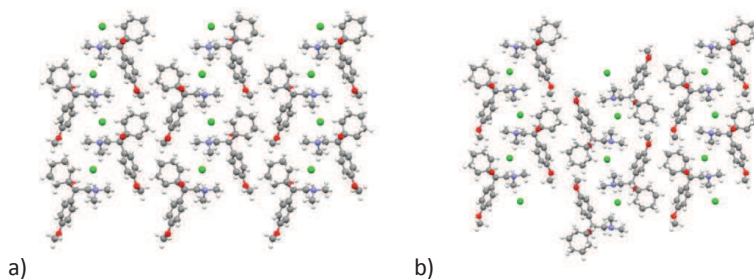
Molecular crystals can also be made up of molecules having two or more different conformations. In these cases, more than one molecule will be present in the asymmetric unit. An example of this is Linezolid, an antibacterial agent. Linezolid can crystallize in two anhydrous polymorphs, one of which is made up of two crystallographic independent molecules existing in two different conformations. [11] The two different molecules, shown in Figure 1.8, are arranged in a "head-to-tail" fashion, favored by polar interactions, forming non-centrosymmetric dimers (as Linezolid is optically active and cannot have an inversion as a symmetry element).

Figure 1.8. Two crystallographic independent molecules, Linezolid Form IV.
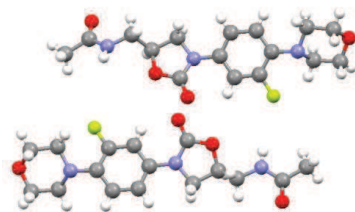
Molecular crystals, being composed of at least partially organic molecules, usually contain hydrogen bond donors and acceptors. The formation of different hydrogen bonding patterns between molecules in the solid state is often the driving force for polymorphism of molecular compounds.

1.2.1 Structure-Properties Relations

Structural differences cause differences in all the properties of the solid state of different polymorphs, *in primis* thermodynamic stability and solubility (usually anti-correlated). This is obviously a very important factor in considering a polymorph for use in the pharmaceutical industry, as solubility is often correlated with bioavailability. A very famous example of this is the antiretroviral drug Ritonavir (shown in Scheme 1.1), which can crystallize in two different anhydrous forms with very different solubilities.

Scheme 1.1. Ritonavir

While form I was formulable as semi-solid gel capsules, the appearance of the less soluble form II caused crystals to form inside the capsules. Form II could not be formulated in the same way as form I. [12]

The large difference in solubility between forms I and II of ritonavir is due to their structures, in particular to the differences in the hydrogen bond motifs. The molecule of ritonavir is very large and has many potential hydrogen bond donors and acceptors. As a result, the hydrogen bond scheme in both forms I and II is very complex. Form II contains stronger hydrogen bonds, as all the strong hydrogen bond donors and acceptors are saturated. A key difference is that in form II the hydroxyl group of an alcohol acts both as donor and acceptor, while in form I the same hydroxyl group acts only as a donor, as is shown in Scheme 1.2. In form II, this causes a synergic effect which makes both hydrogen bonds stronger.

Scheme 1.2. Hydrogen bond scheme around the hydroxyl group for a) form
I and b) form II.

a)

b)
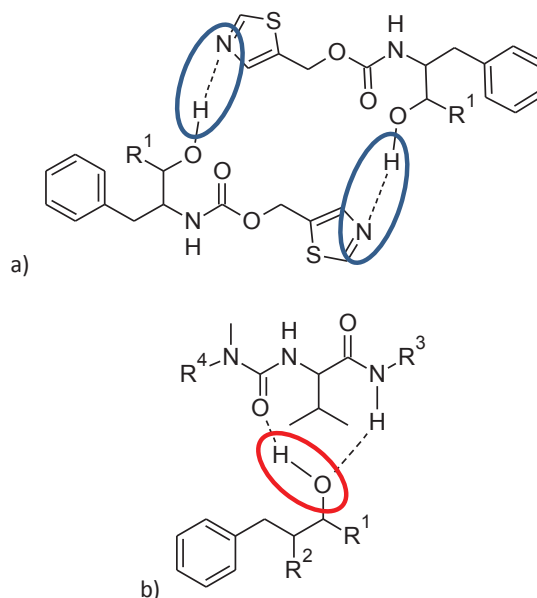
Moreover, crystal growth for the two forms is different and results in
crystals of form I having a greater percentage of their surface area with exposed
hydrogen bond donors compared with crystals of form II. As the cleavage of
hydrogen bonds is the first step of solubilization, these differences cause form II
to be much less soluble with respect to form I. [13]

Just as marked structural differences can cause crystal forms to have very
different properties, structural similarities lead to crystal forms having similar
properties. An example of this is Nortriptyline hydrochloride, a triclyclic
antidepressant which will be discussed in detail in Chapter 4 of this work.
Nortriptyline hydrochloride can exist in two crystalline anhydrous forms known as
α and β. [14, 15, 16] The two forms have very similar properties, including
stability, solubility and hygroscopicity. Structural analysis of the two forms
showed many strong analogies as shown in Figure 1.9, which help explain the
similar properties.

Figure 1.9. Crystal Structure of nortriptyline hydrochloride, forms a) α and b) β.
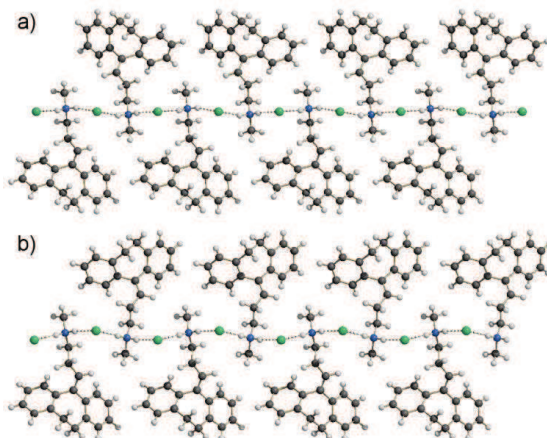
The cases illustrated above suggest how structural knowledge is more than an academic exercise, as it can offer insight on the behavior of different crystal forms, help explain solid state transformations (or lack thereof) and allow to predict properties of different polymorphs.

1.2.2 Thermodynamic relations between polymorphs

One of the most important questions to be addressed when characterizing polymorphic systems is relative stability between different crystal forms. When more than one crystal form is available, knowledge of thermodynamic relationships is critical to understanding solid-state behavior.

One way of representing thermodynamic relationships between polymorphs is using energy-temperature diagrams. Energy-temperature diagrams are schematic plots of the energetic situation of forms in relation to temperature. The most common representations are curves of Gibbs free energy (G) and enthalpy (H) as functions of temperature.

As $G = H - TS$ (where G and H are as defined above, T is absolute temperature and S is entropy) and by the definition of molar heat capacity at

constant pressure (C_p), the dependences of G and H with temperature are given by the following equations:

$$\left(\frac{\partial H}{\partial T}\right)_P = C_p \quad ; \quad \left(\frac{\partial G}{\partial T}\right)_P = -S \qquad (1.1)$$

Both the molar heat capacity and entropy monotonically increase with temperature and are always greater than zero. Therefore, the curve $H(T)$ will increase monotonically, while the curve $G(T)$ will decrease monotonically. When plotting on a diagram the $G(T)$ and $H(T)$ of a solid and a liquid, as is depicted in Figure 1.10, the G curves will cross in correspondence of the melting point of the solid.

When studying the thermodynamic relations between polymorphs, it is useful to plot the G and H curves of both forms on the same graph. In general, given any two polymorphs of a substance, two possible thermodynamic relations are possible: the two forms can either be monotropically or enantiotropically related. Monotropically related means that one of the two forms is thermodynamically more stable at every temperature below the melting point. This means that the curves for G of the two solids never cross below the melting point. This situation is depicted in Figure 1.11.

The crossing of the G curves of the two solids (**G_{s1}** and **G_{s2}**) with the G curve of the liquid (**G_l**) represent the melting points of the two solids. Form 1 can interconvert into form 2, ignoring kinetic considerations, at any temperature below fusion, and the enthalpy of conversion is the difference between **H_{s1}** and **H_{s2}** at the temperature the conversion occurs.

In the case of enantiotropically related forms, **G_{s1}** and **G_{s2}** curves cross before encountering **G_l** (*i.e.* before the melting points). This results in one form being thermodynamically more stable above the temperature at which **G_{s1}** and **G_{s2}** cross (**T_t**) and the other being thermodynamically more stable below **T_t**. This case is depicted in Figure 1.12.

Figure 1.10. Energy-Temperature diagram for a liquid and a solid at constant pressure

H_l = enthalpy of the liquid

H_s = enthalpy of the solid

G_s = Gibbs free of the solid

G_s = Gibbs free energy of the liquid

ΔH_{fus} = fusion enthalpy

T_{fus} = fusion temperature
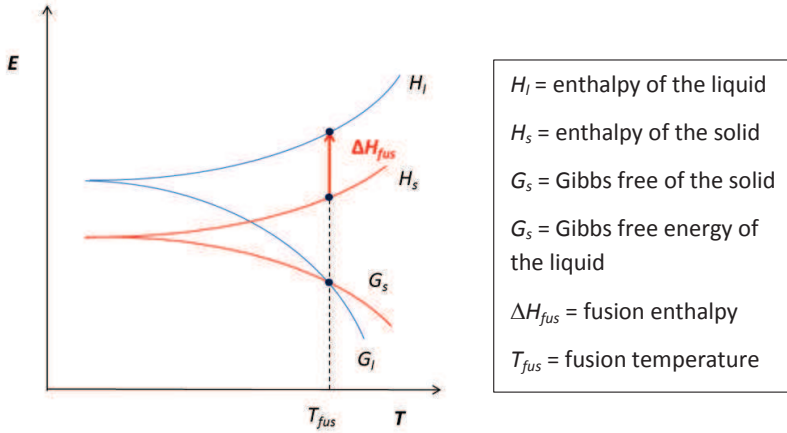
Figure 1.11. Energy-Temperature diagram for two monotropically related forms

H_l = enthalpy of the liquid
H_{s1} = enthalpy of form 1
H_{s2} = enthalpy of form 2
G_{s1} = Gibbs free of form 1
G_{s1} = Gibbs free of form 2
G_s = Gibbs free energy of the liquid
ΔH_{s1} = fusion enthalpy for form 1
ΔH_{s1} = fusion enthalpy for form 2
T_{s1} = fusion temperature of form 1
T_{s2} = fusion temperature of form 2
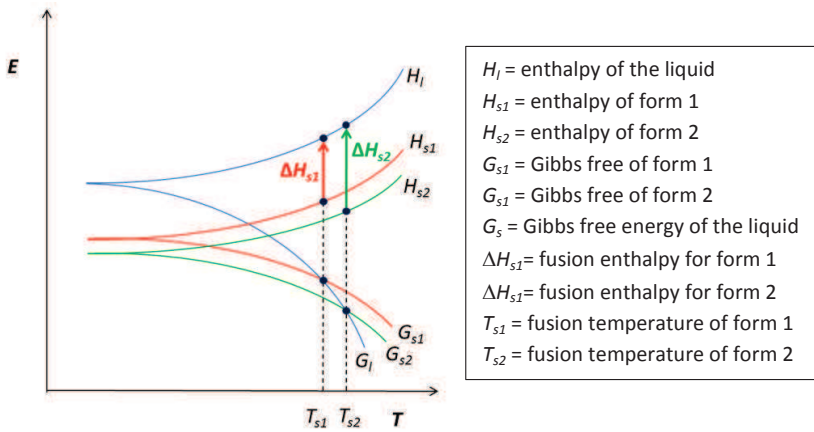
Figure 1.12. Energy-Temperature diagram for two enantiotropically related forms

H_l = enthalpy of the liquid
H_{s1} = enthalpy of form 1
H_{s2} = enthalpy of form 2
G_{s1} = Gibbs free of form 1
G_{s1} = Gibbs free of form 2
G_s = Gibbs free energy of the liquid
ΔH_{s1}= fusion enthalpy for form 1
ΔH_{s1}= fusion enthalpy for form 2
ΔH_t= transition enthalpy 1→2
T_{s1} = fusion temperature of form 1
T_{s2} = fusion temperature of form 2
T_t = transition temperature 1→2
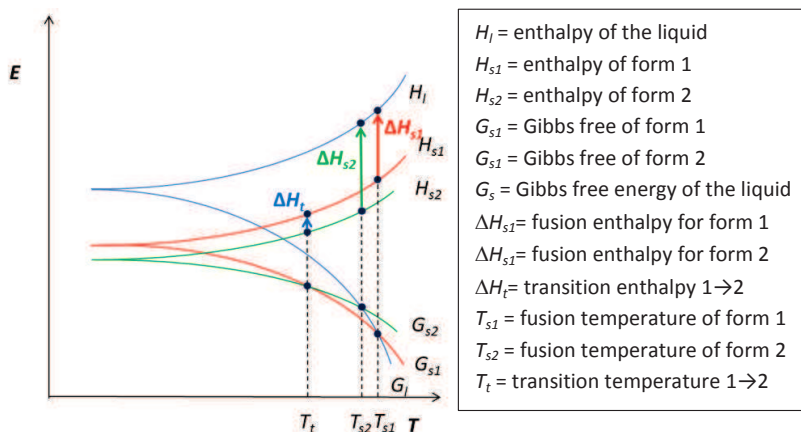
Obviously, crystal forms which are thermodynamically less stable than others can still be stable for kinetic reasons. If the conversion into other forms is kinetically hindered, the net result will be in a "practical" stability of the less stable forms. If this weren't the case, only one crystal form would exist for any compound at any given temperature.

1.2.3 Graph Set Notation

Because understanding and describing hydrogen bonding plays a very important part in understanding molecular polymorphism, a way to effectively define and categorize hydrogen bonding motifs is useful, as it can make comparison of different crystal structures easier. One of the most used methods to define and describe hydrogen bonding is the Graph Set Notation. [17, 18]

The idea behind the Graph Set Notation is to break down complex hydrogen bond schemes into simpler patterns which can be then analyzed separately. This also allows the hydrogen bonding scheme for different crystalline forms to be directly compared.

There are four types of basic hydrogen bond types, classified according to the patterns they form and identified by a single upper case letter:

1) Chains (C)
2) Rings (R)
3) Intramolecular Bonds (S)
4) Other discrete patterns (D)

The letter identifying the pattern is then accompanied by two numbers, a subscript and a superscript, detailing the number of hydrogen bond donors and acceptors, respectively. A third number, indicated in parenthesis, indicates the number of atoms involved in the pattern. When the indicators are equal to one, they can be omitted. Therefore, every hydrogen bond basic pattern can be described by the following identifier:

$$G_d^a(n)$$

> **G** = hydrogen bond pattern type
> **a** = hydrogen bond acceptors
> **d** = hydrogen bond donors
> **n** = number of atoms involved in the pattern

This method allows to quickly and simply describe many different hydrogen bond patterns. A couple of examples of patterns and their Graph Set identifiers are reported in Scheme 1.3.

Patterns containing only one type of hydrogen bond as described above are called motifs and represent the simplest level of hydrogen bond pattern description. The term "one type" also takes into account the chemical identity of the donors and acceptors. If a molecule has more than one hydroxyl group and each donates to a carbonyl, the motifs will be as many as the chemically different hydroxyl groups present.

More complex patterns can arise as different motifs (more than one type of hydrogen bond) combine to form more complex structures and networks. These constitute superior order hydrogen bond networks. If two motifs combine, the network formed is second order. If three motifs combine, the network is third

order, and so on. An example of second order network is represented in Scheme 1.4.

Scheme 1.3. Examples of Hydrogen Bond Motifs

The chain motif represented in a) can be found for example in Nortryptiline hydrochloride, discussed in further detail in Chapter 4. The ring motif represented in b) can be found in Bupropion hydrohalides, discussed in detail in Chapter 3.

a)

$C_4^2(4)$

b)

$R_4^2(8)$
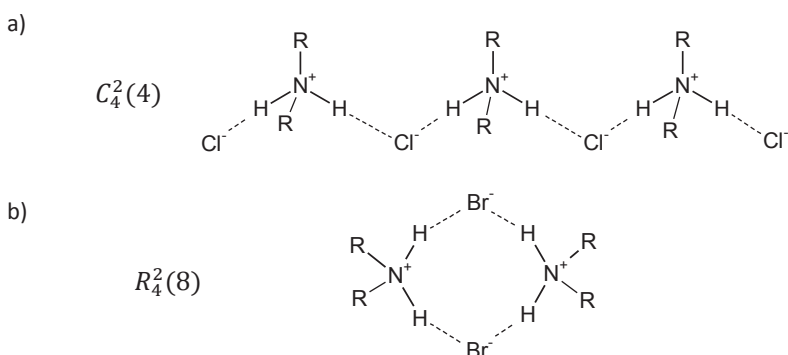
Scheme 1.4. Example of Second Order Hydrogen Bond Network

First Order motifs
N_1: a=D ; b=D
Second Order pattern
N_2: $R_2^2(8)$
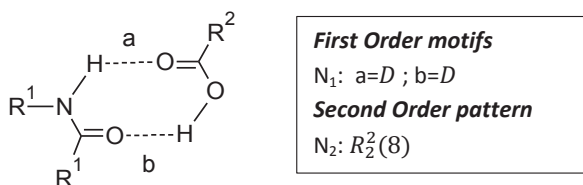
1.3 Importance of Polymorphism in the Pharmaceutical Industry

The occurrence of polymorphism in active pharmaceutical ingredients (APIs) has an enormous importance for many different reasons. Firstly, the structural differences between polymorphs of a compound can cause the solids to have different properties and characteristics, some of which can influence handling, safety, stability and efficacy of a drug product or substance. The knowledge of the properties of the different solid forms of an API can therefore

lead to the choice of the form with the most suitable characteristics, leading to a better bioavailbility, longer shelf-life, easier formulation or more robust process control.

1.3.1 Crystal Form Choice

In the previous paragraphs, the importance of thermodynamic stability was discussed. A desirable solid form obviously will have good crystallographic and chemical stability to ensure shelf-life and consistent bioavailability. However, the more thermodynamically stable forms will generally have the lowest solubilities, therefore the lowest bioavailabilities. In some instances, for example for very insoluble APIs, the chosen form might not be the most stable but the most soluble. Furthermore, other characteristics have to be taken into account. For example, the crystal habit, which may depend on crystal form, can play a fundamental role in the ease of handling and processablity of a pharmaceutical powder. Powders made of needle-shaped crystals, for example, will generally have poor flow and electrostatic properties, while those containing prism-shaped crystals will have a higher bulk density and will be much easier to handle industrially. Moreover, needle shaped crystals will generally create additional process complications, for example having higher filtration resistance. [19]

An example of the influence crystal habit can have in bulk properties can be found in the polymorphs of Linezolid mentioned in paragraph 1.2. Figure 1.13 shows pictures of crystals of forms II and IV. While form II crystallizes as needle-shaped crystals having poor bulk properties, form IV crystallizes as prism-shaped crystals having much better characteristics. [20]

Different crystal forms may also exhibit different compressability, being more or less suitable for tableting. As tablets are the preferred pharmaceutical form when possible, this is a very important issue. Hygroscopicity is also a very important property to take into account because it can have an effect on the stability of the formulated product. An example of different crystalline forms (though not strictly polymorphic) having different hygroscopicities is found among the hydrates of Rabeprazole sodium salt.

Figure 1.13. Crystals of Linezolid forms a) II and b) IV.

a)   b)
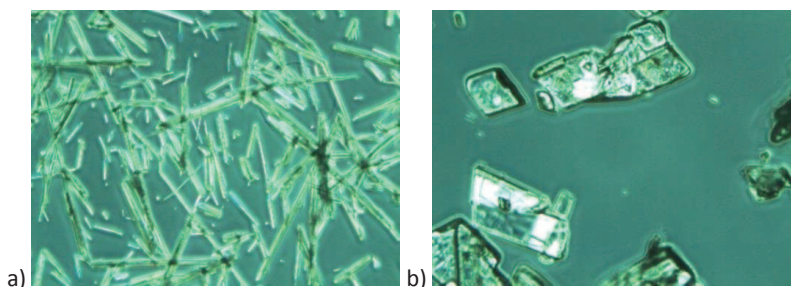
Rabeprazole sodium salt, shown in Scheme 1.5, is a proton pump inhibitor. It is known to exist in several crystalline hydrated forms, including a hemihydrate, a monohydrate and a sesquihydrate. While the hemihydrate and the sesquihydrate are hygroscopic, the monohydrate is not and also exhibits a better chemical stability. [21]

Scheme 1.5. Rabeprazole sodium salt
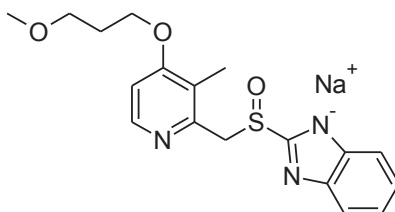
Many different solid-state properties of crystals have therefore to be taken into account when choosing the most suitable solid form for formulation. The complete characterization of all forms is therefore crucial to make correct and informed choices.

1.3.2 Biopharmaceutics Classification System

In order to correctly understand and assess the impact of solubility on bioavailability of a drug product, a useful tool, especially used in regulatory issues, is the Biopharmaceutics Classification System (BCS). [22, 23] This is a

differentiation of active substances into four groups depending on their water solubility and their permeability through the gastro-intestinal membrane. It is widely used for regulatory purposes to help establish bioavailability and bioequivalence, but can also give information regarding which properties can limit bioavailability for a specific substance. [24] Details on BCS classes and solubility boundaries are given in Table 1.1.

The Biopharmaceutics Classification System is important when dealing with different solid forms of pharmaceutical substances because it gives indication as to whether or not polymorphism will have an impact on the bioavailability of the formulated product. A very soluble substance, for instance, belonging to classes I or III, will not have bioavailability limited by drug solubility. In these cases, polymorphism will have small influence on the efficacy of the finished product. Conversely, where solubility is low, for example in classes II and IV, polymorphism can be an issue in the bioavailability of the formulated drug.

Table 1.1. Biopharmaceutics Classification System

A drug substance is considered HIGHLY SOLUBLE when the highest dose strength is soluble in < 250 ml water over a pH range of 1 to 7.5. It is considered HIGHLY PERMEABLE when the extent of absorption in humans is determined to be > 90% of an administered dose, based on mass-balance or in comparison to an intravenous reference dose.

Class I	High Permeability	High Solubility
Class II	High Permeability	Low Solubility
Class III	Low Permeability	High Solubility
Class IV	Low Permeability	Low Solubility

1.3.3 Crystal Forms and Patents

A major role in the importance of solid state issues in the pharmaceutical industry is played by patentability of solid forms and the protection that this can offer. A patent is the granting by a national government of the right to exclusively exploit a particular invention for a limited period of time in exchange for making the invention available to society. As patents are granted by individual national governments, the rules on what is patentable and what protection can be

obtained can vary from country to country. On some level, international organizations exist which try to make the granting of patents as homogenous as possible throughout groups of countries. An example of this is the EPO, or European Patent Organization.

The two main patent systems when dealing with polymorphism of APIs generally are considered to be the EPO (European Patent Organization) and the USPTO (United States Patent and Trademark Office), as these cover the main global markets for pharmaceuticals. Of course, many other patent systems can have deep impact and importance in many specific cases, but only EPO and USPTO are briefly discussed here.

Both EPO and USPTO consider solid forms to be inventions and therefore patentable. However, the rules for patentability change slightly from one system to the other. In general, in order to be granted a patent, the invention must be novel, inventive and useful or industrially applicable. When referred to a crystalline form, the novelty is quite easy to define, as a specific solid form must not have been prepared before. The inventiveness is less clear-cut and is defined differently by the EPO and the USPTO. For the EPO, inventiveness requires a technical problem to be solved, for example if the known crystalline forms are hygroscopic, the disclosure of a new, non-hygroscopic form will be considered inventive, as this solves an existing problem. For the USPTO, the term "non-obviousness" is used to describe inventiveness. One of the main requirements of patentability is that the invention being patented is not obvious, meaning that a "person having ordinary skill in the art" would not know how to solve the problem at which the invention is directed by using exactly the same mechanism. This definition of inventiveness is less rigorous, and therefore the granting of patents on crystalline forms are generally slightly easier to obtain with the USPTO than with the EPO. [25]

As far as usefulness and industrial applicability are concerned, while a new crystalline form is considered intrinsically industrially applicable by the USPTO (as it can be formulated and sold), the EPO requires the new form to have some advantageous characteristic over the state of the art. Again, this gives rise to differences between what is granted on either side of the Atlantic Ocean.

Of course, not only solid forms but also specific solid state characteristics (for example a specific range of particle size [26]) and the processes used to obtain them are considered inventions and can be protected by patents in many patent systems, including EPO and USPTO. This adds considerably to the scope of protection obtainable concerning solid-state issues.

There is another issue regarding solid-state and patents which is gaining importance and attracting attention in the pharmaceutical industry: when a crystal form is patented, the holder of the patent can in principle not only start a litigation against competitors for using it, but also for having small amounts of it in their product. For example, according to the American legal system, under 35 U.S.C. § 271(a), any infringement, even *de minimis* infringement, is actionable. If a competitor has any amount of a crystalline form patented by others, the patent holder can file law suits. There is as of yet no legal precedent brought to trial in the United States, so there is no case law to establish a precedent, but the quantitation of damages could be calculated according to two different approaches: 1) the damages due could be proportional to the amount of patented crystalline form or 2) the damages due could be proportional to the whole loss of revenue, independently of the amount of patented crystalline form present. [25] Of course, in case 1) precise quantitation is a big issue, while in case 2) the detection limits of the available methods are crucial. In the light of this, quantitation methods with lower and lower detection limits are gaining importance.

As the money involved in pharmaceutical development, production, formulation and sales is considerable, the importance that patent protection may assume, when blocking or hindering competitors, is proportionately considerable.

1.3.4 Crystal Form Characterization

The existence of patent issues regarding the solid state in the pharmaceutical industry adds importance to the necessity of structural characterization of polymorphs. In fact, very often scientific issues fall in the background of purely legal issues. For instance, there are cases in the patent literature where mixtures of polymorphs are taken for a different form. The determination of the crystallographic cell through indexing of the powder

diffractogram would ascertain the monophasic nature of a sample, avoiding these kinds of situations. Another example of lack of sound science in the patent literature are cases when the same crystalline form is object of several different patent applications under different names. An example of this discussed in the scientific literature is Cefdinir (Scheme 1.6). [27]

Scheme 1.6 – Cefdinir
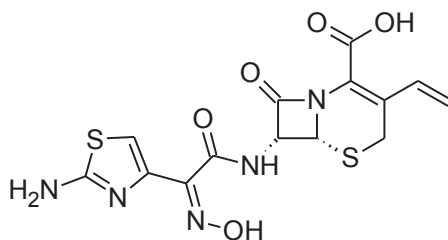
Cefdinir is a potent antibiotic [28] which can exist in several different crystalline forms, both anhydrous and hydrated. This case has been object of a patent litigation in 2009. Interestingly, a monohydrate form has been object of six different patent applications under different names. [29, 30, 31, 32, 33, 34] In all cases, the crystalline form was characterized by XRPD of varying quality. This instance is not uncommon in pharmaceutical patent literature and underlines the importance of high quality characterization of solid forms.

1.3.5 Crystal Form Quantitation

In the light of the scientific, legal and practical importance that crystal form quantitation can have in the pharmaceutical industry, quantitation methods also have a role to play in polymorphism and solid state analysis of pharmaceuticals. Many quantitation methods exist, making use of IR spectroscopy [35], SS-NMR [36], DSC (only for solvates and hydrates [37]) and other techniques. [38] However, the most precise methods which also tend to have the lowest LODs are based on powder diffraction. [18] The lowest LODs obtained to date make use of XRPD using synchrotron radiation. [39,40] This will be further discussed in Chapter 2 (section 2.1.6).

The approaches which can be used for XRPD crystal form quantitation are varied. The most used methods are the Rietveld method and the single peak method, both having strengths and drawbacks.

The Rietveld method makes use of the full diffraction profile of samples. The knowledge of the crystal structures of all phases involved, necessary for the application of this method, allows to construct the theoretical XRPDs and to compare them with the XRPD of the unknown mixture. The theoretical basis and mathematical procedure are discussed in more detail in Chapter 2. With the Rietveld method, it is possible to get the best precision and accuracy as well as the lowest LODs for the same radiation source. The main strength of this method is the fact that it uses the full diffraction profile, so the influence of preferred orientation and other aberrations due to sample preparation is minimized.

As for the single peak method, its main strength is that it does not require the knowledge of the crystal structures of the phases involved. In fact, very often the structure of pharmaceutical polymorphs is not only not known, but very difficult if not impossible to determine with single crystal methods. However, the single peak method is heavily influenced by preferred orientation, as a single representative peak is chosen for each phase under analysis. The method requires the construction of a calibration curve for all phases involved, and therefore pure monophasic standards of all phases are necessary. A more detailed discussion of quantitation methods can be found in Chapter 6.

1.4   Aims and Scope

The main aim of this work is to explore the possibilities offered by structural analysis and to apply them to active pharmaceutical ingredients, in order to study their solid-state landscape and offer insight into the behavior of different crystalline forms. Also, the vast majority of the analyzed structures have been obtained using state-of-the-art powder diffraction methods for structure solution, highlighting the usefulness and versatility of the technique.

Chapters 3, 4 and 5 of this work are dedicated to structural analysis applied to active pharmaceutical ingredients. The deeper understanding of the properties of different crystalline forms can help, as explained in the previous paragraphs, in all phases of drug production, in patent issues, in life cycle management and in

the correct reading and interpretation of the information available in the scientific and patent literature.

In Chapter 3, the rich and varied solid-state landscape of Bupropion hydrohalides is analyzed and discussed making extensive use of structure solution from powder data, bringing to light interesting features, similarities and differences between phases. In particular, all phases analyzed are constituted by bupropion molecules in similar dimer conformations, differing only in the packing arrangement of the dimers. Conformational analysis using gas phase molecular modelling is also used and discussed.

In Chapter 4, structural analysis is used to explain the polymorphic behavior of Nortriptyline hydrochloride. In particular, the similar properties of the two known polymorphs and their lack of solid-state interconversion are addressed and explained.

In Chapter 5, structure resolution from powder data is used to study the thermal behavior of the anti-inflammatory drug Ibuprofen lysine salt. Ibuprofen lysine salt undergoes a fully reversible conversion into a different crystalline form upon heating. Structural and thermal analysis offer an explanation of this behavior.

As discussed in the present chapter, quantitative analysis is another crucial issue when dealing with the solid-state of APIs. The knowledge of structures of different crystalline forms can help in quantitative analysis, as it allows the Rietveld method to be successfully applied. However, other Quantitative Phase Analysis (QPA) methods have been reported in the literature which make use of the full diffraction profile (the main advantage of the Rietveld method) but do not require the knowledge of the structure of the phases involved. [41] The possibility to use a similar full profile method without the necessity of the knowledge of the crystalline structures is very promising and interesting for pharmaceutical solids This method has, to our knowledge, been applied only once to APIs, [42] but the full potential of the method was not explored. Therefore, one aim of this work is to apply a structureless full profile method to the quantification of pharmaceuticals and to compare the results obtained with results obtainable by the classical Rietveld method. This is explored in Chapter 6.

The solid-state of Pharmaceutical solids (API's) is a complex and varied field. In this field more than in others, the partnership between Industry and Academia is necessary and sought. The Industrial world is often oblivious to state-of-the-art methods and solutions, while the Academic world does not have a clear view of industrial necessities and problems that need to be addressed. Partnership and team work can benefit both worlds. Both roles, know-hows and points of view are necessary and a synergy is useful for successful problem solving. Reflections on this point together with the work that has been done to promote this kind of knowledge sharing are contained in Chapter 7.

References

1. Mc Crone, W. C., *Physics and Chemistry of the Organic Solid State*, *2* (**1965**) 725-767.

2. Haleblian, J., McCrone, W., *Journal of Pharmaceutical Sciences, 58* (**1969**), 911-929.

3. Miller, S. P. F., Raw, A. S., Yu, L. X., Scientific Considerations of Pharmaceutical Solid Polymorphism in Regulatory Applications, in: *Polymorphism in the Pharmaceutical Industry*, Hilfiker, R. (ed.), Wiley-VCH, Weinheim, **2006.**

4*. "Guidance for Industry – Regulatory Classification of Pharmaceutical Co-Crystals"*, U.S. Department of Health and Human Services, Food and Drug Administration, **2013**.

5. Casati, N., Macchi, P., Sironi, A., *Chemical Communications, 19* (**2009**), 2679-2681.

6. Macchi, P., Casati, N., Marshall, W.G., Sironi, A., *CrystEngComm., 12* (**2010**), 2596-2603.

7. Li, Z. J., Abramov, Y., Bordner, J., Leonard, J., Medek, A., Trask, A. V., *Journal of the American Chemical Society, 128* (**2006**), 8199-8210.

8. Vladiskovic, C., Masciocchi, N., *Crystal Growth & Design, 14* (**2014**), 3603-3611.

9. Vega, D., Fernández, D., Echeverría, G., *Acta Crystallographica, C56* (**2000**), 1009-1010.

10. Sivalakshmidevi, A., Vyas, K., Mahender R. S. , Reddy G. O., *Acta Crystallographica*, E**58**, (**2002**), o1072-o1074.

11. Maccaroni, E., Alberti, E., Malpezzi, L., Masciocchi, N., Vladiskovic, C*., International Journal of Pharmaceutics, 351* (**2008**), 144-151.

12. Chemburkar, S. R., Bauer, J., Deming, K., Spiwek, H., Patel, K., Morris, J., Henry, R., Spanton, S., Dziki, W., Porter, W., Quick, J., Bauer, P., Donaubauer, J.,

Narayanan, B. A., Soldani, M., Riley, D., McFarland, K., *Organic Process, Research & Development*, *4* (**2000**), 413-417.

13. Bauer, J., Spanton, S., Henry, R., Quick, J., Dziki, W., Porter, W., Morris, J., *Pharmaceutical Research*, *18* (**2001**), 859-866.

14. MacCalman, M.L., Roberts, K.J., Hendriksen, B.A., *Journal of Crystal Growth, 128* (**1993**), 1218-1224.

15. Klein, C.L., Banks, T.A., Rouselle, D., *Acta Crysallographica, C47* (**1991**), 1478-1480.

16. Vladiskovic, C., Masciocchi, N., Cervellino, A., *Journal of Pharmaceutical Sciences, 101* (**2012**), 4481-4489.

17. Etter, M.C., MacDonald, J.C., Bernstein, J., *Acta Crystallographica, B46* (**1990**), 256-262.

18. Bernstein, J., *Polymorphism in Molecular Crystals*, Clarendon Press, Oxford, **2002**.

19. Tung, H.-H., Paul, E. L., Midler, M., McCauley, J. A., Polymorphism, in *Crystallization of Organic Compounds – An Industrial Perspective*, John Wiley & Sons (**2009**), Hoboken, New Jersey, pp. 44.

20. Aronhime, J., Koltai, T., Braude, V., International Patent Application WO 2006/004922.

21. Barreca, G., Restelli, A., Allegrini, P., United States Patent US 8,143,409.

22. Amidon, G.L., Lennernas, H., Shah, V.P., Crison, J.R., *Pharmaceutical Research, 12* (**1995**), 413-420.

23. Löbenberg, R., Amidon, G.L., *European Journal of Pharmaceutics and Biopharmaceutics, 50* (**2000**), 3-12.

24. Yu, L.W., Amidon, G.L., Polli, J.E., Zhao, H., Mehta, M.U., Conner, D.P., Shah, V.P., Lesko, L.J., Chen, M.L., Lee, V.H., Hussain, A.S., *Pharmaceutical Research, 19* (**2002**), 921-925.

25. Allegrini, P., Vladiskovic, C., *Chimica Oggi - Chemistry Today*, *3*(15) (**2012**), 30-33.

26. Patil, N.S., Pagire, H.S., Neela, P.K., Pradham, N.S., Valgeirsson, J., United States Patent Application, US 2011/117200.

27. Cabri, W., Industrial Aspects and Legal Issues, in: *Crystallography for Health and Biosciences*, Guagliardi A., Masciocchi, N. (ed.), Insubria University Press, Varese, **2012**.

28. Inamoto, Y., Chiba, T., Kamimura, T., Takaya, T., *J. Antibiotics, 41* (**1988**), 828-830.

29. Sturm, H., Wolf, S., Ludescher, J., US Patent 6,350,869.

30. Manca, A., Sala, B., Monguzzi, R., US Patent Application US 2003/0204082.

31. Kumar, Y., Prasad, A., Prasad, M., International Patent Application, WO 2004/104010.

32. Dandala, S., Sivakumaran, S., United States Patent Application, US 2005/0137182.

33. Singh, G.P. et al., United States Patent Application, US 2005/0245738.

34. Law, D., Henry, R.F., Lou, X., International Patent Application, WO 2005/090361.

35. Bugay, D.E., Newman, A.W., Findlay, W.P., *Journal of Pharmaceutical and Biomedical Analysis, 15* (**1996**), 49-61.

36. Lubach, J.W., Munson, E.J., Solid State NMR Spectroscopy, in: *Polymorphism in the Pharmaceutical Industry*, Hilfiker, R. (ed.), Wiley-VCH, Weinheim, **2006.**

37. Giron, D., *Thermochimica Acta, 248* (**1995**), 1-59.

38. Patel, A.D., Luner, P.E., Kemper, M.S*., Journal of Pharmaceutical Sciences, 90* (**2001**), 360-370.

39. Nunes, C., Mahendrasingam, A., Suryanarayanan, R., *Pharmaceutical Research, 22* (**2005**), 1942-1953.

40. Yamada, H., Masuda, K., Ishige, T., Fujii, K., Uekusa, H., Miura, K., Yonemochi, E., Terada, K., *Journal of Pharmaceutical and Biomedical Analysis, 56* (**2011**), 448-453.

41. Giannini, C., Guagliardi, A., Millini, R., *Journal of Applied Crystallography, 35* (**2002**), 481-490.

42. Giannini, C., Guagliardi, A., Tedesco, E., *Newsletter of Commision on Powder Diffraction, IUCr, 29* (**2003**), 42-43.

2. Techniques for Structural Analysis

2.1 X-Ray Powder Diffraction

2.1.1 Interaction of X-Rays with matter

X-rays are an electromagnetic radiation having a wavelength (λ) between 0.1 and 100 Å. As the energy of electromagnetic radiation is inversely proportional to the wavelength, X-rays, having small values of λ, are highly energetic and therefore have high penetration in matter with a refraction index in any medium very close to 1. [1]

Interaction between radiation and matter (therefore also between X-rays and crystals) can happen in three ways:

a) Elastic (coherent) Scattering. The scattered radiation has the same wavelength as the incident (primary) radiation.
b) Inelastic (incoherent) Scattering (or Compton Scattering). The scattered radiation partially loses energy in the collision and therefore has a different (longer) wavelength from the incident radiation.
c) Absorption.

To fully describe the interaction of X-rays with matter taking into account all three phenomena, the dynamical theory of diffraction is necessary, which is mathematically quite complex. However, when considering specifically the interaction of X-rays with crystals, it is generally sufficient to consider only the

elastic scattering due to electrons according to the Thompson model, therefore using the kinematical theory of diffraction. [2]

When considering the interaction of X-rays with electrons, every electron interacts with the electrical field associated with the electromagnetic radiation by oscillating with the same frequency. Therefore, every electron generates a new spherical wavefront propagating in all directions and having the same wavelength as the incident radiation. This is shown schematically in Figure 2.1. The new wavefronts interact with each other causing interference (both constructive and destructive). The diffracted intensity will be non-zero only when the diffracted radiation from every electron is in phase, therefore where there is constructive interference. As the electron density is higher in the internal electron core, as opposed to the lower electron density of the valence electrons, the diffraction of X-rays will happen mainly around nuclei. This is the principal assumption upon which structural analysis using diffraction of X-rays is based. The organization of the nuclei in space can be evaluated by observing the interference (diffraction) pattern of X-rays generated in the reciprocal space by the real-space lattice.

Figure 2.1. Schematic representation of interference patterns given by the interaction of electrons with X-rays
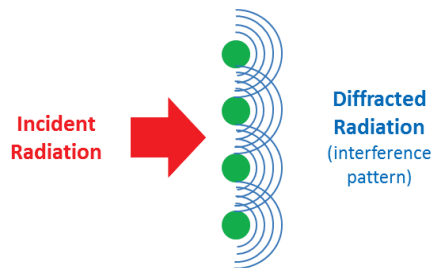
2.1.2 Crystals and Reciprocal Lattice

A crystal can be ideally thought of as an ordered structure of atoms or molecules which continues periodically in all directions. In order to describe a periodic structure, a very convenient thing is to use a lattice. A lattice can be simply described by identifying the smallest repeating unit, called the unit cell.

Given any kind of periodic structure, an infinite number of unit cells can be chosen to describe it, as schematically represented in two dimensions in Figure 2.2.

Figure 2.2. Schematic representation of the crystalline lattice

Given any periodic structure, an infinite number of unit cells can be chosen to describe it. In the case illustrated below, the periodic structure formed by the repeating lightning bolts can be described by any of the cells 1, 2 and 3.
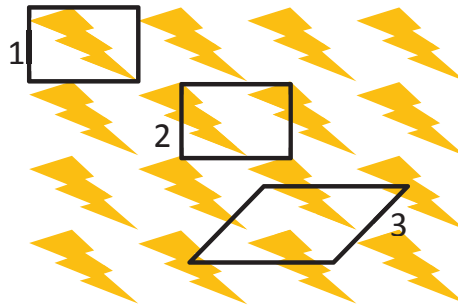
Analogously to the way in which two-dimensional unit cells depicted in Figure 2.2 describes a two-dimensional lattice, a three-dimensional lattice can be described by a three-dimensional unit cell, which in turn can be described by three non-coplanar vectors, **a**, **b** and **c**. Any point in the lattice can then be indicated by a vector q defined by equation (2.1).

$$q = u\mathbf{a} + v\mathbf{b} + w\mathbf{c} \qquad (2.1)$$

Instead of using vectors **a**, **b** and **c**, the same unit cell can be described using six scalar quantities: the lengths of the three vectors, a, b and c, and the angles between the vectors, α, β and γ. This is shown in Figure 2.3.

Figure 2.3. Description of the Unit Cell
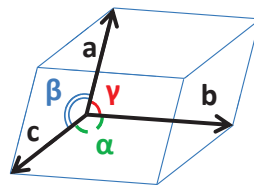
The situation described in Figure 2.2, repeated in Figure 2.4a, is not common, as the full content of the unit cell represents the repeating unit. Usually, only a part of the content of the unit cell will be repeated in space (therefore inside the unit cell as well), describable by simple geometrical transformations called symmetry elements (rotations, inversions, reflections, translations or combinations thereof). This is called the asymmetric unit. As an example, the two-dimensional structure of Figure 2.4b can be described knowing the asymmetric unit (the red lightning bolt), the unit cell (the black box) and the symmetry elements, meaning the geometrical transformations that describe how to obtain the yellow lightning bolts from the red one.

Figure 2.4. Two-dimensional structures and their unit cells

The asymmetric unit of structure a) is represented by the full content of the unit cell, the yellow lightning bolt. The asymmetric unit of structure b) is represented by the red lightning bolt, which can be transformed into the yellow lightning bolt inside the unit cell by inversion around the blue point.
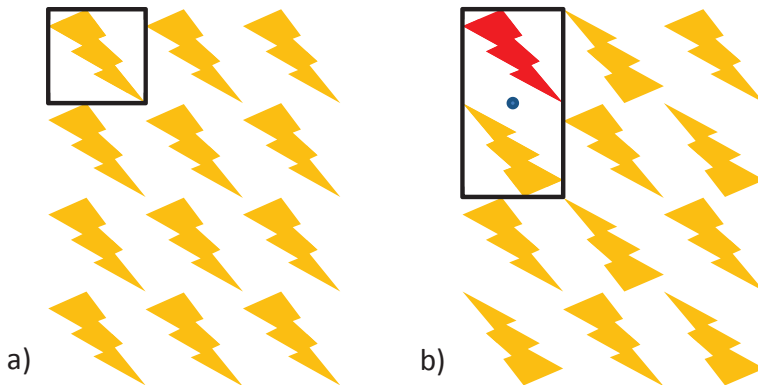
Other useful concepts when dealing with crystal structures are crystallographic planes and the way to describe them. The term "crystallographic plane" is a geometrical concept which really indicates a family of parallel, equidistant planes (where interplanar distance is defined *d*). These can be defined by three numbers *hkl*, called Miller's Indices, which indicate the number of equal

parts into which the first plane of the family next to the origin divides **a**, **b** and **c**. A couple of examples are depicted for clarity in Figure 2.5.

Figure 2.5. Crystallographic Planes

Miller's Indices indicated in round parenthesis are used to identify crystallographic planes.

(010) (200) (011)
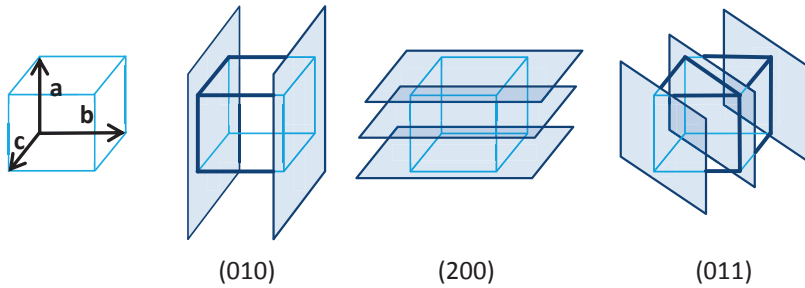
A mathematical concept very useful when dealing with diffraction by crystals is the reciprocal lattice. [2] The reciprocal lattice is defined by three vectors, $\mathbf{a}^*$, $\mathbf{b}^*$ and $\mathbf{c}^*$ (analogously to $\mathbf{a}$, $\mathbf{b}$ and $\mathbf{c}$ already discussed for the real space lattice) constructed so that the following conditions are met:

$$\mathbf{a}^* \cdot \mathbf{b} = \mathbf{a}^* \cdot \mathbf{c} = \mathbf{b}^* \cdot \mathbf{a} = \mathbf{b}^* \cdot \mathbf{c} = \mathbf{c}^* \cdot \mathbf{a} = \mathbf{c}^* \cdot \mathbf{b} = 0 \qquad (2.2)$$

$$\mathbf{a}^* \cdot \mathbf{a} = \mathbf{b}^* \cdot \mathbf{b} = \mathbf{c}^* \cdot \mathbf{c} = 1 \qquad (2.3)$$

As the dot represents the scalar product between two vectors and is equal to the product of the length of the two vectors times the cosine of the angle between them, equation (2.2) implies that $\mathbf{a}^*$ is perpendicular to both $\mathbf{b}$ and $\mathbf{c}$, $\mathbf{b}^*$ is perpendicular to both $\mathbf{a}$ and $\mathbf{c}$ and $\mathbf{c}^*$ is perpendicular to both $\mathbf{a}$ and $\mathbf{b}$. Considering the definitions of both scalar product and vector product, the following can be derived:

$$\mathbf{a}^* = \frac{\mathbf{b} \times \mathbf{c}}{V}; \qquad \mathbf{b}^* = \frac{\mathbf{a} \times \mathbf{c}}{V}; \qquad \mathbf{c}^* = \frac{\mathbf{a} \times \mathbf{b}}{V} \qquad (2.4)$$

$$\mathbf{a} = \frac{\mathbf{b}^* \times \mathbf{c}^*}{V^*}; \qquad \mathbf{b} = \frac{\mathbf{a}^* \times \mathbf{c}^*}{V^*}; \qquad \mathbf{c} = \frac{\mathbf{a}^* \times \mathbf{b}^*}{V^*} \qquad (2.5)$$

(where V and V^* are, respectively, the volumes of the real space and the reciprocal cell).

The families of crystallographic planes described above can also be represented in the reciprocal space with a vector perpendicular to the crystallographic planes having length equal to:

$$d^* = \frac{1}{d} \qquad (2.6)$$

This means than an infinite number of parallel crystallographic planes can be defined by a single vector $\mathbf{d}^*$ having origin in the origin of both the direct space and reciprocal unit cell or by a single point positioned at the end of vector $\mathbf{d}^*$. This is schematically depicted in two dimensions in Figure 2.6.

Figure 2.6. Two-dimensional representation of direct space and reciprocal lattice
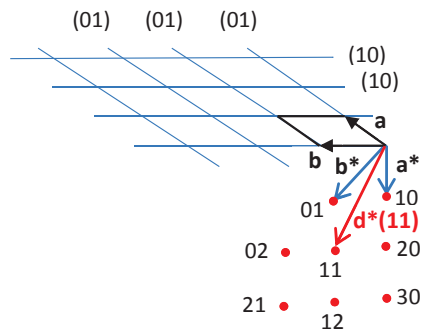
2.1.3 Bragg's Law and Laue's Equations

There are two ways to describe the mathematical conditions of constructive interference, Bragg's law and Laue's equations. In its most simple interpretation, Bragg's law considers a crystallographic plane, described by Miller's indices *hkl*, to act as a mirror for x-rays. Constructive interference will therefore only happen when the path difference for two rays reflecting off different parallel planes is a multiple of the wavelength and will depend on the incident angle θ. This condition

44

can be calculated by simple geometrical considerations. This is depicted in figure 2.7.

Figure 2.7. Graphical representation of Bragg's Law
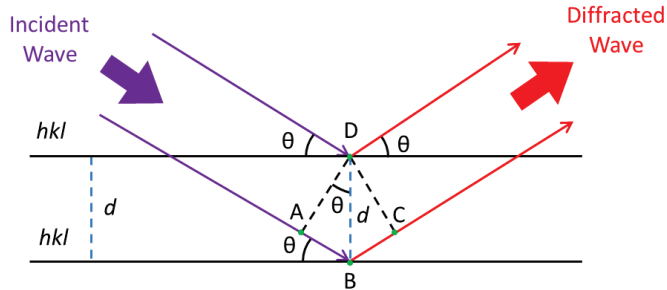
The condition for constructive interference is that the path difference between the wave that reflects two different crystallographic planes having the same *hkl* values is equal to a multiple of the wavelength of the incident radiation. In the picture, where two crystallographic planes *hkl* have an interplanar distance of *d*, this condition is fulfilled if AB + BC = *n*λ. As AB = BC and AB = *d* sinθ from simple trigonometric considerations, the geometrical condition of constructive interference can therefore be expressed by equation (2.7), which represents Bragg's Law:

$$2d \sin \theta = n\lambda \qquad (2.7)$$

Laue's equations are a different way to describe the mathematical conditions of constructive interference when x-rays interact with a crystal. [3] Considering a scattering vector **S** defined as

$$\mathbf{S} = \frac{(s - s_0)}{\lambda} \qquad (2.8)$$

where s_0 is the direction of propagation of the incident radiation, **s** is the direction of observation and λ is the wavelength of the radiation, the conditions for constructive interference are

$$\boldsymbol{a} \cdot \mathbf{S} = h \; ; \qquad \boldsymbol{b} \cdot \mathbf{S} = k \; ; \qquad \boldsymbol{c} \cdot \mathbf{S} = l \qquad (2.9)$$

45

Equations (2.9) are known as Laue's equations and must be satisfied simultaneously with *h*, *k* and *l* assuming integer values for constructive interference. Laue's equations can also be expressed differently making use of the reciprocal space:

$$\frac{(s-s_0)}{\lambda} = \boldsymbol{S} = h\boldsymbol{a}^* + k\boldsymbol{b}^* + l\boldsymbol{c}^* = \boldsymbol{d}^* \qquad (2.10)$$

In other words, as $h\boldsymbol{a}* + k\boldsymbol{b}* + l\boldsymbol{c}*$ is another way to express **d*** as defined in paragraph 2.1.2, the scattering vector **S** has module, and therefore diffraction intensity, greater than zero, where it coincides with vector **d***$_{(hkl)}$, therefore terminating on a point of the reciprocal lattice.

2.1.4 X-Ray Powder Diffraction Apparatus

The aim of any diffraction experiment is the measurement of the intensity profile in reciprocal space. [4] When X-rays hit a sample, radiation will be diffracted where constructive interference is possible, as described in the previous paragraph. If the sample is a single crystal, the diffraction will happen along the points of the reciprocal lattice where Laue's equations are satisfied, as shown in Figure 2.8a. If the sample contains more crystals having different orientations, the reciprocal lattices of the various crystals will superimpose (Figure 2.8b). Il the sample is constituted by an infinite number of crystals randomly oriented, the diffraction pattern will be made up of continuous lines (Figure 2.8c). A ray of the concentric circles obtained represents the powder diffraction pattern observed during an X-ray Powder Diffraction (XRPD) experiment.

Figure 2.8. Diffraction by a Single Crystal a), several crystals b), and a powder sample c).
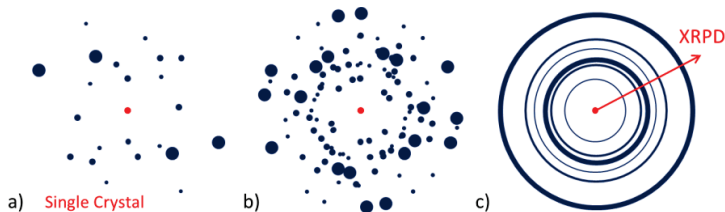
A diffraction experiment substantially needs three components:

1) a radiation (X-ray) source
2) a crystalline sample
3) a detector to measure the diffracted intensity

In between these components, other (optical) components may be added to modify the X-ray beam. The three main components listed above can be placed in different geometrical conformations. The two geometries most used in laboratory XRPD experiments are Bragg-Brentano (or parafocusing, or reflection) and Debye-Scherrer (or transmission).

In Bragg-Brentano geometry, the sample analyzed is packed flat and the diffracted radiation is measured after reflection off the sample. This is schematically shown in Figure 2.9a. The advantages of this method are in the easy and quick sample preparation, while the main disadvantage is that the diffracted intensity is highly influenced by sample characteristics, above all preferred orientation.

In transmission geometry, the radiation passes through the sample before reaching the detector. The sample can be packed in different ways, for example in cylindrical capillaries or in flat discs. The most used configuration is the cylindrical sample. This instrument configuration is showed in Figure 2.9b. Data collected in transmission geometry is generally less influenced by sample effects like preferred orientation, but sample preparation is longer and more complex.

Figure 2.9. Bragg-Brentano (Reflection) a) and Debye-Scherrer (Transmission) b) Geometries
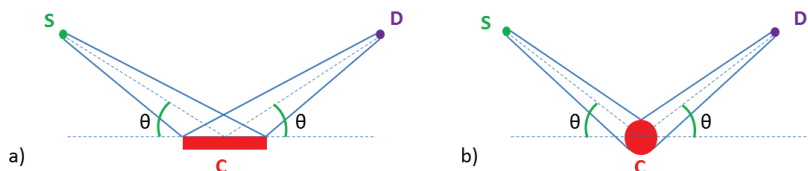
There are many different types of X-ray sources. In this section, only laboratory X-ray sources will be dealt with. [2] For synchrotron and other high

energy sources, see paragraph 2.1.5. The two most common laboratory sources of X-rays are sealed tubes and rotating anode tubes.

Sealed tubes are made up of a fixed anode coupled with a cathode sealed under high vacuum inside a metal and glass or ceramic tube. Electrons are emitted by the anode, generally tungsten, and accelerated towards the cathode by a high electrostatic potential (generally around 40 kV). The high-energy electrons impact against the cathode, displacing core electrons and causing X-ray emission. Metal filters are then used to cut off some of the unwanted wavelengths, making the radiation as monochromatic as possible (other monochromators can be used as optical components if necessary). As most of the energy supplied to the tube is converted into heat, sealed tubes require very efficient cooling to maintain working conditions.

The wavelength and emission profile of the obtained X-rays depends on the material of the cathode. Some of the most common materials used for cathodes and the resulting wavelengths are reported in Table 2.1, together with the metal used as a filter. For the analysis of molecular crystals, which tend to have relatively large crystalline cells and therefore many diffraction peaks at high interplanar spacings (therefore low angles) a longer wavelength allows a better resolution of diffraction peaks, distributing the peaks over larger angular ranges. Copper is generally the cathode of choice for XRPD as it is the most versatile, allowing for good resolution while avoiding the necessity of large angular ranges.

Table 2.1. Materials generally used for cathodes and resulting wavelengths. [2]

Anode Material	$K\alpha_1$ [Å]	$K\alpha_2$ [Å]	$K\beta$ [Å]	Filter
Cr	2.28975	2.293652	2.08491	V
Fe	1.93608	1.94002	1.75664	Mn
Co	1.78900	1.79289	1.62082	Fe
Cu	1.54059	1.54441	1.39225	Ni
Mo	0.709317	0.71361	0.63230	Zr

Rotating anode tubes have a better thermal efficiency than sealed tubes. This is achieved using bulky anodes which are rotated, therefore constantly moving a more chilled portion of the anode towards the impact zone. A higher brightness of X-rays is achievable. However, this radiation source is less durable than the sealed tube and is therefore used only for specific applications.

When analyzing powder samples, it is important for the sample to have certain characteristics. [5] First of all, the sample should contain all possible orientations of the crystals randomly distributed. Secondly, the crystallites should be as homogenous in size and shape as possible. Crystal shape can deeply influence peak intensity, especially in Bragg-Brentano geometry, because anisotropic shapes (for example rods or plates) will preferentially offer the incident beam a series of crystal faces which will be more represented than others. Careful grinding and preparation of the sample can minimize these effects. The use of transmission geometry with a cylindrical sample can also minimize preferred orientation effects. Sample preparation considerations are especially important for quantification purposes or when trying to solve structures from powders.

Several different types of detectors are available for laboratory instrumentation. As the characteristics (and the prices!) of detectors vary considerably, the detector choice is important when considering laboratory equipment. Until a few years ago, scintillation point detectors based on fluorescent crystals like sodium iodide (NaI) doped with 1% thallium were the most commonly used. The crystals present in the detector absorb X-rays and emit blue photons. The blue photons are multiplied by a photomultiplier and then converted into electric current. Scintillation detectors have the advantage of high linearity, high stability and long working life, together with a relatively low price. However, over the last few years, they have been gradually replaced by solid-state detectors, which have the advantage of being potentially very small and therefore can be mounted in arrays (both linear and two-dimensional). This shortens considerably measurement time, yielding high signal-to-noise ratio.

In fact, over the last few years, silicon or germanium solid-state detectors have become more and more used in powder diffractometry. A silicon or germanium single crystal doped with lithium interacts with an X-ray photon

causing electron vacancies proportional in number to the energy of the incoming photon. This generates an electric current which can be amplified and measured. The mounting of these kinds of crystals in an array allows to individually measure the current coming from each point of the array, therefore providing information about the incoming radiation from every specific location of the detector. This can shorten measurement times by two orders of magnitude, with a limited loss of resolution. The main disadvantage of this type of detector, apart from the considerably higher price compared to the scintillator, is that is has poor linearity for high photon fluxes. This can cause artefacts when observing particularly intense peaks.

In this work, two different types of diffractometers have been used for data collection, one working in reflection geometry on flat samples and one working in transmission geometry on cylindrical samples. The experimental conditions used are reported below.

Refection XRPD on Flat Sample – Experimental Conditions: The flat sample diffractograms were acquired on a Bruker D8 Advance ϑ:ϑ diffractometer equipped with a silicon strip detector (LynxEye) and having a goniometer radius of 300 mm. Nickel-filtered CuKα was used. The samples were generally placed in an aluminum sample holder equipped with a quartz monocrystal plate or in a silicon monocrystal sample holder (both 0.2 mm deep). When necessary, the samples were gently ground in an agate or glass mortar with a pestle.

When the analysis was run for identification or indexing purposes, the range investigated was generally 5-55° in 2ϑ with a step size of 0.02° and a scan speed of 0.5 sec/step. When the analysis was run for structure resolution or Rietveld refinement, the range investigated was 5-105° in 2ϑ with a step size of 0.02°. The diffractogram was then acquired for about 15 h in recycling mode.

Transmission XRPD on cylindrical samples – Experimental Conditions: The transmission diffractograms on cylindrical samples were acquired on a Bruker D8 Advance ϑ:ϑ diffractometer equipped with a silicon strip detector (LynxEye) and having a goniometer radius of 280 mm. Nickel-filtered CuKα was focused on the detector through the sample using a focusing mirror. The samples were gently ground in an agate or glass mortar with a pestle and then packed in glass

capillaries having a diameter of 1 mm. The capillary was rotated at 30 rpm during the measurement. The data, generally to be used for structure solution or Rietveld refinement, were acquired in the 5-105° in 2ϑ with a step size of 0.02°. Diffractograms were generally acquired for 15 or 64 h in recycling mode.

Single Crystal XRPD Analysis – Experimental Conditions: *The single crystal data contained in this work were collected on an Enraf-Nonius diffractometer using graphite monochromated MoKα radiation (λ=0.71073 Å). Data collection and data reduction strategy followed standard procedures implemented in the diffractometer's software. The structures were solved by direct methods using SIR97 program* [6] *and refined on F^2 by full-matrix least-squares procedure using SHELXL-97,* [7] *with anisotropic factors for all non-hydrogen atoms. Hydrogen atoms (apart from the hydrogen atoms of the molecule of 1-propanol of the 1-propanol solvate of Bupropion hydrobromide, see Chapter 3) were placed in geometrically calculated positions and refined by a riding model.*

2.1.5 Non-ambient Diffractometry

As XRPD is a relatively quick and easy technique which requires minimal sample preparation, it is well-suited for other applications like studying the sample in non-ambient conditions. The variables typically explored are temperature and pressure. For pharmaceutical solids, variable temperature XRPD can be extremely useful because API production, handling and formulation can cause at various stages the solid to undergo heating. The knowledge of behavior upon heating can therefore yield precious information. Moreover, variable temperature XRPD is extremely useful when studying desolvation processes or when establishing thermodynamic relationships between polymorphs.

The conditioning of the sample during an XRPD experiment can be achieved using a furnace chamber mounted inside the diffractometer connected with an automated temperature controller. Some of the issues to be addressed during variable temperature XRPD experiments are the need for homogeneous heating while avoiding oxidation or degradation of the sample. This is usually achieved by creating an enclosed, controlled atmosphere environment inside the furnace.

In this work, a custom-made controlled-temperature sample holder (shown in Figure 2.10) was successfully used for several variable temperature XRPD studies. The sample is heated in air, therefore care must be taken to ensure no thermal degradation or oxidation occurs. Moreover, thermal gradients can be generated on the sample, so careful and critical data evaluation is necessary. However, when studying pharmaceutical solids, transitions and other events are normally observed at relatively low temperatures (usually below 200°C), therefore an open chamber is usually well-suited for the desired applications.

Figure 2.10. Temperature controlled open sample holder (Officina Elettrotecnica di Tenno, Ponte Arche, Italy).
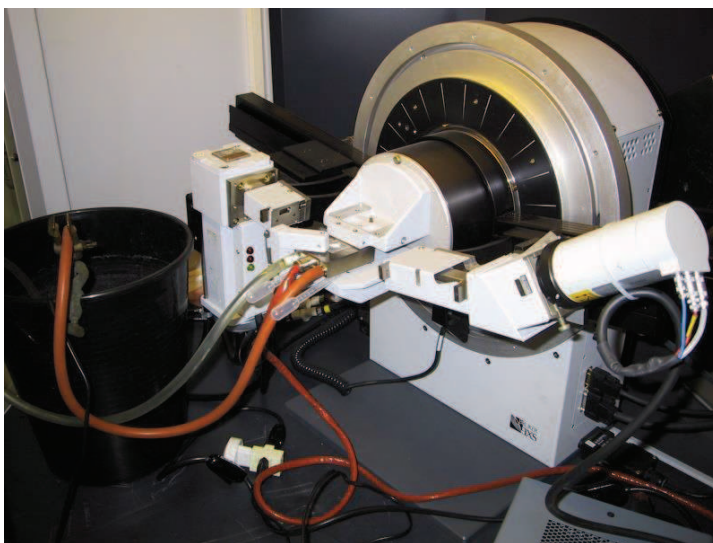
Variable temperature XRPD – Experimental Conditions: *The variable temperature XRPD experiments were run on a Bruker D8 Advance ϑ:ϑ diffractometer equipped with a silicon strip detector (LynxEye) and having a goniometer radius of 300 mm. Nickel-filtered CuKα was used. Samples were placed in an open, custom-made aluminum sample holder capable of heating the sample in air from room temperature up to 500 °C. (supplied by Officina Elettrotecnica di Tenno, Ponte Arche, Italy).*

Generally, a significant 2ϑ range, usually about 15° wide depending on the aim of the experiment, was chosen and data was acquired after heating of the sample in 10° or 20°C steps, using a step size of 0.02° in 2ϑ and a scan speed of 0.5 sec/step. After reaching the desired maximum temperature (generally the end of the observed event, typically either melting or complete conversion into a different phase), the sample was cooled using the same temperature steps used in heating and the diffractograms acquired again. Once room temperature was reached, the sample was visually inspected and a final analysis was run in the 5-55° in 2ϑ range to check both the chemical and the crystallographic purity. When deemed necessary, the chemical purity was also checked by solution ^{1}H-NMR (for experimental details, see paragraph 2.3.2).

2.1.6 Synchrotron Radiation

Synchrotron radiation can be fruitfully employed in powder diffraction experiments because of its elevated brilliance and coherence. Moreover, the wide emission X-ray spectrum makes it possible to select very specific wavelengths and highly monochromatic radiation. These factors make XRPDs collected with synchrotron radiation very high quality, having a low signal-to-noise ratio and narrow diffraction peaks.

When electrons moving at relativistic speeds are subjected to centripetal accelerations in curved trajectories, electromagnetic radiation is emitted. [8] The wavelengths obtained range from radio frequencies to short-wavelength X-rays. Electrons circulating with energies in the order of the GeV are maintained in large storage rings (tens or even hundreds of meters in diameter). They can then be subjected to centripetal accelerations, therefore emitting radiation, in different devices:

1) Bending Magnets – A magnetic field forces the change in trajectory.
2) Insertion Devices – electrons are forced into sinusoidal trajectories by a linear sequence of alternating magnets.

The radiation which can be obtained by synchrotron sources for XRPD experiments is many orders of magnitude more energetic than that obtained by laboratory sources. This gives many advantages, starting from very quick experiments (coupled with fast area or linear detectors) and very low detection

limits for trace amounts of contaminating crystalline forms. [9, 10] This, as discussed in Chapter 1, can be a very important issue to address when dealing with polymorphism of pharmaceutical substances.

Synchrotron Radiation XRPD Experiments: The synchrotron data contained in this work were acquired at the Powder diffraction station of the X04SA-MS beamline of the SLS synchrotron facility at the Paul Scherrer Institute, from samples loaded in 0.5 mm Lindemann glass capillaries, using Debye–Scherrer geometry and 15 keV radiation (λ=0.827006 Å), partial He beam path, and a Mythen detector covering 120° 2ϑ with 0.0038° resolution. Data were carefully absorption-corrected and subtracted for air and capillary scattering contributions before analysis.

2.2 Structure solution from Powder Diffraction Data and Quantitation methods

As discussed in Chapter 1, structure solution can be extremely useful and in some cases necessary in the study of pharmaceutical polymorphism. The traditional single crystal analysis, though offering structures of better quality and reliability, is seldom available for pharmaceutical applications for many reasons. Not all crystal forms can crystallize in specimens suitable for analysis, or crystal forms may come from desolvation or heating processes and can therefore be available only in polycrystalline form. In cases such as these, structure solution from powder data is the only viable method. [11]

Traditionally, in order to solve a structure from X-ray diffraction data, it is necessary to extract integrated intensities for each reflection. The integrated intensities depend on the squares of the modules of the structure factors **F_h**. The structure factor is a mathematical function describing the amplitude and phase of a wave diffracted from a specific crystallographic plane *hkl*. Solving a structure substantially implies solving for the phases of the structure factors knowing the modules. When no structure information is known *a priori*, the methods are called *ab-initio*. There are substantially two different approaches to the problem, reciprocal space methods (here, for simplicity, Direct methods only are considered) and real-space methods. [2]

Direct Methods operate in reciprocal space and are generally used with single crystal data. The only initial information required is the unit cell description and the knowledge of the cell content. No information regarding atom connectivity is used. The working assumptions are atomicity and positivity, meaning the electron density is considered concentrated around the atoms (atomicity) and it is treated mathematically as having positive value in every point (positivity). These methods are not widely used for solving structures of molecular solids from powders.

Real-space methods, operating by definition in real space, make use of the prior information usually accessible about atom connectivity, bond length, etc. The molecule is therefore initially described as a rigid body, with the addition of the necessary torsion angles to describe conformational freedom. Using a rigid body as starting geometry, the bond lengths and angles are already described. The only variables explored are torsion angles and the relative positioning and orientation of the molecules inside the unit cell. This is not only feasible but efficient for several reasons: first of all, bond lengths and angles don't vary much from one molecule to another and can be well described using molecular modelling with widely available force fields. Secondly, when dealing with crystal structures of polymorphic phases, the important information is not the length of every single bond, but the relative position of the various functional groups and interactions between them (above all hydrogen bonding), which can be successfully described by exploring torsion angles and molecular position and orientation only.

These characteristics make real-space methods particularly suitable for solving structures of small-molecule pharmaceutical solids. In fact, the molecular formula is obviously known and the size and conformational flexibility of the molecules are generally well-suited to the method.

The process of solving structures from powder data can be divided into several successive well-defined steps, assuming that high-quality diffraction data has been acquired on a pure monophasic sample of the desired crystalline form:

1) Indexing. Determining cell parameters and attributing *hkl* indices to every diffraction peak observed.

2) Space group determination. Assigning of a space group based on the volume of the cell, the approximate molecular volume and systematic absences.
3) Structure solution. An approximate solution is obtained using an *ab-initio* method.
4) Structure refinement. The solution obtained in point 3 is refined using the Rietveld method.

Each one of the steps described above has different critical points. In order for structure solution to be successful, every step is essential.

2.2.1 Indexing and Space Group Determination

Indexing means determining the cell parameters and attributing to each reflection observed in the reciprocal space a unique triplet *hkl.* When working on single crystal data, this is relatively simple, but working with powder data, the unavoidable overlapping of diffraction peaks (especially when dealing with molecular crystals) makes the procedure more complicated.

First of all, the position of the peaks must be very precisely evaluated, while the intensities do not matter at all. The diffraction peaks must be narrow, to avoid overlapping as much as possible. This can be achieved using very thin samples when operating in flat-sample geometry.

Having a series of precise peak values (generally about 20), the peak positions are expressed as Q_{obs}, defined as

$$Q_{obs} = \frac{1}{d^2} = \left(\frac{2\sin\theta}{\lambda}\right)^2 \qquad (2.11)$$

The process of indexing requires then finding the parameters of the reciprocal unit cell a_{ij} (with i,j = 1,3), which are the same for each reflection observed, and three values *hkl* which are different for every reflection observed. The described parameters have to satisfy the following condition:

$$Q_{obs} - \Delta < h^2a_{11} + k^2a_{22} + l^2a_{33} + hka_{12} + kla_{23} + hla_{13} < Q_{obs} + \Delta \quad (2.12)$$

where Δ represents the pre-assigned tolerance value.

56

Letting the observed Q_{obs} values be N, the number of variable to determine is $6+3N$. The problem is therefore always underdetermined and yields an infinite number of possible solutions, meaning a theoretically infinite number of possible cells. The correct one has to be chosen on the basis of several criteria. Firstly, knowing the molecular formula and shoichiometry all the components of the solid under examination, it is possible to estimate the molar volume in the solid state. A very rough estimate can be obtained by multiplying the number of non-hydrogen atoms by 18 Å^3, a less rough estimate can be obtained using tables of average atomic molar volumes in the solid state [12]. Secondly, all reflections present must be indexed or attributable to known impurities.

In order to help with the choice of crystal cell, several numerical criteria have been devised to help validate possible solutions. Aside from the considerations regarding density and volume described above, two figures of merit are often used, M_{20} (or De Wolff figure of merit) and F_N (or Smith and Snyder figure or merit).

The De Wolff figure of merit [13] is defined as

$$M_{20} = \frac{1}{N_{poss}} \times \frac{Q_{20}}{2|\Delta Q|} \qquad (2.13)$$

where Q_{20} is the Q-value of the 20th indexed peak, N_{poss} is the number of possible independent reflections for $Q<Q_{20}$ and $|\Delta Q|$ is the average absolute difference between the observed and calculated Q.

The Smith and Snyder figure of merit [14] is calculated as

$$F_N = \frac{N}{N_{poss}} \times \frac{1}{|2\theta|} \qquad (2.14)$$

where N is the number of the observed Bragg peaks, N_{poss} is the number of possible independent reflections up to the Nth observed peak and $|2\theta|$ is the absolute average difference between the observed and calculated 2θ values.

The space group must then be assigned, taking into consideration the number of molecules in the unit cell and the systematic absences (the absence of specific *hkl* reflections based on cell symmetry). This is done using the correlation tables present in the International Tables for Crystallography, Vol A. [15]

Both to verify the cell and space group determined and to refine cell parameters, it is very useful to apply Whole-Pattern Profile Fitting (WPPF) methods. The obtained cell and space groups can be used to simulate a pattern with peak positions determined by the unit cell and variable peak intensities. This can be done for example with the Le Bail method. [16]

Peak shapes, important in WPPF methods, can be described in different ways. Several mathematical functions are available: Gaussian curves, Lorentzian curves, Voigt (a convolution of a Gaussian and a Lorentzian curve), pseudo-Voigt (linear combination of Gaussian and Lorentzian curves) and Pearson VII (a generalized Lorenzian-Gaussian mixture different from the pseudo-Voigt). These mathematical approaches are based on finding a mathematical function able to correctly describe the shape of the diffraction peak observed. A different approach is to describe peak shape considering the various contributions from experimental configuration (goniometer radius, slits, radiation profile, geometry used, etc.) and using separate functions to describe each contribution. Peak shape is then described with a convolution of the different contributions. This approach is called the Fundamental Parameters Approach (FPA) and is schematically reported in Figure 2.11. [17]

Figure 2.11. Graphical Representation of the convolution procedure for peak description with the Fundamental Parameters Approach.

| Bragg Peak | Emission Profile | Slit Width | Axial Divergen | Crystallit e Size | Peak Description |
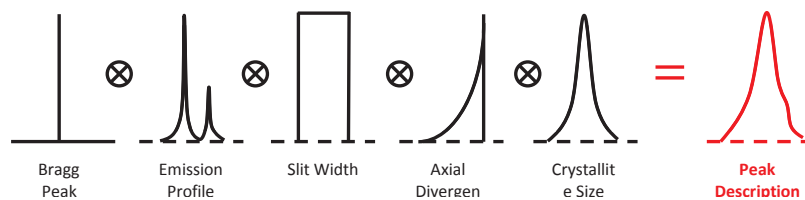
Indexing and Space Group Determination, general procedure: A general protocol was applied to all phases studied. Exact peak positions of the different phases were determined using standard peak search methods followed by profile fitting methods incorporated in the program TOPAS-R [18], also used for indexing and determining approximate cell parameters for each phase. The unit cell parameters were then refined with the structureless Le Bail mode of the Rietveld method. For

58

each XRPD dataset, the background was modeled using a Chebyshev polynomial, peak profiles were described by the Fundamental Parameters Approach and an average isotropic thermal factor was attributed to all atoms. Density considerations and the analysis of systematic absences lead to space group determination and Z-evaluation.

2.2.2 Structure Solution

The aim of the structure solution step is to derive an approximate structural model to be later refined. In real-space methods, as described at the beginning of section 2.2, this is achieved by constructing an initial molecular fragment (generally using molecular modelling when a previously solved structure of a different polymorph is not available) based on known atom connectivity and moving it in real-space. [19] The positions of the atoms of the molecular fragments can be described either by Cartesian coordinates or by a Z-matrix carrying internal coordinates (bond lengths, bond angles and torsion angles). The powder diffraction profile is then calculated and compared with the experimental powder data using a cost function (CF). The aim is to find an absolute minimum of the cost function, which should correspond to an approximate solution.

The position of a molecular fragment can be described by the coordinates of its center of gravity x, y and z, by three angles which describe its orientation ϕ_1, ϕ_2 and ϕ_3 and by the necessary torsional angles τ_1, τ_2, τ_3.... These parameters are included in the so-called parameter vector $\mathbf{P}$:

$$\mathbf{P} = \{x, y, z, \phi_1, \phi_2, \phi_3, \tau_1, \tau_2, \tau_3 \dots\} \qquad (2.15)$$

A trial parameter vector $\mathbf{P}$ is used to calculate intensities y_{ic} for all i points of the diffraction pattern. These are then compared with the observed y_{io} for all points using a cost function CF:

$$\mathrm{CF}(\mathbf{P}) = \sum_i w_i \left[y_{io} - y_{ic}(\mathbf{P}) \right]^2 \qquad (2.16)$$

where w_i is the statistical weight of the single i point and is generally taken as $1/y_{io}$. The parameter vector is then changed (randomly or otherwise) and the cost function is calculated again. The new configuration can then be discarded or

accepted depending on a pre-chosen criterion, and the iterations continue. The way in which the new parameter vector is generated and the acceptance criteria vary depending on the method (Monte Carlo, Simulated Annealing, Genetic Algorithm, etc.), but the idea is always to find the parameter vector $\mathbf{P_o}$ which minimizes the cost function and is therefore a possible structural solution.

Structure Solution, general method: Approximate structure solutions were generally found by employing a semirigid molecular fragment, typically constructed using the molecular modeling optimization routine of ACD/ChemSketch, version 12.01. The molecule, or molecules, under examination were made flexible about the necessary acyclic torsion angles, for example those of side chains. When necessary, the pertinent halide ion was added as a freely floating atom. If the phase under examination was a solvate, the solvent molecule was also modelled and added. For Ibuprofen lysine salt (see Chapter 5), the molecules of Ibuprofen and lysine were modelled and moved separately, but simultaneously, during structure solution. Approximate location and orientation of the molecular fragments were found using the simulated annealing algorithm incorporated in TOPAS-R. Each simulated annealing was run until a chemically and crystallographically reasonable structure solution was repeatedly found.

The CPU time and iterations necessary to yield a solution varied depending on the number of fragments and torsion angles explored. The background, peak description and thermal factor, already optimized in the Le Bail step described with the indexing procedure, were kept fixed to keep the number of variables as low as possible.

In this phase, the 2ϑ range typically employed was 5-55°.

2.2.3 Rietveld Refinement

The Rietveld method [16] is based on the comparison between a calculated and an experimental diffraction profile. Like in other WPPF methods, the difference is evaluated using a cost function minimized using a non-linear least-squares approach.

The cost function to be minimized is the weighted sum of squares, analogous to the cost function $\mathrm{CF}(\mathbf{P})$ reported as equation 2.16, already used

during structure solution. The values for y_{ic} are calculated according to equation 2.17

$$y_{ic} = S_j \sum_{\mathbf{h}} I_{\mathbf{h}} P(i, \mathbf{h}) \, A(i, \mathbf{h}) O(\mathbf{h}) + y_{ib} \qquad (2.17)$$

where S_j is a scale factor, $P(i, \mathbf{h})$ is the profile shape function, $A(i, \mathbf{h})$ is an asymmetry function, $O(\mathbf{h})$ is the preferred orientation correction, y_{ib} is the calculated background and $I_{\mathbf{h}}$ the calculated intensity of reflection $\mathbf{h}$ as defined in equation 2.18

$$I_{\mathbf{h}} = m_{\mathbf{h}} |F_{\mathbf{h}}|^2 \mathrm{Lp}_{\mathbf{h}} \qquad (2.18)$$

where $m_{\mathbf{h}}$ is the multiplicity of reflection $\mathbf{h}$, $|F_{\mathbf{h}}|^2$ is the square of the modulus of the structure factor for reflection $\mathbf{h}$ and $\mathrm{Lp}_{\mathbf{h}}$ is the Lorentz-polarization correction.

As the structure factors need to be calculated starting from the structure, the Rieltveld method requires knowledge of all structural and instrumental parameters, and allows the refinement of any variable chosen (cell data, background description, scale factors, atomic positions, etc.). In the case of Rietveld refinement after structure solution as described in paragraph 2.2.2, it allows the refinement of cell data, molecular position, orientation and of course of the torsion angles used to describe molecular flexibility (as well as background description and other relevant parameters).

Rietveld Refinement of a structural solution, general procedure*: After an approximate structure solution was found with the simulated annealing method described in paragraph 2.2.2, it was refined using the Rietveld routine embedded in TOPAS-R. The cell parameters, background polynomial, thermal factor attributed to all atoms were optimized together with the molecular fragment positions and orientation and the torsion angles. The full XRPD profile was used in the refinement, typically in the 5-105° 2ϑ range.*

2.2.4 Quantitation Methods

The Rietveld method can also be fruitfully employed for quantification, as briefly described in paragraph 1.3.5. While the calculation of the cost function

(equation 2.16) remains the same, the calculation of the intensity (equation 2.17) can be modified to allow calculation of intensity from more than one structure represented in the sample. As an example, equation 2.19 shows how equation 2.17 would be modified for a sample containing two different phases 1 and 2, while equation 2.18 to obtain values of $I_\mathbf{h}$ remains unchanged.

$$y_{ic} = S_1 \sum_\mathbf{h} I_{1\mathbf{h}} P(i, \mathbf{h}) A(i, \mathbf{h}) O(\mathbf{h}) + S_2 \sum_\mathbf{h} I_{2\mathbf{h}} P(i, \mathbf{h}) A(i, \mathbf{h}) O(\mathbf{h}) + y_{ib} \quad (2.19)$$

From the values obtained for the scale factors S_1 and S_2 it is possible to obtain the relative amounts of the two phases 1 and 2.

As crystal structures of active pharmaceutical ingredients are not always, if not seldom, available, a very interesting Quantitative Phase Analysis (QPA) method proposed in the literature uses the full XRPD profile but does not require the knowledge of the structure of the phases involved. [20] This method uses a Rietveld-like calculation method, modifying the equations to use intensities extracted from the observed diffraction profile. In order to do this, the moduli of the observed structure factors need to be placed on an absolute scale to be comparable with those calculated form the crystal structure. The moduli of structure factors are on an absolute scale when they are expressed relative to the scattering of an isolated electron under the same conditions. The necessary scale factor K_j can be obtained using the Wilson Plot. [21] Equation 2.18 therefore becomes

$$I_\mathbf{h} = m_\mathbf{h} K_j |F_{\mathbf{h}o}|^2 \mathrm{Lp}_\mathbf{h} \qquad (2.20)$$

where K_j is the absolute scale for phase j and $F_{\mathbf{h}o}$ are the observed structure factors. To obtain K_j, the average scattered intensity of the crystal is compared with the theoretical values to be expected form a completely random arrangement of atoms inside a unit cell of the same content, as expressed in equation 2.21,

$$K_j I_{avg} = \sum f_i^2 \, e^{(-2B \sin^2 \theta / \lambda^2)} \qquad (2.21)$$

where I_{avg} is the mean intensity value in a chosen interval of 2θ, f_i^2 are the squares of the atomic structure factors for the atoms present in the unit cell, B is

62

an isotropic atomic thermal vibration factor and λ is the wavelength of the radiation used. Taking the natural logarithm of both sides of equation 2.21 and rearranging, equation 2.22 is obtained.

$$\ln\left(\frac{I_{avg}}{\sum f_i^2}\right) = -\ln K_j - 2B \sin^2 \theta / \lambda^2 \qquad (2.22)$$

Plotting $\ln\left(\frac{I_{avg}}{\sum f_i^2}\right)$ for chosen intervals of 2θ against $\sin^2 \theta / \lambda^2$ a line having intercept equal to $-\ln K_j$ and slope equal to $-2B$ should be obtained. This is called the Wilson Plot.

This QPA method has been implemented in a publicly available software called QUANTO [22] but has been applied, to our knowledge, only once to active pharmaceutical ingredients. [23] Seeing the promising characteristics of the method, as it does not require the knowledge of the crystal structures but only the XRPDs of pure samples of the phases involved for intensity extraction, it was deemed useful to explore the scope of the method when applied to APIs.

Quantitative Phase Analysis (QPA), general procedure: High quality powder data of the pure phases to be used in QPA (acquired as described in paragraph 2.1.4) was analyzed with the software QUANTO. Initially, a Le Bail fit was carried out for each pure phase using and refining the known cell data, generating a list of reflections with the associated moduli of the observed structure factors. For each XRPD dataset, the background was modeled using a Chebyshev polynomial and peak profiles were described with pseudo-Voigt functions. A second run, providing the program with the unit cell contents as well as the refined cell parameters, allowed to extract integrated intensities for each indexed peak, saving the data in a separate file to be used during quantitation. High quality powder data of known mixtures were then analyzed both with a classical Rietveld approach and with the intensities extracted from the pure phases. The program automatically applied the Wilson plot to place extracted intensities on the absolute scale when intensity files were used in place of structure information. Again, the background was modeled using a Chebyshev polynomial and peak profiles were described with pseudo-Voigt functions. More details regarding the whole procedure are reported in Chapter 6.

2.3 Other techniques for Crystal Form Characterization

Many other techniques are available for characterizing various aspects of crystalline phases, for example Infrared spectroscopy (IR), Raman spectroscopy, Nuclear magnetic resonance spectroscopy (NMR), dynamic vapor sorption (DVS), and various thermal methods, including differential thermal analysis (DTA), differential scanning calorimetry (DSC) and thermogravimetric analysis (TGA). In the present work, wide use was made of DSC and NMR to characterize samples.

2.3.1 Differential Scanning Calorimetry (DSC)

When heating a solid sample, thermal events (for example solvent loss, transitions into other forms, melting or thermal decomposition) will be induced. Information can be obtained when heating a sample and an inert reference in the same conditions, measuring the temperature difference between the sample and the reference. Different events will either cause heat to be absorbed or released. This is the basis of Differential Thermal Analysis (DTA). As DTA offers only qualitative but not quantitative information, the technique evolved in Differential Scanning Calorimetry (DSC).

DSC measures the heat flow between the sample and the reference during heating (or cooling). Two different approaches are possible in order to do this:

a) Power compensation – The sample and reference are kept at the same temperature and the power needed to do this is measured.
b) Heat flux – The heat differential between the sample and the reference is measured as a function of temperature.

In both cases, the output is a curve of heat flow (dQ/dt) as a function of temperature. Generally, the heat flow is given in J/g and the temperature in °C, even though using absolute temperature is sometimes considered useful. Endothermic events can be depicted both as above or as below the baseline, depending on the convention used. This is generally clearly marked on the axis to avoid confusion. [24]

Because heat Q depends on the specific heat capacity (C_p) according to $Q = C_p\Delta T$, the heat flow can be correlated with the specific heat capacity, [25] as shown in equation 2.23.

$$\frac{dQ}{dt} = C_p \frac{dT}{dt} \qquad (2.23)$$

Therefore, the DSC trace can also be expressed in C_p as a function of heating. This is of particular significance when the baseline shifts, for example during the glass transition of an amorphous phase.

Integration of equation 2.23 with the temperature shows how the area underlying the curve is proportional to the energy involved in the process, in particular ΔQ. At constant pressure, $\Delta H = \Delta Q - P\Delta V$, where P is pressure and ΔV is change in volume (expansion work). When operating with open crucibles the pressure can be considered constant and, as the phenomena observed are generally solid→solid transitions or solid→liquid transitions, ΔV is negligible. Therefore, $\Delta Q = \Delta H$. DSC therefore gives a direct measurements of the enthalpy change associated with observed phenomena.

DSC analysis can play an important role in studying polymorphism of pharmaceutical compounds because different crystalline forms will in principle have different thermal profiles, including but not limited to different melting points. The phenomena observable with DSC are several. Scheme 2.1 holds the most common types of events observed, classified according to whether they are accompanied by heat release (exothermic) or heat absorption (endothermic). The glass transition, being a shift in the baseline, is classified separately.

DSC is a precious tool in characterizing crystalline forms because it allows to determine, for example, whether a specific form has crystallization solvent, whether it converts before melting into a different phase and whether the transition is exothermic or endothermic. This in particular allows determination of thermodynamic relationships between crystalline forms. [26] As discussed in Chapter 1, this can be of great importance.

Scheme 2.1. Events observable by DSC

Endothermic Events	Exothermic Events
• Melting	• Crystallization
• Solvent Loss	• Exothermic solid→solid
• Endothermic solid →solid	transformation
transformation	• Thermal decomposition
• Glass transition	

DSC is justifiably considered a destructive technique. However, with custom-made temperature programs, it can be a powerful tool to prepare specific crystalline forms. For example, it is possible to achieve controlled desolvations and study other solid-solid transitions. [27]

Throughout this work, DSC has been extensively used to characterize solid forms. Moreover, custom-made temperature programs have been used to prepare previously unknown crystalline forms. This use of preparative DSC is further described and discussed in Chapter 3.

Differential Scanning Calorimetry Experiments: Differential Scanning Calorimetry measurements contained in the present work were run on a Mettler-Toledo 822e calorimeter. The samples (typically, in the 3-5 mg range) were loaded in aluminum pans with pierced lids and generally heated at 10 °C/min (depending on the aim of the experiment) under a flow of nitrogen (80 ml/min). The temperature range explored, depending on the aim of the experiment, was generally between 30 and 300°C. When the experiment required it, custom-made temperature programs were designed with cooling steps as well as heating steps, depending on the desired outcome.

Transition temperatures in the DSC traces were determined using the onset method, the temperature at which the tangent segment taken in the first inflection point of the curve crosses the baseline.

When required for analytical purposes, the pans were opened after the analysis and the recrystallized or otherwise modified solids analyzed via XRPD and/or solution ^{1}H- and ^{13}C-NMR (see sections 2.1.4 and 2.3.2 for details).

2.3.2 Nuclear Magnetic Resonance (NMR)

Nuclear Magnetic Resonance (NMR) spectroscopy is a technique which allows to obtain information on the chemical environment of nuclei based on the study of the interaction of nuclear angular momentum with an externally applied magnetic field. The application of a strong external magnetic field causes formerly degenerate energy levels of the nuclei to split in $2I+1$ states, where I is nuclear spin quantum number of the nucleus under exam. The energy difference between adjacent states ΔE is equal to

$$\Delta E = \gamma \hbar B_0 = \hbar \omega_0 \qquad (2.24)$$

where γ is the gyromagnetic ratio, $\hbar$ is the reduced Plank constant, B_0 is the applied magnetic field and ω_0 is the Larmor frequency. What is measured during an NMR experiment is ω_0. This depends on the chemical environment of the single nuclei and is therefore used to extract a lot of chemical information.

With several modifications, the NMR technique can be applied both to molecules in solution and molecules in the solid-state. The kind of information obtained in the two cases is rather different. In solution, molecular tumbling mediates to isotropic values many anisotropic contributions (for example dipole coupling and quadrupole coupling). This causes NMR spectra recorded in solution to have sharp signals, mainly used for chemical identification purposes. Solid-State NMR yields information of different nature, because the anisotropic contributions are not mediated by molecular tumbling. In principle, solid-state NMR therefore offers more information than solution NMR.

Some techniques are available which simplify the spectrum enough to make the information acquirable and readable. For example, Magic Angle Spinning (MAS) allows to mediate some anisotropic contributions and high power decoupling is used to eliminate J-coupling. Solid-State NMR can therefore be used to extract important information about the solid state, complementary to those which can be obtained from powder diffracion. For example, SS-NMR can be used to determine how many crystallographically non-equivalent molecules are present in the asymmetric unit. This is crucial information to have when attempting to solve structures form powder data. An example of this is the solving of the

structure of form IV of Linezolid from powder data reported in the literature. [28] SS-NMR allowed to determine the presence in the asymmetric unit of two crystallographic independent molecules, forming non-centrosymmetric dimers in the structure.

In the present work, SS-NMR has not been used, but wide use has been made of solution ^{1}H- and ^{13}C-NMR to study the chemical composition of phases, to verify the chemical identity after thermal treatments or other procedures and to gather relevant chemical information.

Nuclear Magnetic Resonance Experiments in Solution: ^{1}H- and ^{13}C-NMR experiments were run on a Mercury 300 Varian spectrometer generally using d6-DMSO as a solvent. Sample concentration was in the range 0.01-0.04 M.

Proton Spectra for chemical identification were generally acquired with a delay of 1 second between acquisitions for 16 acquisitions. When the aim of the spectrum was to quantify the solvent present, the delay was brought to 30 seconds. Carbon spectra were generally acquired with a delay of 4 seconds between acquisitions for about 15 h (about 10000 acquisitions).

Chemical Shift values are given in ppm using TMS as an external reference. Signal attribution was based on chemical shift and signal multiplicity. When deemed necessary, exchange of the mobile protons with deuterated water was carried out to confirm signal attribution.

2.4 Preparation of Crystal forms

Crystal forms can be prepared in many different ways. The main method employed industrially is crystallization from solution, as this allows purification as well as control of particle size and crystal shape, in addition to easy separation of the finished product from the mother liquor. Moreover, it is easily industrially applicable and highly controllable. However, not all crystalline forms can be prepared from crystallization from solution. Other techniques are available, like desolvation, heating, grinding, vapor digestion, slurry conversions, solvent removal by evaporation, spray drying or freeze drying, anti-solvent precipitation, crystallization from the melt, sublimation and more. [29]

2.4.1 Crystallization

Crystallization from solution is the most employed technique not only because of the purification issues and industrial applicability, but also because many parameters can be varied and managed, allowing control on the outcome of the crystallization. Choice of the solvent, temperature, stirring, concentration, cooling rates, ripening times can all affect crystallization outcome. Understanding the parameters involved and their influence on the process is vital to successfully controlling a crystallization procedure.

The driving force of any crystallization is the supersaturation, the difference between the concentration in solution of the species to be crystallized and the equilibrium solubility concentration at a given temperature. [30] Once supersaturation is achieved, crystallization occurs through two mechanisms, nucleation and crystal growth. The kinetics of the two processes is different, and therefore nucleation and crystal growth can occur at different supersaturation levels. Typically, crystal growth can occur at lower supersaturations than nucleation. A metastable zone therefore exists below the solubility curve where crystal growth could occur, but in the absence of nuclei it does not. Only at the edge of the metastable zone does spontaneous nucleation occur. At this point, the supersaturation decreases while crystallization occurs. This is depicted in Figure 2.12.

Figure 2.12. Solubility Curve, Supersaturation and Metastable Zone Width
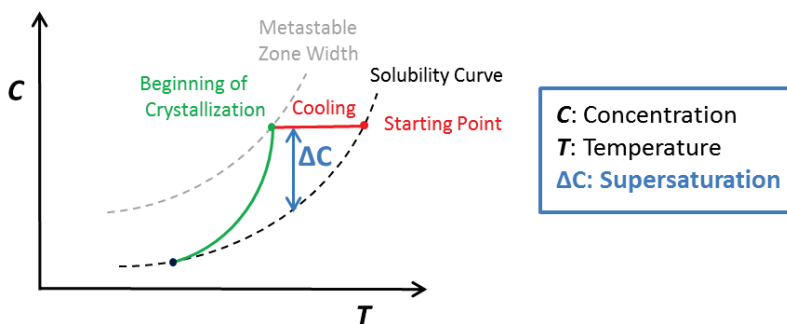
As crystallization is driven by supersaturation which is tied to solubility, the understanding of solubility is essential to understanding (and controlling) crystallization. To understand how solubility, a thermodynamic property, is tied to thermodynamic stability, it is useful to consider chemical potential μ. When a crystalline form 1 is thermodynamically more stable than another form 2, as explained in Chapter 1, $G_1 < G_2$. This, at constant pressure, implies $\mu_1 < \mu_2$. Since $\mu = \mu^0 + RT \ln a$, where R is the universal gas constant, T is temperature and a is activity, the chemical potential can be linked to the concentration of the species in solution. In fact, the activity can be assumed equal to the concentration admitting an activity coefficient of 1. At equilibrium, therefore,

$$\mu_1 = \mu^0 + RT \ln S_1 \; ; \qquad \mu_2 = \mu^0 + RT \ln S_2 \qquad (2.25)$$

where S_1 and S_2 are the solubilities of the two forms at the temperature T. As $\mu_1 < \mu_2$, this implies that $S_1 < S_2$. This means that not only the most thermodynamic stable form always has lower solubility, but also that the solubility curves for the different crystal forms follow the trend of Gibb's free energy (discussed in Chapter 1). Therefore, the relationships between solubility curves for monotropic and enantiotropic polymorph pairs are depicted in Figure 2.13.

Analogously to what previously discussed in Chapter 1, kinetic considerations are very important in understanding crystallization outcome. Different cooling rates will achieve different supersaturations before spontaneous nucleation sets in. This allows to control which crystalline form nucleates and grows.

Figure 2.13. Solubility curves for a) monotropic and b) enantiotropic polymorph pairs
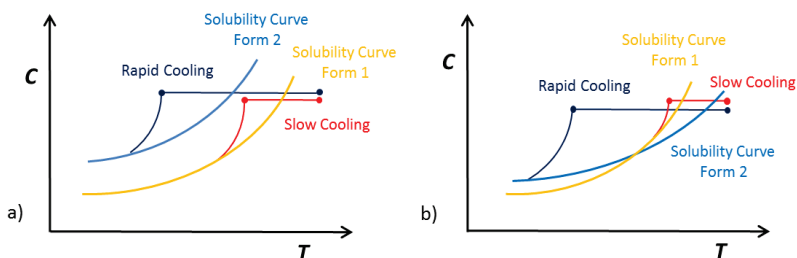
Crystallization experiments, general procedure: The active pharmaceutical ingredients used in this work have been donated by Dipharma Francis S.r.l., Baranzate (MI), Italy. The solvents and other reagents used were purchased from Sigma-Aldrich (St. Louis, MO, USA) and used without further purification. Crystallization of the different pharmaceutical compounds studied in this work were generally carried out on 2-5 g of substance. Typically, the solid was placed in a round-bottomed flask equipped with a thermometer and a reflux condenser and placed under magnetic stirring in inert atmosphere, generally nitrogen gas. The solid was suspended in an initial amount of solvent, the solvent was heated to reflux using an oil bath and more solvent was added portion-wise until complete dissolution was obtained.

When the experiment required fast cooling, the oil bath was removed and immediately replaced by an ice bath. When the experiment required slow cooling, the heating of the oil bath was stopped but the oil bath was left in position to cool naturally. In the cases in which a more controlled cooling was necessary, small double-walled reactors with oil circulation were used. The temperature of the circulating oil was controlled by electronic programmable thermo-cryostats, allowing to design specific cooling ramps.

The crystallized solid obtained was typically retrieved by filtering the suspension on Buchner, Hirsch or Gooch filters. The solids were generally analyzed wet using the necessary techniques, then dried under vacuum and analyzed again.

Once a metastable crystalline form is generated in solution, it can still evolve into a more stable form, especially if suspended in a solvent. This not only means waiting time between crystallization and filtration is important, but it is also the principle used in slurry transformations (generally called Solvent-Mediated Phase Transitions, or SMPT). [31] Different solvents can be used to promote different phase transitions. This is especially true when the species involved are solvates, therefore having solvent molecules in the crystalline structure. In this work, slurry experiments have been used to transform one solvate form into another (see Chapter 3 for more details).

Slurry Experiments, general procedure: The active pharmaceutical ingredients used in this work have been donated by Dipharma Francis S.r.l., Baranzate (MI),

Italy. When necessary for the experiments, the solids were crystallized and/or otherwise treated before the slurry experiment. The solvents used were purchased from Sigma-Aldrich (St. Louis, MO, USA) and used without further purification. Slurries of the different crystal phases treated were generally carried out on 0.2-2 g of substance. Typically, the solid was placed in a round-bottomed flask equipped with a thermometer and a reflux condenser and placed under magnetic stirring in inert atmosphere, generally nitrogen gas, at room temperature. The amount of solvent used varied depending on phase solubility. When necessary to work at non-ambient temperatures, a heated oil bath was used. The slurry times were generally between ten minutes and 2 hours.

2.4.2 Other techniques

Many other less conventional techniques are available when seeking to prepare a specific (or new) crystalline form, as mentioned at the beginning of this section. The only crystallization method apart from crystallization from solution that was used in this work is heating. Heating can be effective in promoting phase transitions and desolvation processes.

Heating to induce desolvation and/or phase transition*: In the instances where heating was required to obtain phase transitions, this was obtained by different means. When a vacuum was necessary to favor desolvation, a laboratory oven (operating in the 30-120°C renge) was used and connected to a mechanical vacuum pump. When heating at very specific and precise temperature was necessary, the heating was carried out until phase transition occurred directly in a DSC pan, as described in paragraph 2.3.1.*

References

1. Milanesio, M., Diffrazione da Materiali Policristallini I: Principi e Campi di Applicazione, in *Analisi di Materiali Policristallini mediante Tecniche di Diffrazione*, Guagliardi, A., Masciocchi, N., (ed.), Insubria University Press, Varese, **2007**.
2. Pecharsky, V.K., Zavalij, P.Y*., Fundamentals of Powder Diffraction and Structural Characterization of Materials*, 2nd Ed., Springer, New York, **2009**.

3. Bürgi, H.B., Introduction to Structural Crystallography, in *Crystallography for Health and Biosciences*, Guagliardi A., Masciocchi, N. (ed.), Insubria University Press, Varese, **2012**.

4. Artioli, G., Diffrazione da Materiali Cristallini II: Geometrie e Componenti Strutturali, in *Analisi di Materiali Policristallini mediante Tecniche di Diffrazione*, Guagliardi, A., Masciocchi, N., (ed.), Insubria University Press, Varese, **2007**.

5. Masciocchi N., Preparazione del Campione, in *Analisi di Materiali Policristallini mediante Tecniche di Diffrazione*, Guagliardi, A., Masciocchi, N., (ed.), Insubria University Press, Varese, **2007**.

6. Altomare, A., Burla, M. C., Cavalli, M., Cascarano, G. L., Giacovazzo, C., Guagliardi, A., *Journal of Applied Crystallography*, *32* (**1999**), 115-9.

7. Sheldrick, G. M., SHELXL-97, University of Göttingen, Germany, **1997**.

8. Fornasini, P., X-rays and Neutron Sources, in *Crystallography for Health and Biosciences*, Guagliardi A., Masciocchi, N. (ed.), Insubria University Press, Varese, **2012**.

9. Nunes, C., Mahendrasingam, A., Suryanarayanan, R., *Pharmaceutical Research, 22* (**2005**), 1942-1953.

10. Yamada, H., Masuda, K., Ishige, T., Fujii, K., Uekusa, H., Miura, K., Yonemochi, E., Terada, K., *Journal of Pharmaceutical and Biomedical Analysis, 56* (**2011**), 448-453.

11. Masciocchi N., Vladiskovic, C., Structural Analysis by Powder Diffraction Methods, in *Crystallography for Health and Biosciences*, Guagliardi A., Masciocchi, N. (ed.), Insubria University Press, Varese, **2012**.

12. Hofmann, D. W. M., *Acta Crystallographica, B57* (**2002**), 489-493.

13. De Wolff, P.M., *Journal of Applied Crystallography, 1* (**1968**), 108-113.

14. Smith, G.S., Snyder, R.L., *Journal of Applied Crystallography, 12* (**1979**), 60-65.

15. Hahn, T., *International Tables for Crystallography* (**2006**), Vol. A, Ch. 7.1, 112-717.

16. Le Bail, A., Duroy, H., Fourquet, J.L., *Mater. Res. Bull. 23* (**1988**), 447-452.

17. Cheary, R. W., Coelho, A., *Journal of Applied Crystallography, 25* (**1992**), 109-121.

18. Coelho, A.A., TOPAS-R, v3.0 (**2005**), Bruker AXS, Karlsruhe, Germany.

19. Rizzi, R., Analisi Strutturale II: Tecniche di Global Optimization, in *Analisi di Materiali Policristallini mediante Tecniche di Diffrazione*, Guagliardi, A., Masciocchi, N., (ed.), Insubria University Press, Varese, **2007**.

20. Giannini, C., Guagliardi, A., Millini, R., *Journal of Applied Crystallography, 35* (**2002**), 481-490.

21. Wilson, A.J.C., *Acta Crystallographica, 2* (**1949**), 318-321.

22. Altomare, A., Burla, M. C., Giacovazzo, C., Guagliardi, A., Moliterni, A. G. G., Polidori, G., Rizzi, R., *Journal of Applied Crystallography, 34* (**2001**), 392-397.

23. Giannini, C., Guagliardi, A., Tedesco, E., *Newsletter of Commision on Powder Diffraction, IUCr, 29* (**2003**), 42-43.

24. Craig, D. Q. M., Characterization of Polymorphic Systems Using Thermal Analysis, in *Polymorphism in the Pharmaceutical Industry*, Hilfiker, R. (ed.), Wiley-VCH, Weinheim, **2006**.

25. Battacharya, S., Brittain, H. G., Suryanarayanan, R., Thermoanalytical and Crystallographic Methods, in *Polymorphism in Pharmaceutical Solids*, Brittain, H. G. (ed.), Informa Healthcare, New York, **2009**.

26. Giron, D., *Thermochimica Acta, 248* (**1995**), 1-59.

27. Vladiskovic, C., Masciocchi, N., *Crystal Growth & Design, 14* (**2014**), 3603-3611.

28. Maccaroni, E., Alberti, E., Malpezzi, L., Masciocchi, N., Vladiskovic, C*., International Journal of Pharmaceutics, 351* (**2008**), 144-151.

29. Hilfiker, R., De Paul, S. M., Szelagiewicz, M., Approaches to Polymorphism Screening, in *Polymorphism in the Pharmaceutical Industry*, Hilfiker, R. (ed.), Wiley-VCH, Weinheim, **2006**.

30. Barrett, P., Smith, B., Worlitschek, J., Bracken, V., O'Sullivan, B., O'Grady, D., *Organic Process Research & Development*, *9* (**2005**), 348-355.

31. Mangin, D., Puel, F., Veesler, S., *Organic Process, Research & Development, 13* (**2009**), 1241-1253.

3. Packing Polymorphism of Bupropion Hydrohalides

Bupropion, or (±)-2-(*tert*-butylamino)-1-(3-chlorophenyl)propan-1-one, depicted in Scheme 3.1, is an atypical antidepressant belonging to the class of aminoketones. It is chemically unrelated to tricyclic antidepressants and, while its neurochemical mechanism of action is not well known, it is thought to act as a serotonin, norepinephrine and dopamine reuptake inhibitor. [1] Bupropion is used mostly as a smoking cessation aid and for Seasonal Affective Disorder (SAD). [2]

Scheme 3.1. Bupropion free base
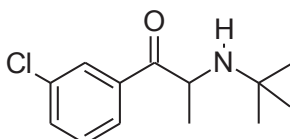
Even though Bupropion has a stereocenter and has been successfully separated into the *R* and *S* enantiomers, it is generally used as a racemate because the enantiomers undergo rapid racemization. [3] Bupropion, now marketed under several names, was first prepared and studied in the early 1970's. [4] As Bupropion has an amine group and can form acid addition salts, it is marketed in salt form. In particular, it was initially prepared as hydrochloride salt, and was later introduced as hydrobromide salt, reported to have better characteristics, being more stable and less hygroscopic. [5]

Both Bupropion hydrochloride and hydrobromide have high solubility in water, belonging to Class I of the Biopharmaceutics Classification System [6, 7] (high solubility and high permeability). This implies that bioavailability is not limited by solubility, and that polymorphism can therefore have little impact on the safety and efficacy of the final product. However, solid-state issues can still be crucial for manufacturing and handling, particularly at the production and formulation stages (as is shown in this case by the introduction of the better performing hydrobromide salt over the hydrochloride salt).

Both Bupropion hydrochloride and hydrobromide salts have been shown to exist in different polymorphic solid forms. In particular, two different anhydrous and unsolvated forms are known for each of the hydrochloride [8, 9] and hydrobromide [10] salts. Both salts have also been shown to form solvates. [15, 11]

Several crystal structures have been solved, both for the hydrochloride and the hydrobromide salts. In particular, the structures of the two anhydrous polymorphs of bupropion hydrochloride have been solved from powder data before the beginning of this work, while the two anhydrous polymorphs of bupropion hydrobromide have been solved from single crystal [12] after we had solved (but not published) the structures form powder data. The published structures confirm the data, here presented, obtained by us. In scientific and patent literature, the solved structures for an ethanol solvate of bupropion hydrochloride and a propanol solvate of bupropion hydrobromide have also been reported. [15, 11]

The structures of both the anhydrous and the solvated phases show many interesting similarities, which will be discussed in detail in the following sections. The richness of the solid-state landscape of bupropion makes it a good research field for structural analysis, because it allows to explore similarities and differences between crystal phases, highlighting the key factors in crystal form diversity. In other words, by performing detailed structural analysis on a large number of crystalline structures with similar components, it may be possible to draw some conclusion and make some predictions regarding crystal forms and their properties.

Isostructural salts, salts of different acids which show identical crystal packing, are particularly interesting because variations in solid state properties can be attributed mainly to the distinct properties of the different acids involved. This can be explained by the fact that crystal lattice contributions will be similar, therefore the main differences will be due to the acids involved. [13]

In order to add to the solid-state landscape of bupropion and to explore further the possibility of isostructural salts, the pharmaceutically uninteresting but structurally relevant hydroiodide salt was prepared and studied, yielding four different anhydrous non-solvated polymorphs. Moreover, studying the desolvation of the known ethanol solvate of the hydrochloride salt, two additional non-solvated forms were observed. This yielded a total of ten anhydrous phases of bupropion salt with three different hydrohalide acids.

As the known solvates of bupropion salts also showed interesting structural similarities, the solvation behavior of bupropion was also explored by preparing four new different solvates of bupropion hydrobromide and solving their structures from powder diffraction data. The crystal structure reported in the literature for the 1-propanol solvate of bupropion hydrobromide [11] presented some inconsistent features compared with the known structures of bupropion, so we decided to solve the structure again from single crystal. The data here presented for the propanol solvate of bupropion hydrobromide are therefore original.

The solid forms of bupropion hydrohalide salts here characterized and explored are therefore ten anhydrous and un-solvated phases (four hydrochloride, two hydrobromide and four hydroiodide polymorphs) and six solvated phases (an ethanol solvate of the hydrochloride salt and five different solvates of the hydrobromide salt).

3.1   Anhydrous Bupropion Hydrohalides

The structures of two new bupropion hydrochloride polymorphs and the four new bupropion hydroiodide polymorphs, as well as the structures of the two known hydrobromide polymorphs, were solved by state-of-the-art powder diffraction methods and compared with the known structures of the hydrochloride salt. A total of ten crystalline structure were therefore compared

for structural similarities. For clarity, Table 3.1 summarizes the nomenclature of all known salts and their polymorphs, together with literature references and brief comments regarding the identity of the forms. In particular, we believe the forms reported in the literature as forms II and IV to be the same form. This is further discussed in paragraph 3.1.1.

3.1.1 Identity of Bupropion hydrobromide forms reported in the literature

Hu and co-workers report in [12] the structure of an anhydrous form of Bupropion HBr they call form IV. Form IV is considered different from Bupropion HBr form II described in US 7,241,805 on the basis that the declared positions of the diffraction peaks are different. However, US patent US 7,241,805 does not report diffraction peak positions. Peak positions for form II are reported in patent application WO 2010/015692 and are reproduced in Table 3.2 alongside the peak positions declared by Hu and co-workers for form IV. The middle column of Table 3.2 holds the difference between the corresponding peak positions reported for the two forms. The peak positions for Bupropion hydrobromide forms II and IV show that the two forms correspond in reality to the same crystal phase. The presence of a small systematic error in peak positions can be due to sample displacement or to other instrumental artifacts.

In order to confirm the identity of Bupropion hydrobromide forms II and IV, the XRPD trace reported in the patent literature for form II was compared with the calculated powder pattern obtained from the structure of form IV (the structure designation in the Cambridge Structural Database is ICEPOX01).

As the XRPD trace for form II (shown in Figure 3.1a) showed heavy preferred orientation and significant peak broadening, suitable corrections were performed to make the XRPD traces comparable. In particular, the program TOPAS-R was used to calculate a powder pattern from ICEPOX01. The preferred orientation along *hkl* direction (001) was taken into account by using the March-Dollase formula (*r*=0.48). Beam overflow was added to the calculations to account for the low intensity of the peaks at lower angles. A small crystal size was employed to account for peak broadening. The calculated XRPD trace obtained is reported in Figure 3.1b. Figure 3.1c reports the calculated XRPD trace obtained

from ICEPOX01 without beam overflow, crystal size and preferred orientation corrections for comparison.

The comparison of the XRPD traces confirms that Bupropion HBr forms II and IV correspond to the same crystalline phase.

Table 3.1. References and nomenclature of Bupropion salts and polymorphs.

Solid Form	Literature Reference	Comments	Nomenclature used in this work
Bupropion · HCl Form I	[8]		BCl_I
Bupropion · HCl Form II	[9]		BCl_{II}
Bupropion · HCl Form III	[14]		BCl_{III}
Bupropion · HCl Form IV	[14]		BCl_{IV}
Bupropion · HBr Form I	[12]	This form was initially characterized in [10] only by XRPD and DSC; subsequently the its crystal structure was published in [12]	BBr_I
Bupropion · HBr Form II	[10]	This form was characterized in the patent literature by XRPD and DSC and corresponds to Bupropion·HBr Form IV published in [12]. See paragraph 3.3.1 for details.	BBr_{II}
Bupropion · HBr Form IV	[12]	The structure here reported corresponds to Bupropion·HBr Form II published in [10]. See paragraph 3.1.1 for details.	BBr_{II}
Bupropion · HI Form I	[14]		BI_I
Bupropion · HI Form II	[14]		BI_{II}
Bupropion · HI Form III	[14]		BI_{III}
Bupropion · HI Form IV	[14]		BI_{IV}

Table 3.2. Comparison of XRPD peak positions for Bupropion hydrobromide forms II and IV.

Peaks attributed to Bupropion HBr Form II in WO 2010/015692 [° in 2θ]	Difference between first and third column (average 0.12(3)°)	Peaks attributed to Bupropion HBr form IV in *Chinese J. Struct. Chem.* **2011**, *30*(11), 1591-1596 [° in 2θ]
6.53	0.15	6.38
12.18	0.10	12.08
-	-	12.78
13.03	0.13	12.90
14.18	0.14	14.04
15.92	0.16	15.76
16.52	0.12	16.40
18.01	0.11	17.90
18.83	0.08	18.75
19.28	0.07	19.21
-	-	20.34
20.67	0.10	20.57
21.64	0.09	21.55
21.95	0.13	21.82
23.11	0.13	22.98
24.18	0.09	24.09
25.75	-	-
25.83	0.12	25.71
26.83	0.11	26.72
27.14	0.19	26.95
27.87	0.13	27.74
28.81	0.13	28.68
29.67	-	-
30.07	0.14	29.93
31.82	0.14	31.68
32.42	0.12	32.30

Figure 3.1. Comparison of the XRPD trace of form II and the calculated powder pattern of form IV.

a) Extract from WO2010/015692, Powder Pattern for Bupropion HBr form II
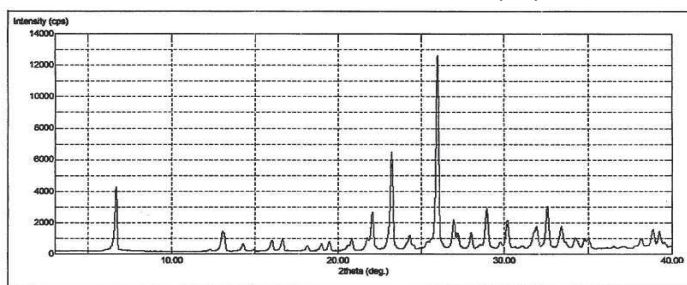
b) Calculated Powder Pattern for ICEPX01 corrected for Preferred Orientation and Beam Overflow
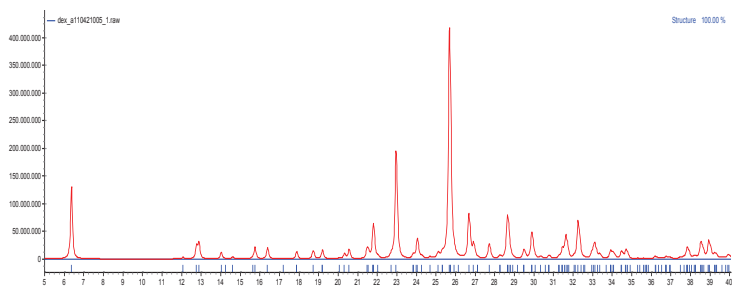
c) Calculated Powder Pattern for ICEPOX01, no corrections
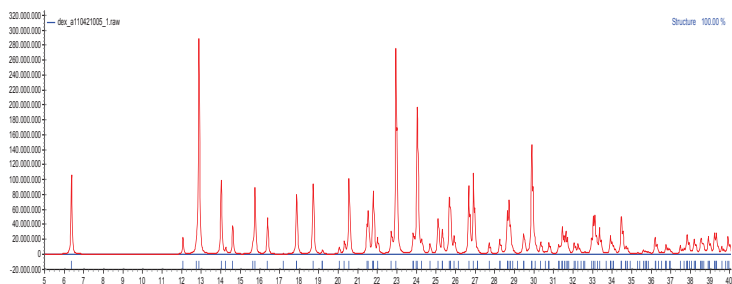
3.1.2 Crystal Form Preparation

The two new bupropion hydrochloride crystal forms were found by performing controlled desolvation of the ethanol solvate of bupropion hydrochloride (see section 3.2) using reduced pressure, variable temperatures and preparative DSC. The two forms, denominated forms III and IV (**BCl$_{III}$** and **BCl$_{IV}$** in this work) were never obtained as monophasic samples, but only in mixtures. Powder diffraction allows to solve structures from non-monophasic samples, as long as the structure and composition of the contaminant phase is known. It was therefore possible to solve the structures of all phases.

The previously reported ethanol solvate of Bupropion hydrochloride [15] was obtained by dissolving 2 g of bupropion hydrochloride in 8 mL of ethanol at reflux and rapidly cooling the resulting solution in an ice bath to obtain crystallization. Different desolvation protocols were specifically tailored to obtain a mixture rich in **BCl$_{III}$** or in **BCl$_{IV}$**.

A mixture rich in form **BCl$_{III}$** was obtained by slow desolvation of the ethanol solvate at room temperature under reduced pressure. The XRPD of the mixture was recorded after several weeks and found to be a mixture of **BCl$_{III}$** and **BCl$_{I}$** (about 15%). As the structure for form **BCl$_{I}$** was known, it was possible to solve the structure of form **BCl$_{III}$** from the mixture of the two forms obtained.

A mixture rich in form **BCl$_{IV}$** was obtained during a specifically designed preparative DSC experiment: after heating the ethanol solvate in a pierced aluminum sample holder to 110°C at 10°C/min under a flow of nitrogen, the DSC pan was opened and a mixture of **BCl$_{IV}$** (85%) and **BCl$_{III}$** (15%) was retrieved. The data for form **BCl$_{III}$** was then used to solve the structure for form **BCl$_{IV}$** from the mixture rich in **BCl$_{IV}$** .

The chemical identity of the sample after thermal treatment was confirmed by ^{1}H-NMR analysis. Slightly different desolvation experiments yielded mixtures of different compositions, but never pure phases.

Bupropion hydrobromide was obtained by dissolving 3 g of Bupropion hydrochloride in 7 mL of water and slowly adding aqueous KBr at room temperature under magnetic stirring until the formation of a precipitate was observed. The mixture was then heated to obtain complete dissolution and slowly

cooled to crystallize **BBr$_{II}$**. The identity of the halide ion was confirmed by precipitation of the silver halide from a clear aqueous solution of the obtained solid using a 0.1 M solution of AgNO$_3$. The yellow precipitate confirmed the identity of the bromide ion.

A monophasic sample of **BBr$_I$** was prepared by dissolving 20.0 g of **BBr$_{II}$** in refluxing isopropanol (100 mL) and water (8 mL) and rapidly cooling the mixture with an ice bath. The crystallized solid (pure **BBr$_I$**) was isolated by filtration at 0°C.

The structures of **BBr$_I$** and **BBr$_{II}$** were solved by powder diffraction methods, but during the course of this work the two single crystal structures discussed in previous paragraphs were published. The single crystal structures matched the structures solved by us by powder diffraction. In this work, the crystal and structural data obtained by powder diffraction are presented and used in the structural comparisons.

Bupropion hydroiodide was obtained by dissolving 3 g of Bupropion hydrochloride in 7 mL of water at room temperature and adding aqueous KI drop by drop under stirring until the precipitation of a white solid was observed. The solid obtained, recovered by filtration at room temperature, was a mixture of **BI$_I$** and **BI$_{II}$**. The identity of the halide ion was confirmed by precipitation of the silver halide with 0.1 M AgNO$_3$ from a clear aqueous solution. The yellow coloring of the precipitate confirms the halide to be iodide and not chloride.

Monophasic **BI$_I$** was obtained by recrystallizing 0.5 g of Bupropion hydroiodide in 5 mL of isopropanol and recovering the solid by filtration, while monophasic **BI$_{II}$** was obtained by recrystallizing 0.5 g of Bupropion hydroiodide in 2 mL of water and filtering the crystallized solid at 0°C. **BI$_{III}$** was obtained during a specifically designed preparative DSC experiment by heating **BI$_{II}$** in a pierced aluminum pan under nitrogen flow to 198°C at 10°C/min, holding at 198°C for six seconds and quench cooling to room temperature. The DSC pan was opened and monophasic **BI$_{III}$** was retreived. The chemical identity of the sample after heating was confirmed by ^{1}H-NMR.

Form **BI$_{IV}$** was obtained by dissolving of 4.1 g of Bupropion hydroiodide in 5 mL of refluxing trifluoroethanol. The clear solution obtained was then slowly concentrated at room temperature by evaporating the solvent under a flow of nitrogen. A white solid crystallized and was recovered by filtration. The sample of

form **BI$_{IV}$** used for structure solution contained traces of KI, clearly visible in the powder diffraction trace as weak, sharp peaks.

3.1.3 Crystal Data

As the main aim of this work was structural comparison between the different phases, the first step was to compare the cell data from all forms analyzed. This is reported in Table 3.3. Figure 3.2 shows the final Rietveld refinement plots for the crystal forms solved from powder samples during this work, and Appendix A reports the atomic coordinates of the phases.

Table 3.3. Comparative crystal cell data of different solid forms of Bupropion hydrohalides (E.s.d.'s in parentheses).

	BCl$_I$	BCl$_{II}$	BCl$_{III}$[δ]	BCl$_{IV}$	BBr$_I$[£]	BBr$_{II}$*	BI$_I$	BI$_{II}$	BI$_{III}$	BI$_{IV}$
Ref	[8]	[9]	[14]	[14]	Unpublished Results	Unpublished Results	[14]	[14]	[14]	[14]
Formula	C$_{13}$H$_{19}$Cl$_2$NO	C$_{13}$H$_{19}$Cl$_2$NO	C$_{13}$H$_{19}$Cl$_2$NO	C$_{13}$H$_{19}$Cl$_2$NO	C$_{13}$H$_{19}$ClNOBr	C$_{13}$H$_{19}$ClNOBr	C$_{13}$H$_{19}$ClNOI	C$_{13}$H$_{19}$ClNOI	C$_{13}$H$_{19}$ClNOI	C$_{13}$H$_{19}$ClNOI
FW [g mol^{-1}]	276.22	276.22	276.22	276.22	320.65	320.65	367.66	367.66	367.66	367.66
SG	P2$_1$/c	Pbca	P-1	P-1	P-1	Pbca	C2/c	C2/c	P-1	P2$_1$/n
a [Å]	14.326(2)	27.2853(5)	7.7477(2)	7.5154(3)	7.6939(2)	27.7040(8)	8.5910(2)	14.6084(3)	7.9819(4)	8.2635(5)
b [Å]	8.753(2)	8.7184(3)	8.1124(1)	7.8712(3)	7.9366(2)	8.6328(6)	14.6100(3)	8.0869(2)	8.2163(5)	9.7799(3)
c [Å]	11.885(3)	12.0422(3)	13.1768(3)	13.7033(6)	13.8498(3)	12.4092(9)	25.6710(6)	27.0461(4)	13.7557(8)	20.2113(6)
α [°]	90	90	117.02(2)	88.12(3)	85.938(2)	90	90	90	84.51(4)	90
β [°]	78.07(2)	90	81.34(2)	86.41(2)	85.593(2)	90	92.626(2)	92.760(1)	84.75(4)	99.98(3)
γ [°]	90	90	89.00(2)	67.78(2)	65.961(2)	90	90	90	63.07(4)	90
V [Å^3], Z	1458.2, 4	2864.7, 8	725.9, 2	748.9, 2	769.3, 2	2967.8, 8	3218.7, 8	3192.0, 8	799.4, 2	1608.6, 4
V/Z	365	358	363	374	385	371	402	399	400	402
T [K]	298	298	298	298	298	298	298	298	298	298
λ [Å]	1.5418	1.5418	1.5418	1.5418	1.5418	1.5418	1.5418	1.5418	1.5418	1.5418
ρ$_{calc}$ [g cm^{-3}]	1.281	1.281	1.264	1.225	1.384	1.435	1.517	1.530	1.527	1.518
μ(CuKα) [mm^{-1}]	3.89	3.96	3.91	3.79	5.14	5.33	17.11	17.26	17.24	17.12
R$_{Bragg}$	0.077	0.056	0.047	0.027	0.071	0.112	0.038	0.047	0.034	0.057

[δ]The cell reported is not the reduced cell. This is to make it structurally comparable with other forms, as is shown in Figure 4.

[£]The values for a and b shown here are the supplementary of the values used in structure solution for direct comparison with other P-1 forms.

*The values of the crystal axes were inverted compared to the values used in structure solution for direct comparison with form BCl$_{II}$.

Figure 3.2. Final Rietveld refinement plots for a) **BCl**$_{III}$, b) **BCl**$_{IV}$, c) **BBr**$_{I}$, d) **BBr**$_{II}$, e) **BI**$_{I}$, f) **BI**$_{II}$, g) **BI**$_{III}$ and h) **BI**$_{IV}$ with difference plot and peak markers at the bottom. The insert shows the high angle region, magnified 5×.
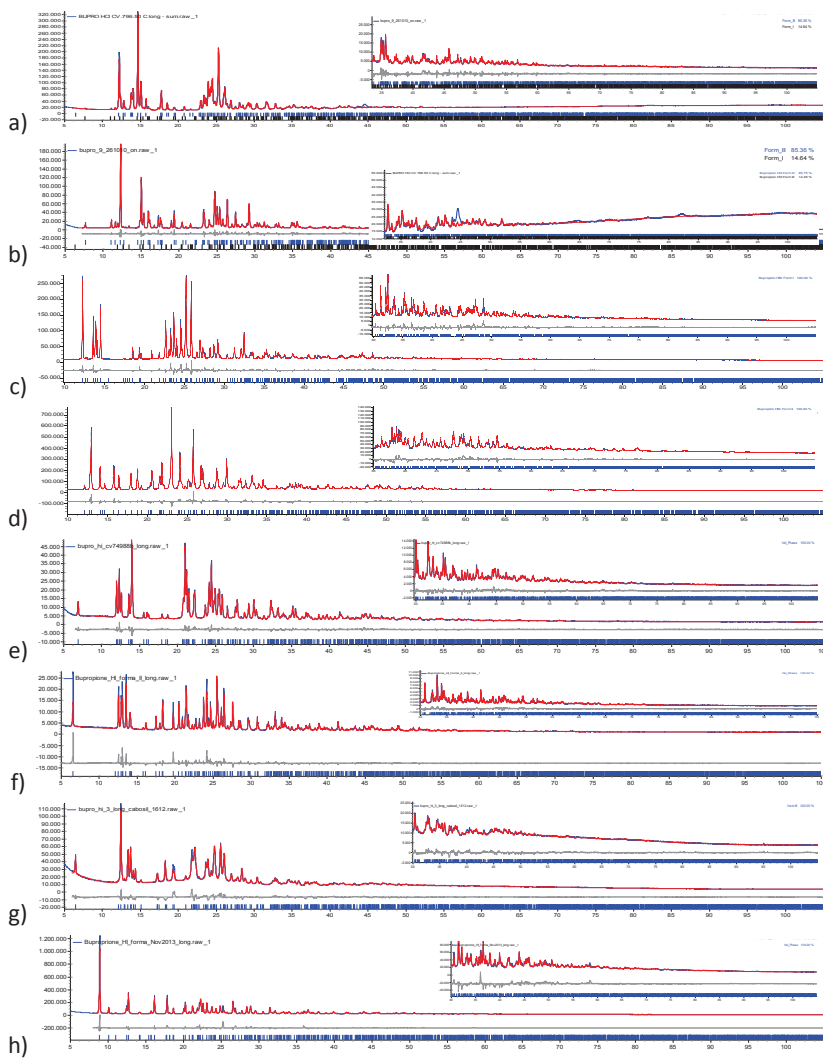
Careful comparison of the cell data for all forms analyzed reveals several interesting similarities. Firstly, the cells for the previously known forms **BCl$_{II}$** and **BBr$_{II}$** are very similar to one another, having not only the same space group but also similar lattice constants. The small difference in volume can be explained by the larger size of the bromide ion compared with the chloride ion.

Secondly, the cells for **BCl$_{III}$**, **BCl$_{IV}$**, **BBr$_I$** and **BI$_{III}$** have similar lattice constants, which may suggest the occurrence of an isostructural group. However, the marked difference in the interaxial angles between **BCl$_{III}$** and the other three solid forms, not recoverable by any cell transformation, suggests the occurrence of two different (triclinic) supramolecular arrangements.

Finally, the cells of **BI$_I$** and **BI$_{II}$** appear to have some correlation, as the space group is the same and the cell axes have similar values, although scrambled. This suggests structural similarities to be explored and analyzed.

The reported observations regarding space groups and cell constants constituted a starting point for our crystal packing analysis, further discussed in paragraph 3.1.3. Also, other interesting observations may be made regarding crystal density. The V/Z values for the different phases were charted and compared, showing, predictably, a trend in the molar volumes of the phases according to the identity of the hydrohalide ion involved. This is reported in Figure 3.3. Worthy of note, the point which lies outside the expected trend refers to the V/Z value of **BBr$_{II}$**. This value has been confirmed by single crystal data, as discussed in previous paragraphs. [12]

Figure 3.3. V/Z Values of anhydrous and unsolvated Bupropion hydrohalides
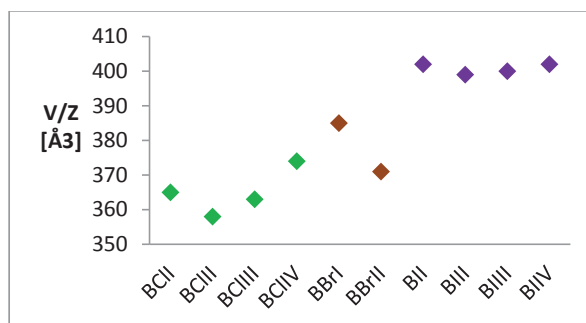
3.1.4 Bupropion molecular conformation

Molecular conformation is an important aspect when studying crystalline phases, as it can offer insight on how stable a phase is and how likely it is to form. Conformational analysis and comparison are addressed by observing the freely rotating dihedral angles (also used for structure solution, see Chapter 2), like for example those describing side chains. The relevant dihedral angles used in describing molecular conformation (and during structure solution from powder diffraction data) of the bupropion molecule are shown in Scheme 3.2.

Scheme 3.2. Bupropion ammonium ion and the torsion angles used to describe molecular conformation
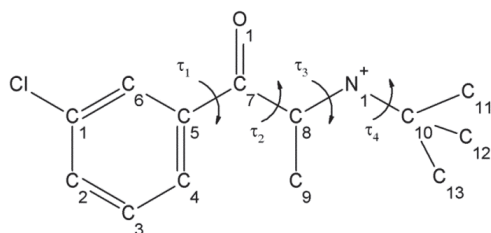
The side chains of bupropion molecules in all phases analyzed adopt a similar conformation, the observed values being summarized in Table 3.4a. As expected, the most variable conformational descriptor in the different forms is τ_4, addressing the *syn* (C_6-C_5-C_7-C_8 torsion near 180°) or *anti* (near 0°) disposition of the Cl-Ar and CO residues. The rest of the molecule, in particular the side chain, adopts the same conformation (or very nearly so) in all the phases analyzed.

Table 3.4. Synoptic collection of the most relevant conformational features of the bupropion molecule a) in the different solid forms of Bupropion hydrohalides and b) in the conformations calculated with molecular modelling tools

a)

	Ref.	τ_1 [°] C_8-N_1-C_{10}-C_{Me}	τ_2 [°] C_7-C_8-N_1-C_{10}	τ_3 [°] C_5-C_7-C_8-N_1	τ_4 [°] C_6-C_5-C_7-C_8	Class
BCl$_I$	[8]	179.0(3)	-79.9(3)	148.2(1)	-154.8(2)	*syn*
BCl$_{II}$	[9]	169.9(4)	-84.9(4)	152.3(2)	-15.0(3)	*anti*
BCl$_{III}$	[14]	175.7(5)	-80.9(4)	147.6(2)	178.0(3)	*syn*
BCl$_{IV}$	[14]	179.6(5)	-82.1(4)	148.4(2)	3.5(2)	*syn*
BBr$_I$	Unpublished Results	-176.6(6)	-83.2(6)	151.1(3)	-177.7(3)	*syn*
BBr$_{II}$	Unpublished Results	171(1)	-83(1)	155.2(5)	-24.0(7)	*anti*
BI$_I$	[14]	166.3(8)	-82.6(6)	154.7(3)	174.6(4)	*syn*
BI$_{II}$	[14]	176.7(8)	-77.6(7)	145.2(3)	-169.5(4)	*syn*
BI$_{III}$	[14]	176(1)	-74(1)	148.5(5)	173.4(5)	*syn*
BI$_{IV}$	[14]	169(1)	-78(1)	169.3(5)	-18.9(3)	*anti*

b)

	Relative Energy [kcal mol^{-1}]	τ_1 [°] C_8-N_1-C_{10}-C_{Me}	τ_2 [°] C_7-C_8-N_1-C_{10}	τ_3 [°] C_5-C_7-C_8-N_1	τ_4 [°] C_6-C_5-C_7-C_8	Class
Most Stable	0	163.2	-175.6	152.9	1.2	*anti*
Most Stable *syn*	+ 0.23	163.3	-175.8	152.7	-178.8	*syn*
Restrain on τ_2	+ 3.83	172.3	**-80**	146.9	177.8	*syn*

The fact that all crystalline forms so far isolated contain the Bupropion molecule in very similar conformation suggests that it is energetically very favored. In order to verify and analyse this, molecular mechanics optimizations were performed for Bupropion molecules in the gas phase [16]. A conformational scan was run, yielding several local minima. The potential energy values derived using the MM3 force field for the two best (but significantly different) conformations (*syn* and *anti,* addressed by τ_4) are nearly identical (see Table 3.4b), the calculated energy difference between the two conformations being only 0.23 kcal mol^{-1} (τ_1, τ_2 and τ_3 differing by 0.2° or less). Worthy of note, angles τ_1 and τ_3 have values similar to those observed in the solid state. This suggests that this conformation is indeed energetically favored. However, τ_2 (in the gas phase approaching the -175° value) is significantly different from that observed in the solid state (with absolute values falling in the narrow 74-85° range). The significance of the values of the dihedral angles is that in the gas phase calculations, the main side chain of bupropion is positioned in an "all *trans*" conformation, while in the solid state, the main chain is positioned in a *gauche* conformation at dihedral τ_2. A closer inspection of the dihedral angles of bupropion and their significance on overall conformation shows that τ_2 is responsible for the orientation of the hydrogen atoms bonded to the nitrogen atom, therefore affecting the ability of the molecule to form hydrogen bonds. This is particularly significant because of the hydrogen bond scheme found in all bupropion crystalline phases described in the next paragraph. A *gauche* conformation at τ_2 causes the hydrogen atoms on the nitrogen to be more available for hydrogen bonding. Molecular modelling calculations in the gas phase and comparison with the conformation in the crystal structure of a solvated form of bupropion have also been carried out by Froimovitz and others, [15] substantially confirming our findings.

All ten phases of anhydrous bupropion hydrohalides show the same hydrogen bond motif, being made up of bupropion molecule dimers held together by hydrogen bonding between two bridging halide ions and two NH_2^+ moieties, as schematically shown in Figure 3.4, generating a centrosymmetic unit. According to the graph set notation discussed in Chapter 1, [17] this hydrogen bond motif is classified $R_4^2(8)$, as it is a ring structure made up of 8 atoms and held together by

four hydrogen bond donors (the hydrogen atoms covalently bonded to the nitrogen atoms) and two hydrogen bond acceptors (the halide ions).

Figure 3.4. Supramolecular arrangement of bupropion hydrohalide dimers

*(The form depicted is **HBr_{II}**, which possesses an anti conformation)*
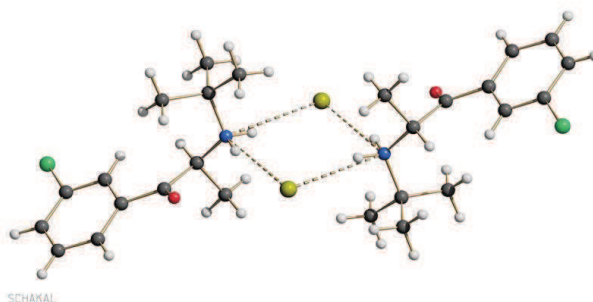
The formation of a dimer is an optimal supramolecular arrangement for Bupropion hydrohalide molecules, as it allows hydrophilic and charged groups to interact with one another within the dimer core (in particular the halide ions and the ammonium groups), leaving the more hydrophobic and less polarized groups on the outside (the methyl and *terz*-butyl group on the side chain). All dimers are generated by crystallographic inversion symmetry, as an inversion point is positioned at the center of the rhombus formed by the halide ions and ammonium groups). This suggest that the enantiopure salts, prepared by others [18] but not studied here, may show a different supramolecular arrangement.

On the basis of these results, it is possible that in relatively concentrated solutions, Buproprion hydrohalides may also exist as dimers, possibly detectable by DOSY NMR experiments. In the ^{1}H-NMR experiments in solution conducted on the different hydrohalide salts (the values of peak positions, attributions and J-couplings are reported in Table 3.5) using a concentration ranging from 0.03 to 0.08 M, however, the chemical shifts of the ammonium protons, independent of sample concentration, suggest that at the concentrations analyzed and using a hydrogen bond acceptor as a solvent (*d6*-DMSO), an ionic pair is maintained, but the interaction between the halide ion and the ammonium group of the

Bupropion molecule happens with one ammonium proton only. This is suggested by the fact that the two ammonium protons (the attribution was confirmed by exchanging with D_2O) have different resonance frequencies, as shown in Table 3.5. Moreover, one of the two protons (arbitrarily called H_{N2} in Table 3.5) has different frequencies in the three salts. This is justified only if the proton interacts with the halide ion, as the bupropion ammonium ion is identical in the three cases. Also, while the signal of H_{N1} (being a multiplet) shows both the geminal coupling with H_{N2} and the vicinal coupling with the hydrogen on the carbon atom the nitrogen is bonded to, the signal for H_{N2} (a doublet) only shows the geminal coupling. Assuming that there is free rotation in solution around the N-C bond and therefore the vanishing of this coupling cannot be attributed to a specific blocked conformation, we tentatively attribute this phenomenon to the formation of hydrogen bonding with the halide ion with significant elongation and polarization of this N-H bond.

In order to understand and explain fully the conformation of the bupropion molecules in the hydrogen-bonded dimers, more molecular modelling calculations in the gas phase were carried out. In search for a local minimum of the potential energy hypersurface which could geometrically approach the conformations observed in the different polymorphs, the value of τ_2 was arbitrarily restrained to -80° (chosen because it is close to the value τ_2 adopts in the solid state to allow the hydrogen bonding scheme present in the dimer). The most stable conformer obtained in this way (third row in Table 3.4b) closely matches the geometry of the *syn* Bupropion molecules found in the solids, with an energy difference of only +3.83 kcal mol^{-1} above the absolute minimum. Obviously, this small energy difference can be easily compensated by the solid state stabilizing effects (mainly hydrogen bond interactions).

Table 3.5. ^{1}H-NMR frequencies (given in ppm using TMS as external standard) for Bupropion hydrochloride, hydrobromide and hydroiodide salts (in solution in d6-DMSO).
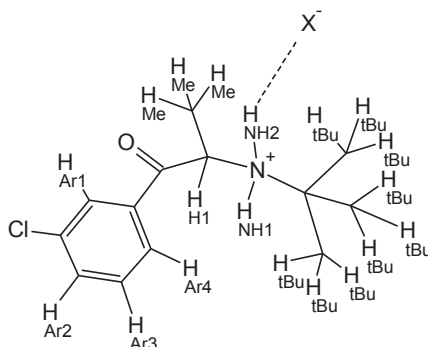
Hydrogen	Bupropion HCl	Bupropion HBr	Bupropion HI
H_{tBu}	1.30 (s)	1.29 (s)	1.28 (s)
H_{Me}	1.52 (d, J=7.0 Hz)	1.49 (d, J=7.0 Hz)	1.47 (d, J=7.2 Hz)
H_1	5.28 (m)	5.30 (m)	5.28 (m)
H_{Ar3}	7.64 (m)	7.65 (m)	7.66 (m)
H_{Ar4}	7.82 (d, J=8.1 Hz)	7.84 (d, J=7.9 Hz)	7.84 (d, J=8.1 Hz)
H_{Ar2}	8.15 (d, J=8.1 Hz)	8.15 (d, J=7.9 Hz)	8.14 (d, J=8.1 Hz)
H_{Ar1}	8.24 (s)	8.25 (s)	8.25 (s)
H_{N1}	8.59 (broad m)	8.58 (broad m)	8.56 (m)
H_{N2}	9.52 (d, J=12.3 Hz)	9.16 (d, J=11.7 Hz)	8.93 (d, J=12.3 Hz)

3.1.5 Crystal Packing Analysis

As all bupropion hydrohalide phases analyzed and discussed so far show the same dimer structure held together by hydrogen bonding, the differences between crystal structures must originate from different packing of the dimer structures. The packing motifs of the different phases must therefore be the key to crystal structure diversity.

As discussed in paragraph 3.1.1, the cell data for forms **BCl$_{II}$** and **BBr$_{II}$** appear to be very similar. A closer look at crystal packing reveals the two phases to be

indeed isostructural, differing only in the identity of the halide ion. This is shown in figure 3.5.

Figure 3.5. Comparision of the structures of a) **BCl$_{II}$** and b) **BBr$_{II}$**.

a)

b)
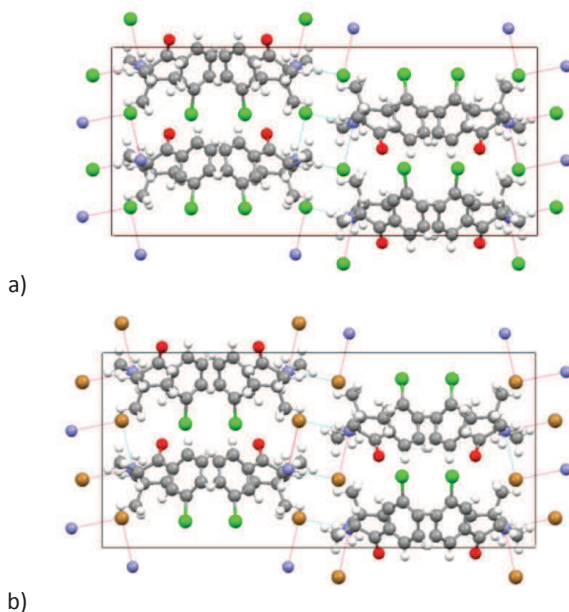
The similarity of the cell axis lengths and the identity of the space group in **BCl$_{III}$**, **BCl$_{IV}$**, **BBr$_I$** and **BI$_{III}$** may suggest the occurrence of an isostructural group. However, there is a marked difference in the interaxial angles between **BCl$_{III}$** and the other three solid forms, not recoverable by any cell transformation. This suggests the occurrence of two different (triclinic) supramolecular arrangements. A closer look at the packing of the molecule dimers confirms this observation. In fact, while in forms **BCl$_{IV}$**, **BBr$_I$** and **BI$_{III}$** the dimers are stacked in straight rows, in **BCl$_{III}$** the stacks are canted in slanted rows. This is particularly evident when viewing the structures along the **a** axis, as shown in Figure 3.6. Forms **BCl$_{IV}$**, **BBr$_I$** and **BI$_{III}$** are therefore isostructural, differing only in the identity of the halide ion, while form **BCl$_{III}$** is different. Incidentally, all four forms contain molecules in the *syn* conformation.

94

Figure 3.6. Comparison of the bupropion hydrohalide structures of space group P-1: a) **BCl$_{IV}$**, b) **BBr$_I$**, c) **BI$_{III}$** and d) **BCl$_{III}$**.

a)   b)

c)   d)
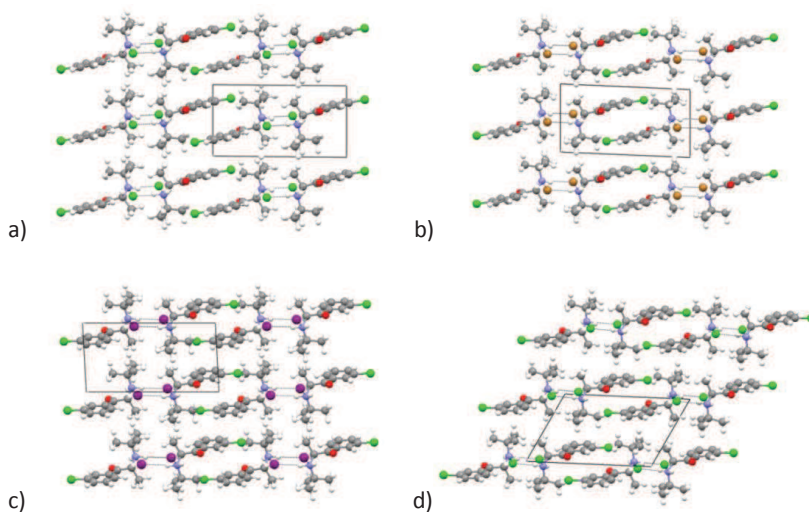
BI$_I$ and **BI$_{II}$** have unit cell dimensions and space group symmetry different from any other form, but they appear to be similar to one another, as they crystallize within the same space group and with similar cell constants, though scrambled. This alone implies a different internal symmetry. In fact, a more accurate analysis of the packing shows significant differences. In both cases, dimers are stacked along the short axis (which represents the "height" of two stacked bupropion dimers) and organized in long chain-like structures parallel to the long axis but, while in **BI$_{II}$** the dimers are stacked vertically when viewed along the medium axis, in **BI$_I$** the stacks are slanted. Moreover, when projecting the packing down the short axis to view the chain-like structures, the bupropion dimers are organized in a greek key motif in **BI$_I$** and in straight lines in **BI$_{II}$**. This is clearly shown in Figure 3.7.

Figure 3.7. View of a) **BI$_I$** and b) **BI$_{II}$** along the short axis (**a** for **BI$_I$**, **b** for **BI$_{II}$**).

a)

b)
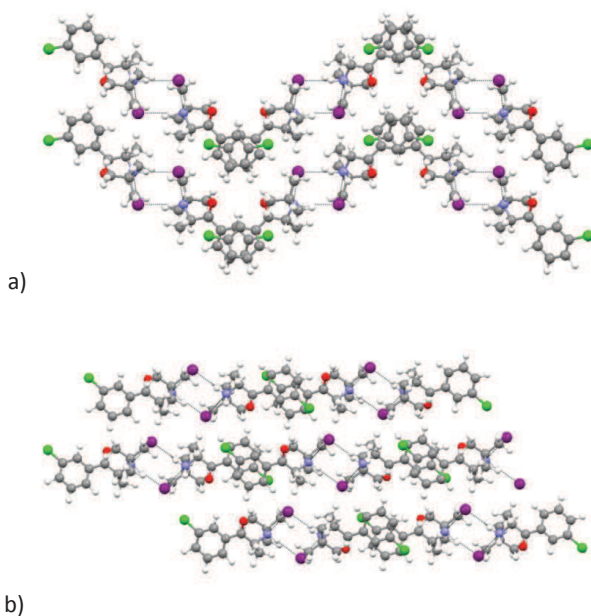
Finally, forms **BCl$_I$** and **BI$_{IV}$** appear to be structurally unrelated to all other bupropion hydrohalide forms previously observed. While they are still made up of bupropion hydrohalide molecules (respectively, of the *syn* and *anti* type) mutually embraced in the "usual" $R_4^2(8)$ hydrogen bond motif encountered previously, both packings are different from that of any other structure analyzed. In form **BCl$_I$** the dimers are packed in alternating slanted columns, while in form **BI$_{IV}$** the dimers are packed in a herringbone pattern, as shown in Figure 3.8.

Figure 3.8. Crystal packing of a) **BCl$_I$** viewed along the **c** axis and of b) **BI$_{IV}$** viewed along the **a** axis.

a) b)
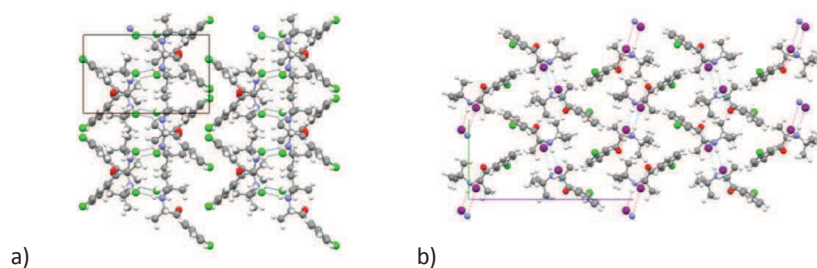
3.1.6 Energetic Considerations

As discussed in Chapter 1, the thermodynamic relations between polymorphs are often crucial for understanding relative stability and thermal behavior. However, straightforward and simple conclusions are not always easy to achieve, especially when more than two different polymorphs of the same substance are to be compared.

The previously known forms of the hydrochloride salt, **BCl$_I$** and **BCl$_{II}$**, have been reported to be enantiotropically related to one another, **BCl$_{II}$** being more stable at low temperatures. [9] Unfortunately, as described above, forms **BCl$_{III}$** and **BCl$_{IV}$** were obtained only in mixtures by partially controlled (to the best of our abilities) desolvation of the ethanol solvate. This made it impossible to determine the thermodynamic relationships of forms **BCl$_{III}$** and **BCl$_{IV}$** with the known hydrochloride forms.

The thermal behavior of the two known forms of the hydrobromide salt has been discussed in the literature. [19] The endothermic conversion from **BBr$_{II}$** to **BBr$_I$** at high temperature, together with fact that the molar volume for form **BBr$_{II}$** is much lower than the molar volume of form **BBr$_I$** (see Figure 3.3) demonstrates that forms **BBr$_I$** and **BBr$_{II}$** are also enantiotropically related, with form **BBr$_{II}$** more stable at low temperatures.

As for the hydroiodides, the thermodynamic relations between the different forms are not easy to unravel. Not only are the molar volumes very close for the different forms, but the DSC traces, shown in Figure 3.9, offer little information. Forms **BI_I** and **BI_{IV}** show no event before the melting point (195.6°C and 193.7°C, respectively). Form **BI_{II}** melts (m.p. 192.7°C) and then recrystallizes into form **BI_{III}** (m.p. 200.2°C) , but this observation alone does not allow to determine if the two forms are monotropically or enantiotropically related. [20]

Figure 3.9. DSC traces for a) **BI_I** b) **BI_{II}** and c) **BI_{IV}**.
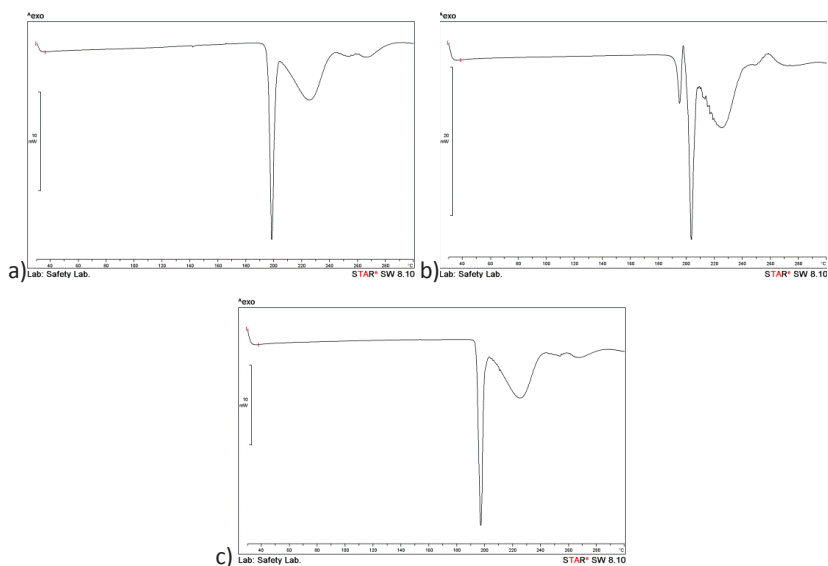
3.2 Isostructural Burpopion Hydrohalide Solvates

In addition to the two known solvates, an ethanol solvate of bupropion hydrochloride (**BCl_{EtOH}** in the text) and a 1-propanol solvate of bupropion hydrobromide (**BBr_{PrOH}**), the structures of which are reported in the literature, four new solvates of bupropion hydrobromide were prepared and three of the four structures solved from powder data. In particular, the forms observed are solvated with ethanol (**BBr_{EtOH}**), trifluoroethanol (**BBr_{TFE}**), ethylene glycol (**BBr_{Gly}**)

and tetrahydrofuran (**BBr$_{THF}$**). It was not possible to solve the structure for **BBr$_{THF}$** due to rapid loss of solvent and conversion into a different form. It was only possible to determine its crystallographic cell constants.

As is described in the following paragraphs, all solvated form are made up of centrosymmetric dimers like already observed for the un-solvated phases. However, the crystal structure of **BBr$_{PrOH}$** reported in the literature [11] is described as made up of non-centrosymmetric dimers constituted by two crystallographic independent but very similar bupropion molecules. Analyzing the structure with the publicly available software Platon, [21] it was found that the molecules had very little deviation from a centro-symmetric dimer (the largest deviation on a single atom was 0.3 Å). The attribution of space group P1 instead of P-1 is a relatively common mistake, as is reported in the literature, [22] and as the structure reported for **BBr$_{PrOH}$** did not seem to us consistent with the rest of the structures observed, it was decided to solve the structure again from single crystal data. The structure here reported for **BBr$_{PrOH}$** is therefore determined by us on original data.

3.2.1 Solvate Form Preparation

Form **BCl$_{EtOH}$** was obtained by dissolving 2 g of bupropion hydrochloride in 8 mL of ethanol at reflux and rapidly cooling the resulting solution in an ice bath to obtain crystallization. Single crystals of **BBr$_{PrOH}$** were obtained by dissolving a few milligrams of bupropion hydrobromide in a couple of milliliters of 1-propanol and leaving the solution to slowly evaporate at room temperature. Form **BBr$_{EtOH}$** was obtained by slow cooling of a solution containing 4.0 g of Bupropion hydrobromide in 20 ml of ethanol heated to reflux. Form **BBr$_{EtOH}$** thus obtained was not monophasic, but contained trace amounts of form **BBr$_I$** visible in the XRPD spectrum. This was taken into consideration during structure solution and refinement. Monophasic **BBr$_{Gly}$** was obtained by crystallizing 20 g of Bupropion hydrobromide in 27 ml of ethylene glycol. After filtration on a Buchner funnel, the solid was washed with small amounts of acetone to remove the excess ethylene glycol. Forms **BBr$_{TFE}$** and **BBr$_{THF}$** were obtained by slurrying **BBr$_{Gly}$** in different solvents at room temperature. Monophasic **BBr$_{TFE}$** was recovered after slurrying 2.0 g of **BBr$_{Gly}$** in 2 ml of trifluoroethanol at room temperature overnight. A mixture containing **BBr$_{THF}$** (in our best attempt) was obtained by slurrying 1.0 g of

BBrGly in 3 ml of tetrahydrofuran for about fifteen minutes at room temperature. The sample thus obtained, being a mixture of **BBr**THF, **BBr**Gly and **BBr**I, was only suitable for indexing and crystal cell determination.

3.2.2 Crystal Data

The crystal data for all six solvates of bupropion hydrohalide salts are reported in Table 3.6. Figure 3.10 shows the final Rietveld refinement plots for the phases solved by powder diffraction methods, **BBr**EtOH, **BBr**TFE and **BBr**Gly. Appendix A reports the atomic coordinates of the phases.

Figure 3.10. Final Rietveld refinement plot for a) **BBr**EtOH (containing small amounts of **BBr**I) b) **BBr**TFE and c) **BBr**Gly with difference plot and peak markers at the bottom. The insert shows the high angle region, magnified 5×.
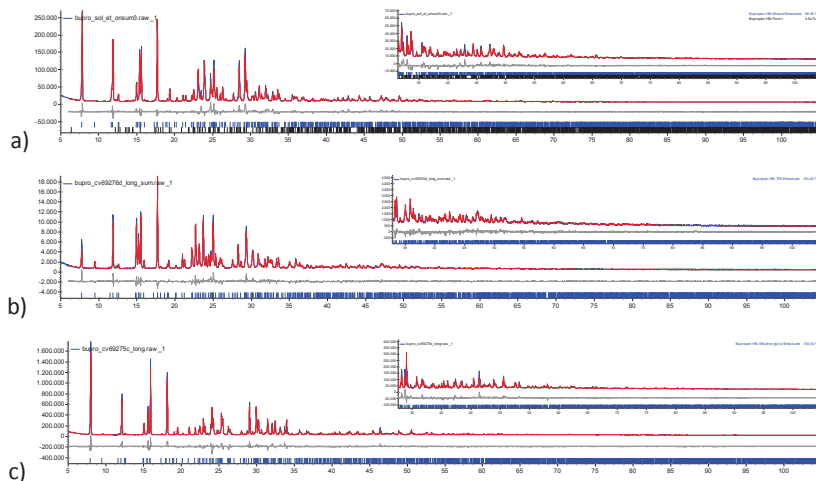
Table 3.6. Comparative crystal cell data of different solid forms of Bupropion hydrohalides (E.s.d.'s in parentheses).

	BCl$_{EtOH}$*	BBr$_{PrOH}$	BBr$_{EtOH}$	BBr$_{TFE}$	BBr$_{Gly}$	BBr$_{THF}$ §
Ref	[15]	Unpublished Data	Unpublished Data	Unpublished Data	Unpublished Data	Unpublished Data
Formula	C$_{13}$H$_{18}$ClNO ·HCl ·½(C$_2$H$_5$OH)	C$_{13}$H$_{18}$ClNO ·HBr ·½(C$_3$H$_7$OH)	C$_{13}$H$_{18}$ClNO ·HBr ·½(C$_2$H$_5$OH)	C$_{13}$H$_{18}$ClNO ·HBr ·½(C$_2$H$_2$F$_3$OH)	C$_{13}$H$_{18}$ClNO ·HBr ·½(C$_2$H$_6$O$_2$)	C$_{13}$H$_{18}$ClNO ·HBr ·½(C$_4$H$_8$O)
FW [g mol^{-1}]	299.23	350.70	343.6	376.6	351.6	356.6
Crystal System	Triclinic	Triclinic	Triclinic	Triclinic	Triclinic	Triclinic
Space Group	P-1	P-1	P-1	P-1	P-1	P-1
a [Å]	7.571(1)	7.827(6)	7.7746(2)	7.9000(2)	7.8338(2)	7.804
b [Å]	9.310(1)	9.392(6)	9.3626(3)	9.3673(2)	9.3544(2)	9.438
c [Å]	11.687(1)	11.838(9)	11.6801(2)	11.7354(3)	11.5267(2)	12.113
α [°]	85.42(1)	85.70(6)	85.99(1)	86.425(1)	87.05(1)	86.72
β [°]	101.49(1)	101.75(7)	101.39(2)	102.501(2)	103.42(2)	100.12
γ [°]	89.85(1)	90.37(6)	90.18(3)	91.033(2)	90.29(3)	91.87
V [Å^3], Z	804.5, 2	849.6, 2	828.3, 2	846.2, 2	820.5, 2	876.7, 2
V/Z	402	425	414	423	410	438
T [K]	293	293	293	293	293	293
λ [Å]	1.54178	0.71073	1.54178	1.54178	1.54178	1.54178
ρ$_{calc}$ [g cm^{-3}]	1,235	1.370	1.378	1.455	1.423	-
μ(CuKα) [mm^{-1}]	3.58	2.58 (MoKα)	4.83	4.91	4.92	-
R$_{Bragg}$	-	0.047	0.058	0.048	0.067	-

*Two angles, α and γ, were changed to the supplementary value to make the cell comparable with the other solvates.

§The solvate with THF was observed and the crystal cell obtained, but the structure was not solved, as the sample was obtained only in mixture with other phase. Therefore some data are missing and no E.s.d.'s are available.

Analogously to the unsolvated phases, several interesting similarities between the crystal data of the different phases is observed. First of all, all the solvates appear to belong to the same P-1 space group. Secondly, the lattice constants seem rather similar in all cases, after accounting for the difference in size of the solvent molecules present in the different phases. In order to verify this, the molar volume V/Z for each solvated hydrobromide phase was plotted against the calculated molar volume of the solvent present. The molar volumes of the solvents were calculated form tabulated average atomic volumes. [23] The graph obtained is reported in Figure 3.11, and shows good correlation between the molar volume of the solvates and of the solvents, suggesting structural correlation between the different solvated phases. The only outlier is **BBr$_{Gly}$**, as will be explained in the following paragraphs.

Figure 3.11. Plot of V/Z for the solvates of Bupropion hydrobromide against the calculated molecular volumes of the different solvents.
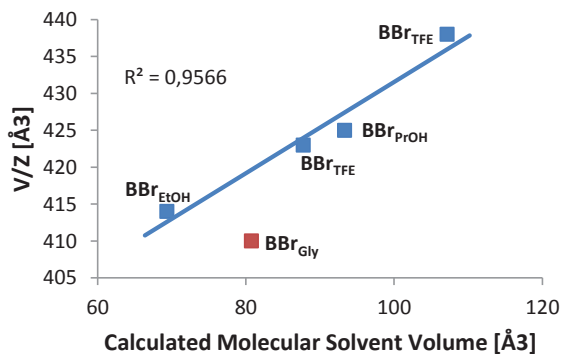
3.2.3 Structural Analysis and Comparison

A first analysis of the conformation of the bupropion molecule in the solvated phases showed not only a similarity in the bupropion molecule (in particular having *syn* conformation of the chlorine atom bound to the aromatic ring with respect to the carbonyl oxygen), but also a strong resemblance with the *syn* conformation present in the non-solvated phases previously analyzed. The

102

values of the dihedral angles describing molecular conformation in the solvated phases are collected in Table 3.7.

Table 3.7. Synoptic collection of the most relevant conformational features of the bupropion molecule in the different solvate forms. Where available, e.s.d.'s are given in parentheses.

	τ_1 [°] $C_8-N_1-C_{10}-C_{Me}$	τ_2 [°] $C_7-C_8-N_1-C_{10}$	τ_3 [°] $C_5-C_7-C_8-N_1$	τ_4 [°] $C_6-C_5-C_7-C_8$	Class
BCl$_{EtOH}$	172.0	-81.2	146.6	170.0	*syn*
BBr$_{PrOH}$	172.2	-83.4	150.4	171.2	*syn*
BBr$_{EtOH}$	179.0(8)	-86.1(6)	144.8(4)	-163.6(4)	*syn*
BBr$_{TFE}$	169.0(7)	-81.4(6)	147.9(3)	-168.7(4)	*syn*
BBr$_{Gly}$	169.3(7)	-83.4(5)	149.5(3)	-163.8(3)	*syn*

Moreover, as is the case with the unsolvated phases, the bupropion hydrohalide structure in all solvated phases is composed of [(bupropionH)$_2$X$_2$] dimers held together by the same NH---X---HN bridging $R_4^2(8)$ hydrogen bond motif.

The analysis of the packing of the bupropion dimers and of the positioning of the solvent molecules shows the isostructurality of all solvates analyzed. Different isostructural (or isomorphous) solvates have the same type of molecular network of the host molecule, inside which the different solvent molecules are accommodated. [24] The phenomenon of isomorphic solvates is not uncommon. Two examples reported in the literature are the solvates of phenylbutazone and finasteride. [25, 26] In this case, the bupropion dimers are stacked diagonally, leaving spaces in the lattice in between the diagonal stacks where the solvent molecules are positioned. The packing of the different solvated phases analyzed (isooriented for easy visual comparison, highlighting the isostructural nature of the solvates) is shown in Figure 3.12.

The solvent molecule is positioned in all cases on an inversion center, therefore resulting always disordered when the molecule is non-centrosymmetric (as is the case with all solvent molecules except for ethylene glycol). The

occupancy of the atoms of the solvent molecules is 0.5, as only half of the sites are occupied (all the phases were found to be emisolvates). During structure solution for forms **BBr$_{EtOH}$** and **BBr$_{TFE}$**, therefore, the solvent molecules were designed using a Z-matrix having a dummy central atom which was placed on an inversion center. The solvent molecule was then rotated but not moved during structure solution, and only during the final Rietveld refinement was the position of the molecule freed. The solvent molecules in all phases form additional hydrogen bonds by acting as hydrogen bond donors, in particular forming a hydrogen bond between their hydroxyl groups and the halide ion. This is depicted in Figure 3.13.

Figure 3.12. Views of the packing of a) **BCl$_{EtOH}$**, b) **BBr$_{PrOH}$**, c) **BBr$_{EtOH}$**, d) **BBr$_{TFE}$** and e) **BBr$_{Gly}$** along the **a** axis.

a)

b)

c)

d)

e)
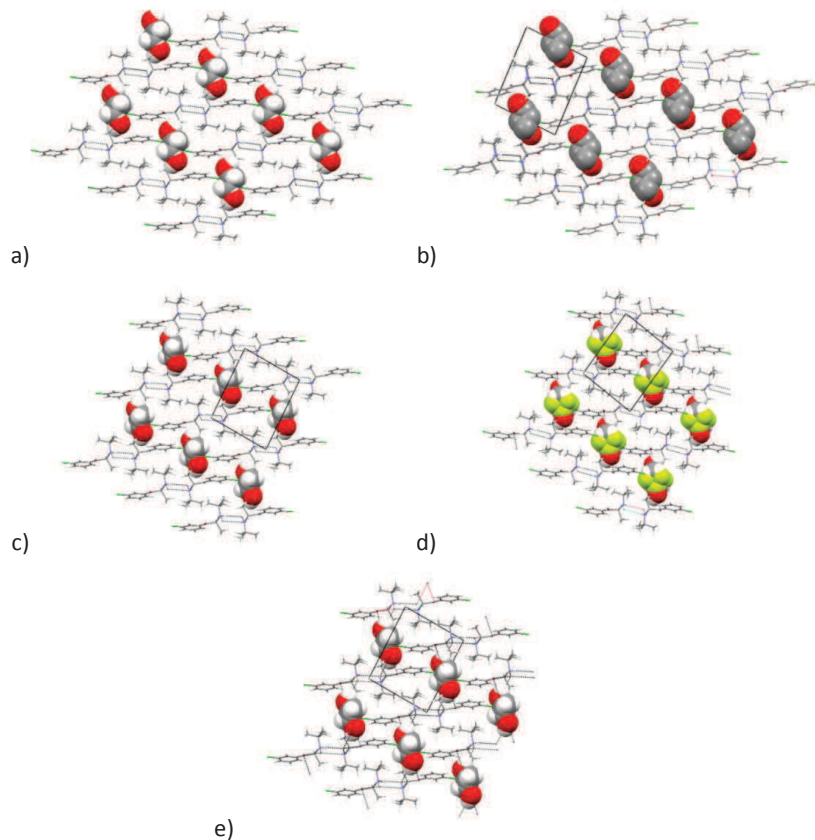
In **BBr$_{Gly}$**, the ethylene glycol molecule is positioned, as is the case with the other solvates, on the center of symmetry of the crystallographic cell and, being a centrosymmetric diol, forms two hydrogen bonds with two different bromide ions, one with each hydroxyl group. This, as shown in Figure 3.14, causes the solvent molecule to be exactly positioned and not disordered, as is the case with the other solvates. The double hydrogen bond between the ethylene glycol molecule and two different bromide ions also causes the molar volume of **BBr$_{Gly}$**

105

to be out of the trend shown in Table 3.11. During structure solution, the ethylene glycol molecule was described by a Z-matrix having a central dummy atom position in an inversion center, but only half of the molecule was described with atoms having occupancy 1, leaving the inversion center to generate the other half of the molecule.

Figure 3.13. Relative positioning of the bupropion dimer and the solvent molecule in a) **BCl$_{EtOH}$**, b) **BBr$_{PrOH}$**, c) **BBr$_{EtOH}$** and d) **BBr$_{TFE}$** to show the disorganized solvent molecules.

a)   b)

c)   d)
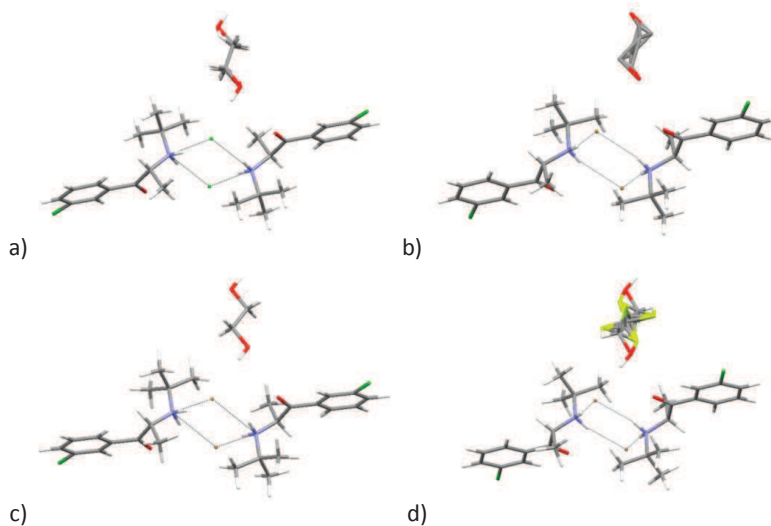
Figure 3.14. Relative positioning of the bupropion dimer and the ethylene glycol molecule in **BCl$_{Gly}$**.
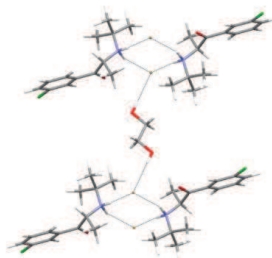
The hydrogen bonding between the solvent molecules and the halogen atom was confirmed by analyzing the atom scheme in all solvated phases. The distances between the oxygen of the hydroxyl group of the solvent and its closest neighbors capable of accepting hydrogen bonding (the halogen ion, the oxygen of the carbonyl group and the chlorine atom on the aromatic ring) were tabulated and corrected for Van Der Waals radii of the neighbors to correctly asses the atomic distance. This, shown in Table 3.8, allows to determine that the solvates indeed form hydrogen bonds with the halide ion.

Table 3.8. Distances between the hydroxyl oxygen of the solvent and its closest neighbors corrected to account for the Van Der Waals radii of the different atoms.

The values were obtained by taking the interatomic distances between the solvent oxygen and the halide ion, the carbonyl oxygen and the chlorine on the aromatic ring and subtracting the Van Der Waals radius of the neighbor. The Van Der Waals radii used are as follows: Cl = 1.75 Å, O = 1.52 Å, Br = 1.85 Å.

	O---X$^-$ [Å]	O---O=C [Å]	O---Cl-Ar [Å]
BCl$_{EtOH}$	1.64	1.74	2.11
BBr$_{PrOH}$	1.61	1.76	2.29
BBr$_{EtOH}$	1.69	1.80	1.96
BBr$_{TFE}$	1.45	1.62	2.16
BBr$_{Gly}$	1.54	1.82	2.26

Even though it was not possible to solve the structure of **BBr$_{THF}$**, having obtained only a mixture of **BBr$_{THF}$**, **BBr$_{Gly}$** and **BBr$_I$**, it was still possible to obtain the cell parameters for **BBr$_{THF}$**. As already discussed, the cell, reported in Table 3.6, appears very similar to the cells of the other solvated phases. Having observed the isostructurality of all the solvated phases analyzed, it is reasonable to conclude that the structure of **BBr$_{THF}$** is also similar to that of the other solvates. The formation of hydrogen bonding between the hydroxyl group of the solvents and the halide ions, previously discussed, also allows to explain the relative stability of the tetrahydrofuran solvate. As the solvent molecule has no hydrogen bond donor, it cannot stabilize the structure via hydrogen bonding. The solvent is

therefore more weakly retained in the structure and the phase undergoes rapid desolvation at ambient temperature and pressure.

In order to understand and try to predict the behavior of the solvates upon desolvation, the crystal structure of the isomorphous solvates of buproprion hydrohalides was compared with the structure of the unsolvated phases. The solvates appear to have a lot in common with the P-1 family of structures discussed in section 3.1, because the bupropion dimers in the solvates appear to be stacked along the **a** axis in slightly rotated stacks, causing the formation of narrow channels along the **a** axis to accommodate the solvent, as is shown in Figure 3.15. This disposition is analogous to the P-1 family of structures, where the dimers are also stacked along the **a** axes and organized in straight (**BCl$_{IV}$**, **BBr$_I$** and **BI$_{III}$**) or slanted (**BCl$_{III}$**) rows. It is therefore reasonable to expect the solvates to convert into a P-1 phase upon desolvation.

Figure 3.15. Schematic comparison between the organization of bupropion hydrobromide dimers a) in the solvates, b) **BCl$_{IV}$** and c) **BCl$_{III}$**.
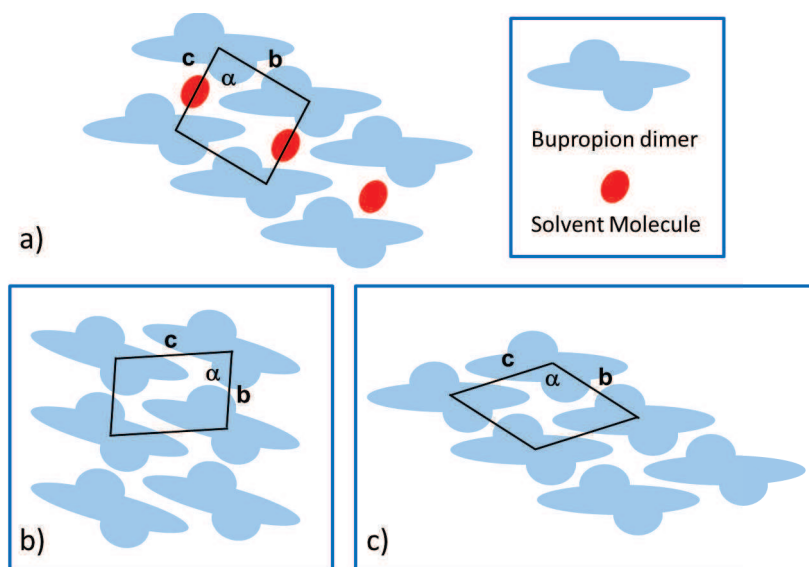
3.2.4 Desolvation Experiments

In order to confirm the hypotheses made regarding the desolvation behavior of solvated phases based upon the structural relations between solvated and non-solvated phases, as discussed in the previous paragraph, various desolvation experiments were carried out on all solvates in different conditions. The desolvation process was studied using ovens operating at reduced pressure and DSC.

The desolvation of **BCl**$_{EtOH}$, described in paragraph 3.1.2, led to mixtures of **BCl**$_{III}$ and **BCl**$_{IV}$, as hypothesized by the structural relation between the phases discussed in the previous paragraph. Mixtures obtained after slow desolvation processes often also contained **BCl**$_I$, probably due to a conversion of **BCl**$_{III}$ or **BCl**$_{IV}$. It was not possible to confirm this due to the fact that **BCl**$_{III}$ or **BCl**$_{IV}$ were never obtained as pure phases.

All solvated phases of bupropion hydrobromide converted into **BBr**$_I$ upon desolvation. The only difference between the different hydrobromide phases was the temperature at which the bulk conversion occurred. For example, while **BBr**$_{Gly}$ is very stable at room temprature and doesn't convert into **BBr**$_I$ when heated at reduced pressure until about 100°C, **BBr**$_{EtOH}$, **BBr**$_{PrOH}$ and **BBr**$_{TFE}$ fully convert into **BBr**$_I$ at much lower temperatures. This is probably due to the fact that the ethylene glycol molecule in **BBr**$_{Gly}$ forms two hydrogen bonds with bromide ions, while the ethanol, propanol and trifluoroethanol molecules, respectively in **BBr**$_{EtOH}$, **BBr**$_{PrOH}$ and **BBr**$_{TFE}$, only form one hydrogen bond each.

Where obtained, monophasic samples of all solvates of bupropion salts were analyzed via DSC. The DSC analyses are reported in Figure 3.16. In all cases, the desolvation event is clearly visible as an endothermic band. The desolvation enthalpies **ΔH**$_{desol}$, collected in Table 3.9, are all very similar to one another, with the exception of **BBr**$_{Gly}$, which has a significantly higher **ΔH**$_{desol}$. This could be attributed to the presence of two hydrogen bonds between the solvent molecule and the rest of the crystalline structure. Also, the shape of the event is different compared with the desolvation events of the other solvates, being apparently made up of two superimposed events. After an event comparable to the desolvation of other solvates, a broad event continues until about 160°C. This phenomenon, highlighted in Figure 3.16e, is tentatively attributed to the fact that,

when the hydrogen bonds are broken and the solvent molecule leaves the structure, ethylene glycol, unlike the other solvents, is still well below its boiling temperature, and needs more energy to vaporize.

BBr$_{THF}$ is less stable than the other solvates examined and very rapidly converts into **BBr$_I$** at room temperature. As discussed above, the decreased stability of **BBr$_{THF}$** compared with the other solvates might be explained by the lack of hydrogen bond donors on the tetrahydrofuran molecule, which makes it impossible for the solvent molecule to form hydrogen bonds with the bromide ion as is the case with the other solvents.

Table 3.9. Desolvation enthalpies for the solvates of Bupropion salts.

	Desolvation enthalpy ΔH_{desol} [kJ mol^{-1}]
BCl$_{EtOH}$	+24.7
BBr$_{PrOH}$	+28.4
BBr$_{EtOH}$	+28.2
BBr$_{TFE}$	+29.9
BBr$_{Gly}$	+37.2

Figure 3.16. DSC analyses for a) **BCl**_{EtOH}, b) **BBr**_{PrOH}, c) **BBr**_{EtOH}, d) **BBr**_{TFE} and e) **BBr**_{Gly}. The unusual shape of the desolvation event for **BBr**_{Gly} is highlighted with a red rectangle.
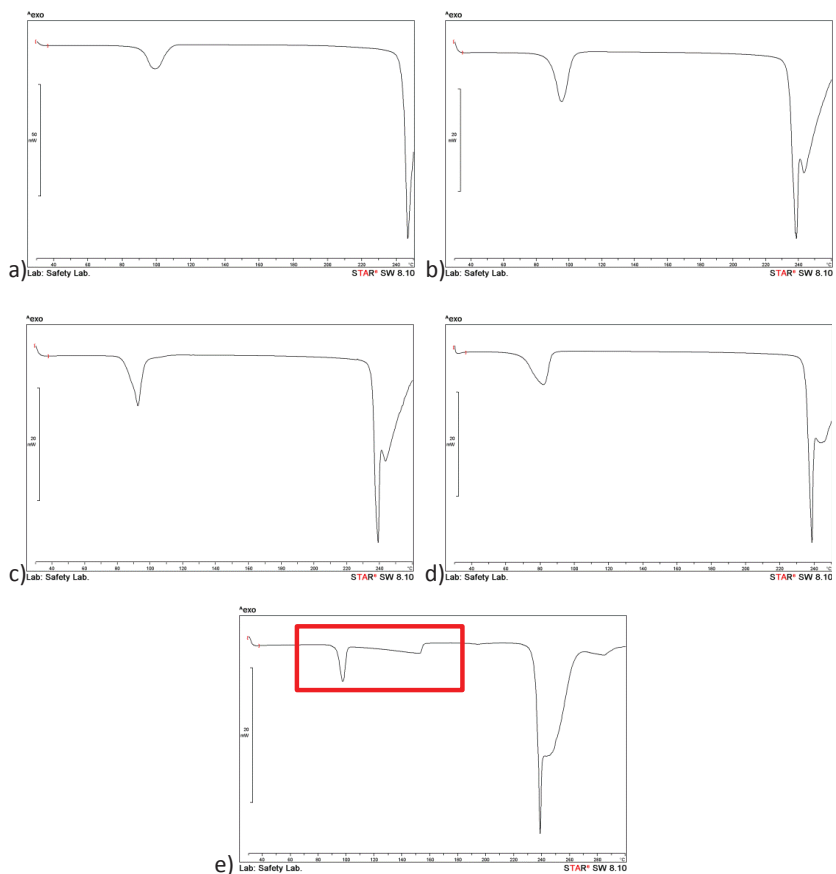
References

1. Kelley, J. L., Musso, D. L., Boswell, G. E., Soroko, F. E., Cooper, B. R., *Journal of Medicinal Chemistry*, *39* (**1996**), 347-349.

2. Metha, N. B., United States Patent, US 3,819,706.

3. Fang, Q. K., Han, Z., Grover, P., Kessler, D., Senanayake, C. H., Wald, S. A., *Tetrahedron Asymmetry, 11* (**2000**), 3659-3663.

4. Metha, N. B., Yeowell, D. A., German Patent Application, DE 2059618.

5. Oberegger, W., Zhou, F., Maes, P., Turchetta, S., Jackson, G., Massardo, P., International Patent Application, WO 2007/002597.

6. Amidon, G. L., Lennernas, H., Shah, V. P., Crison, J. R., *Pharmaceutical Research, 12* (**1995**), 413-420.

7. Yu, L. W., Amidon, G. L., Polli, J.E., Zhao, H., Mehta, M.U., Conner, D.P., Shah, V.P., Lesko, L. J., Chen, M. L., Lee, V. H., Hussain, A. S., *Pharmaceutical Research, 19* (**2002**), 921-925

8. Maccaroni, E., Malpezzi, L., Masciocchi, N., *Journal of Pharmaceutical and Biomedical Analysis, 50* (**2009**), 257-261.

9. Maccaroni, E., Malpezzi, L., Famulari, A., Masciocchi, N., *Journal of Pharmaceutical and Biomedical Analysis, 60* (**2012**), 65-70.

10. Turchetta, S., Zenoni, M., International Patent Application, WO 2010/015692.

11. Liu, M., Hu, X., Gu, J., Tang, G., *Acta Crystallographica, E67* (**2011**), o2772.

12. Hu, X., Xiang, H., Gu, J., Zhang, Y., Chen, L., *Chinese Journal of Structural Chemistry, 30* (**2011**), 1591-1596.

13. Galcera, J., Molins, E., *Crystal Growth & Design, 9* (**2009**), 327-334.

14. Vladiskovic, C., Masciocchi, N., *Crystal Growth & Design, 14* (**2014**), 3603-3611.

15. Froimovitz, M. G., *Journal of Chemical Information and Computer Sciences*, *38* (**1998**), 506-510.

16. Ponder, J. W., TINKER Software Tools for Molecular Design, Version 6.2., **2013**.

17. Bernstein, J., *Polymorphism in Molecular Crystals*, Clarendon Press, Oxford, **2002**.

18. Musso, D. L., Mehta, N. B., Soroko, F. E., Ferris, R. M., Hollingsworth, E. B., Kenney, B. T., *Chirality, 5* (**1993**), 495-500.

19. Zhang, D., Liping, G., Zhang, Z., Wang, L., Shao, M., *Journal of Pharmaceutical Sciences, 101*, (**2012**), 3091-3095.

20. Giron, D., *Thermochimica Acta*, *240* (**1995**), 1-59.

21. Spek, A. L., Acta Crystallographica, *D65* (**2009**), 148-155.

22. Marsh, R. E., *Acta Crystallographica, B55* (**1999**), 931-936.

23. Detlef W. M. H., *Acta Crystallographica, B57* (**2002**), 489-493.

24. Griesser, U., The Importance of Solvates, in: *Polymorphism in the Pharmaceutical Industry*, Hilfiker, R. (ed.), Wiley-VCH, Weinheim, **2006.**
25. Hosokawa, T., Datta, S., Sheth, A. R., Brooks, N. R., Young, V. G. Jr., Grant, D. J. W., *Crystal Growth & Design*, *4* (**2004**), 1195-1201.
26. Schultheiss N., Smit J.P., Hanko J.A., *European Journal of Pharmaceutical Sciences, 38* (**2009**), 498-503.

4. Structural Analysis of Nortriptyline Hydrochloride Polymorphs

Nortriptyline hydrochloride, reported in Scheme 4.1, is a tricyclic antidepressant [1] belonging to a class of similar molecules which have been marketed for various psychiatric disorders for more than fifty years. Tricyclic antidepressants share a similar chemical structure, as well as similar mechanisms of action. In particular, they increase brain levels of norepinephrine and serotonin and block the action of acetylcholine. [2] This class of molecules also has antihistaminic effects and can cause sedation.

Scheme 4.1. Nortriptyline Hydrochloride
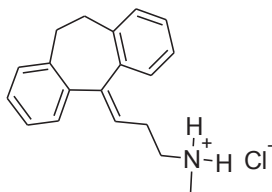
In particular, nortriptyline hydrochloride has been on the market for a long time with many different trade names. The crystal chemistry of nortriptyline hydrochloride, known to exhibit polymorphism, is, however, scarcely investigated. Even though the polymorphic form of nortriptyine hydrochloride will have little or no influence on the bioavailability of the drug as nortriptyline hydrochloride falls in class I of the Biopharmaceutics Classification

System [3, 4] (high solubility and high permeability compounds), knowledge of solid-state features can still be important to address processability or formulability issues at the production and processing levels. For example, it can highlight the conditions of possible interconversions between polymorphs, address their stability ranges and explain unexpected solid-state behaviour.

As discussed in Chapter 1, there can be several different driving forces for polymorphism, for example, different hydrogen bonding scheme, molecular conformations or packing patterns. The comparison of crystal structures of similar molecules can offer insight into the solid-state behaviour of related species. As the class of tricyclic antidepressants is rich in structurally related molecules, similar crystal structures can be used for comparison with nortriptyline hydrochloride. In particular, the most similar compounds with solved crystal structures are the hydrochlorides of amitriptyline [5], cyclobenzaprine [6] and dothiepin [7], shown in Scheme 4.2.

Scheme 4.2. Structural analogues of nortriptyline hydrochloride, a) amitriptyline hydrochloride, b) cyclobenzaprine hydrochloride, c) dothiepin hydrochloride (represented in the protonated form).

a)   b)   c)
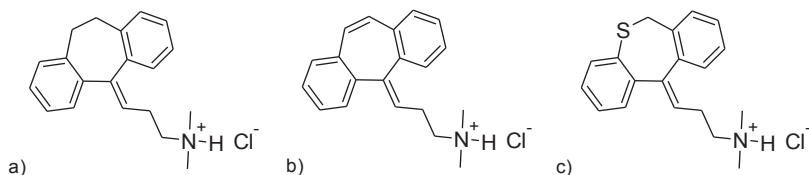
4.1 Nortriptyline Hydrochloride

Nortriptyline hydrochloride exhibits polymorphism, as it can crystallize in two different anhydrous forms. In fact, a paper by McCalman and co-worker [8] reports the crystallization behaviour of the hydrochloride salt of nortriptyline, describing two different polymorphs, α and β (respectively **NOR*HCl$_\alpha$** and **NOR*HCl$_\beta$** in the text). However, little or no information was available until recently in the literature on the properties of the different crystal forms. Actually, while one crystal structure has been known for a long time, [9] it has

116

not been made clear to which polymorph it corresponds until our recent work.
[10]

The two crystalline forms of nortriptyline hydrochloride, forms **NOR*HCl$_\alpha$** and **NOR*HCl$_\beta$**, show very similar properties including solubility, crystal habit and chemical stability. Moreover, both appear indefinitely stable once isolated. In order to investigate the solid state properties, the missing structure was solved by powder diffraction methods and structural comparison was used as a tool to understand polymorphic behavior.

4.1.1 Crystal Data

By comparing XRPD data and the published coordinates, the crystal structure present in the literature was found to be form **NOR*HCl$_\beta$**. The structure of **NOR*HCl$_\alpha$** was therefore solved by powder diffraction methods. Initially, laboratory powder diffraction data was used for indexing, crystal cell determination and structure resolution. However, several unusual characteristics of **NOR*HCl$_\alpha$** were observed. Firstly, the proposed space group, P2/c, is rather unusual. Secondly, the structure found, instead of having one single site for the chloride ion, showed two crystallographically independent sites, each lying on a special position (as will be discussed in paragraph 4.1.2). For these reasons, it was decided to verify the structure using powder diffraction data obtained on a synchrotron source (see Chapter 2). The peculiar characteristics of **NOR*HCl$_\alpha$** were confirmed.

Both forms were found to belong to a monoclinic space group and to have rather similar cell constants, though with a different interaxial angle and different space group symmetry. The crystal data for the two forms are reported in Table 4.1, while Figure 4.1 reports the final Rietveld refinement plot for form **NOR*HCl$_\alpha$**. The atomic coordinates are reported in Appendix A.

Table 4.1. Comparative crystal cell data of forms **NOR*HCl$_\alpha$** and **NOR*HCl$_\beta$** *(E.s.d.'s in parentheses).*

	NOR*HCl$_\beta$	**NOR*HCl$_\alpha$**
Reference	[9]	[10]
Chemical Forumula	$C_{19}H_{21}N \cdot HCl$	$C_{19}H_{21}N \cdot HCl$
Formula weight [g mol^{-1}]	299.84	299.84
Crystal System	Monoclinic	Monoclinic
Space Group	P2$_1$/c	P2/c
a [Å]	5.070(2)	9.99126(6)
b [Å]	34.088(5)	5.10021(3)
c [Å]	9.976(1)	34.1636(1)
β [°]	90.74(2)	98.684(6)
V [Å^3] , Z	1723.97, 4	1720.93, 4
V/Z	431	430
T [K]	295	293
λ [Å]	0.70930	0.827006
$\rho_{(calc)}$ [g cm^{-1}]	1.16	1.16
R$_{Bragg}$	0.046	0.047

Figure 4.1. Final Rietveld Refinement plot for **NOR*HCl$_\alpha$** on synchrotron data with difference plot and peak markers at the bottom. The insert shows the high angle region, magnified 5×.
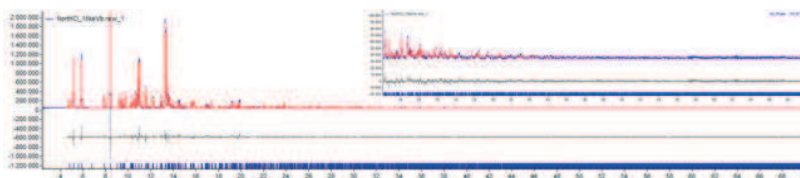
4.1.2 Structural Analysis

The molecule of nortriptyline was characterized by a number of chemically relevant conformational parameters, as well as by the relative conformation of the 1,2-ethylene bridge between the aromatic rings (described by the ψ_{1-4} and

118

$\phi_{1\text{-}2}$ torsion angles, respectively, defined in Scheme 4.3 and synoptically collected in Table 4.2). These torsion angles were used both during structure solution and to compare molecular conformation in the different crystal structures under analysis. Nortriptyline is shown in Scheme 4.3 in its non-protonated neutral form, but it was modelled as protonated in structure solution.

The torsion angles of the N-protonated nortriptyline molecule in both **NOR*HCl$_\alpha$** and **NOR*HCl$_\beta$** phases are very similar, as is shown by the values reported in Table 4.2 and pictorially exemplified in Figure 4.2. Importantly, not only the torsional features of the flexible side chain can be considered analogous (addressed with angles $\psi_{1\text{-}4}$), but also the twisting at the ethylene group (addressed by the $\phi_{1\text{-}2}$ angles), which describe the conformation of the seven-membered ring.

Scheme 4.3. Schematic drawing of the nortriptyline molecule together with the torsion angles discussed.
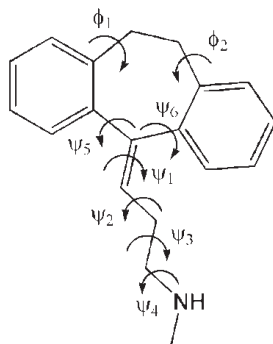
Figure 4.2. Plot of the N-protonated nortriptyline molecules found in **NOR*HCl$_\alpha$** (a) and **NOR*HCl$_\beta$** (b), isooriented for easy graphical comparison.

a)   b)
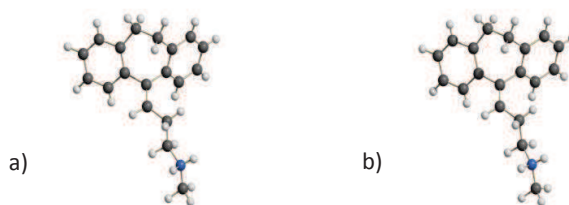
Table 4.2. Synoptic collection of the most relevant conformational features of the nortriptyline molecule *(E.s.d.'s, where available, in parentheses).*

	NOR*HCl$_\beta$	NOR*HCl$_\alpha$
ψ_1 [°]	1.4	3.0(5)
ψ_2 [°]	-113.0	-112.8(4)
ψ_3 [°]	-155.9	-149.2(3)
ψ_4 [°]	-175.1	177.5(3)
ϕ_1 [°]	-7.7	-7.3(1)
ϕ_2 [°]	-71.1	-70.5(2)

The main conformational parameter describing the nortriptyline molecule is the position of the side chain with respect to the (conformationally asymmetric) seven-membered ring. The conformation of the nortriptyline molecules in both **NOR*HCl$_\alpha$** and **NOR*HCl$_\beta$** can be described as *anti,* considering the disposition on opposite sides of the side chain on the exocyclic C=C bond with respect to the fragment defined by the (=C)-aryl-(CH$_2$-CH$_2$-) atoms showing near coplanarity (demonstrated by the small values of the torsion angle ϕ_1). This is better exemplified in Figure 4.3. The other wing of the 7-membered ring manifests a much larger (*ca.* 70°) torsion at the aryl-C$_2$H$_4$ bond (see Table 4.2, torsion angle ϕ_2).

Figure 4.3. Schematic representation of the conformation of the nortriptyline molecules defined as *anti*: the side chain on the exocyclic C=C bond falls on the *opposite* side of the fragment defined by the (=C)-aryl-(CH$_2$-CH$_2$-) atoms showing near coplanarity (the red portion in the drawing).
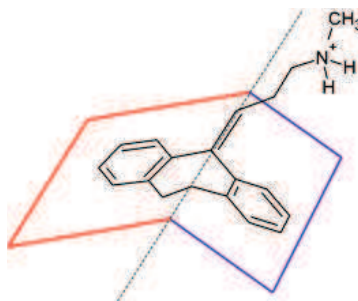
Crystals of **NOR*HCl$_\beta$** crystallizing in the monoclinic P2$_1$/c space group, contain protonated nortryptiline molecules and isolated chloride ions (both lying on a general position), linked by hydrogen bonding between the protonated nitrogen atom and the chloride ions. The $^+$NH$_2$ group donates two hydrogen bonds acting as a bridge between the near chloride ions, which, in turn, accept hydrogen bonds from $^+$NH$_2$ groups of two different nortriptyline molecules (see Figure 4.4b). This creates a chain of hydrogen bonds, which can be described as $C_4^2(4)$ using Graph Set notation (see Chapter 1).

NOR*HCl$_\alpha$ crystallizes in the less common monoclinic P2/c space group, again with the organic molecule in general position, but with two crystallographically independent chloride ions (lying on the twofold axes parallel to **b**). Each chloride ion site has occupancy 0.5. The same kind of hydrogen bond chain already seen in form **NOR*HCl$_\beta$** is also found in form **NOR*HCl$_\alpha$**, with the ammonium group acting as donor with both hydrogens and the chloride ions acting as acceptors from two neighbouring ammonium groups. This creates another $C_4^2(4)$ hydrogen bond motif, analogously to **NOR*HCl$_\beta$**, shown in Figure 4.4a.

Figure 4.4. The one-dimensional chains of μ_2-Cl hydrogen-bonded N-protonated nortryptyline molecules in a) **NOR*HCl$_\alpha$** and b) **NOR*HCl$_\beta$** ($C_4^2(4)$ hydrogen bond motif).
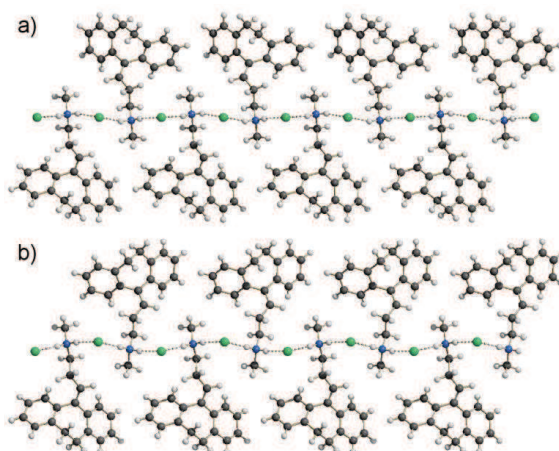
The conformational flexibility of the tricyclic system described above allows the protonated nortriptyline molecule to exist in the solid state in two different *anti* conformations which are non-superimposable mirror images of each other. In solution, on the other hand, the situation changes. Many studies exist on the possible conformations of tricyclic antidepressants in solution, [11, 12] where the flipping from one 7-membered ring conformation to the other is possible, causing two different *syn* conformations to exist. This is exemplified in Scheme 4.4, where all different possible conformations of the nortriptyline molecule are depicted. Variable temperature NMR [13] has demonstrated that, in solution, these kinds of systems can easily flip from one 7-membered ring conformation to the other. In the case of nortriptyline molecules, the flipping from one 7-membered ring conformation to the other also means switching from an *anti* to a *syn* conformation, as the double bond on the chain does not allow rotation. Therefore, one of the possible *anti* conformations is in equilibrium in solution with one *syn* conformation, but not with the other *anti* conformation. This is pictorially summarized in Figure 4.5.

Scheme 4.4. Possible conformations of the nortriptyline molecule, shown here in the neutral form: two *anti* conformations a) and b), and two *syn* conformations, c) and d).

a) **A1**   b) **A2**   c) **S2**   d) **S1**
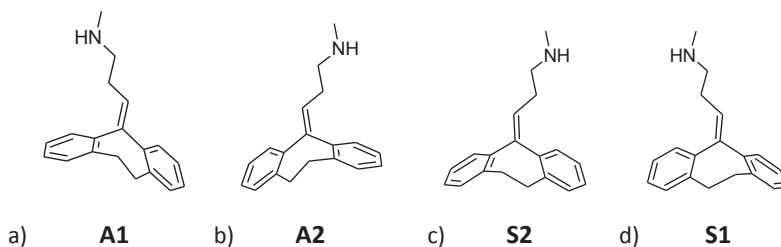
Figure 4.5. Representation of the possible conformations of nortriptyline hydrochloride in solution.

*A1 and A2 represent the two anti conformations which are non superimposable mirror images of one another, while S1 and S2 represent the syn conformations which are in equilibrium with the anti conformations due to the inversion of the 7-membered ring. The two anti conformations crystallize in two different supramolecular structures to give origin to **NOR*HCl$_\alpha$** and **NOR*HCl$_\beta$**, while the two syn conformations do not appear in any known polymorph.*
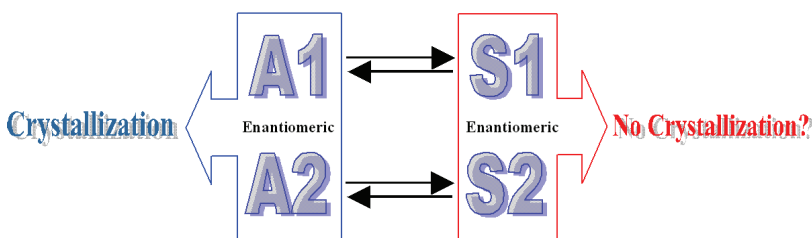
In **NOR*HCl$_\alpha$**, the single hydrogen-bonded chains are built by nortriptyline molecules which are *all* in the same conformation (A1 or A2, as defined in Figure 4.5). The adjacent chain contains nortriptyline molecules in the other (enantiomeric) conformation. Therefore, if we define ↑ and ↓ the two *anti* conformations A1 and A2 of the protonated nortriptyline molecule, **NOR*HCl$_\alpha$** is made up of ↑↑↑↑ and ↓↓↓↓ parallel chains.

In **NOR*HCl$_\beta$**, protonated nortryptiline molecules are again organized in hydrogen bonded chains (as shown in Figure 4.4) and, similarly to **NOR*HCl$_\alpha$**, exist in the solid state in two different non-superimposable mirror image *anti* conformations. In this case, however, each single chain contains molecules which alternate in the two conformations. Thus, using the same notation as above, **NOR*HCl$_\beta$** chains can be described as built by the ↑↓↑↓ sequence.

From the symmetry point of view, the chains found in **NOR*HCl$_\beta$** are generated by glide planes perpendicular to **b** (*pg* frieze group), [14] while in **NOR*HCl$_\alpha$** chain repetition is ensured by the two-fold axes of the *P2/c* space group (*p2* frieze group). Consistently, the axes of the unit cells show very similar values, even though the space group (and therefore axis denomination) is obviously different due to the different symmetry elements of the chains. The

major difference between the cell dimensions of the two polymorphs is the monoclinic β angle, which, *inter alia*, refers to unique axes (**b**) of markedly different lengths.

The differences between the supramolecular organization of **NOR*HCl$_\alpha$** and **NOR*HCl$_\beta$** suggest that solid-state conversion from one form into the other is highly hindered, as it would require the cleavage and reformation of a great number of hydrogen bonds. Such a reorganization would thus be feasible only in solution or upon melting and subsequent recrystallization, as will be discussed in paragraph 4.2.2.

4.1.3 Related Structures

As mentioned at the beginning of the chapter, the class of tricyclic antidepressants contains many different molecules which share marked chemical similarities. In particular, they all contain a tricyclic structure with a long side chain bound to the middle ring. The molecules reported in Scheme 4.2, amitriptyline, cyclobenzaprine and dothiepin, are all marketed in hydrochloride salt form and all have solved crystal structures reported in the literature. [5, 6, 7] They are therefore perfect candidates for structural comparison with nortriptyline hydrochloride. The crystal data for the five different structures to be compared (two crystalline forms of nortriptyline hydrochloride and one each for amitriptyline, cyclobenzaprine and dothiepin hydrochloride) are reported in Table 4.3. The main conformational features of the constituent molecules are reported in Table 4.4. The torsion angles for amitriptyline, cyclobenzaprine and dothiepin are defined in analogy to those of nortriptyline. Worthy of note, among these chemical analogues, cyclobenzaprine is the only species unable to exist in the *syn* and *anti* conformations described above, as it possesses a double bond on the 7-membered ring. The tricyclic system is therefore rigid and possesses no conformational freedom necessary to generate *syn* and *anti* conformers. Moreover, cyclobenzaprine contains two crystallographically independent molecules, and therefore two sets of dihedral angles are necessary. Among this small group of structures, only in dothiepin *chemically different E,Z* species exist, manifested by the existence of two isomers. This is due to the presence, on the ethylene bridge of the seven-membered ring, of a sulphur atom. The known crystal structure of this molecule, however, refers to a single

isomer (*E*), which adopts the same *anti* conformation as the other molecular species collected in Table 4.4.

Table 4.3. Crystal data for **NOR*HCl$_\alpha$**, **NOR*HCl$_\beta$** and three related crystal structures, amitriptyline hydrochloride, cyclobenzaprine hydrochloride and dothiepin hydrochloride. *(E.s.d.'s in parentheses).*

	NOR*HCl$_\beta$	NOR*HCl$_\alpha$	Amitriptyline HCl*	Cyclobenzaprine HCl	Dothiepin HCl
Reference	[9]	[10]	[5]	[6]	[7]
Chemical Forumula	$C_{19}H_{21}N \cdot HCl$	$C_{19}H_{21}N \cdot HCl$	$C_{20}H_{23}N \cdot HCl$	$C_{20}H_{21}N \cdot HCl$	$C_{19}H_{21}NS \cdot HCl$
Formula weight [g mol^{-1}]	299.84	299.84	313.86	311.84	331.90
Crystal System	Monoclinic	Monoclinic	Monoclinic	Tetragonal	Monoclinic
Space Group	P2$_1$/c	P2/c	P2$_1$/c	I4$_1$/a	P2$_1$/c
a [Å]	5.070(2)	9.99126(6)	14.345(4)	32.0959(7)	14.296(5)
b [Å]	34.088(5)	5.10021(3)	9.140(2)	32.0959(7)	9.364(3)
c [Å]	9.976(1)	34.1636(1)	13.812(4)	13.7578(5)	13.724(3)
β [°]	90.74(2)	98.684(6)	96.82(2)	90	97.77(3)
V [Å^3] , Z	1723.97, 4	1720.93, 4	1798.12, 4	14172.6, 32	1820.33, 4
V/Z	431	430	450	443	455

In ref [5], the space group given for amitriptyline hydrochloride is P2$_1$/a. It was chosen here to invert axes **a and **c**, turning it to P2$_1$/a, in order to highlight the similarities with dothiepin hydrochloride.*

Even though amitriptyline and dothiepin belong to the same space group as **NOR*HCl$_\beta$**, P2$_1$/c, they shows no other similarity in the crystallographic cell. Interestingly, amitriptyline and dothiepin show remarkable similarities in their lattice parameters. Crystal data for cyclobenzaprine also does not show any resemblance to the crystal data of the two forms of nortriptyline. However, the conformational features of all molecules show some interesting similarities. First of all, the molecules of nortriptyline, amitriptyline and dothiepin are all in *anti* conformation, as is shown in Figure 4.6 (the molecules of cyclobenzaprine cannot show *syn-anti* conformations, as discussed above). However, the molecules of nortriptyline in the two forms and the molecules of amitriptyline and dothiepin show an important difference in the side chain conformation

addressed by the sign of ψ_2. This is responsible for the orientation of the side chain, as visible in Figure 4.6. While in the two forms of nortriptyline the side chain is oriented almost parallel to the tricyclic moiety, in amitriptyline and dothiepin the side chain is oriented almost perpendicular to it. Cyclobenzaprine, which has two crystallographically independent molecules in the asymmetric unit, exhibits one molecule with the side chain analogous to nortriptyline (see figure 4.6f) and the other with the side chain analogous to amitriptyline and dothiepin (see figure 4.6e).

Figure 4.6. Plots of the molecules present in a) **NOR*HCl$_\alpha$**, b) **NOR*HCl$_\beta$**, c) amitriptyline hydrochloride and d) dothiepin hydrochloride. Cyclobenzaprine has two crystallographically independent molecules, depicted in e) and f).
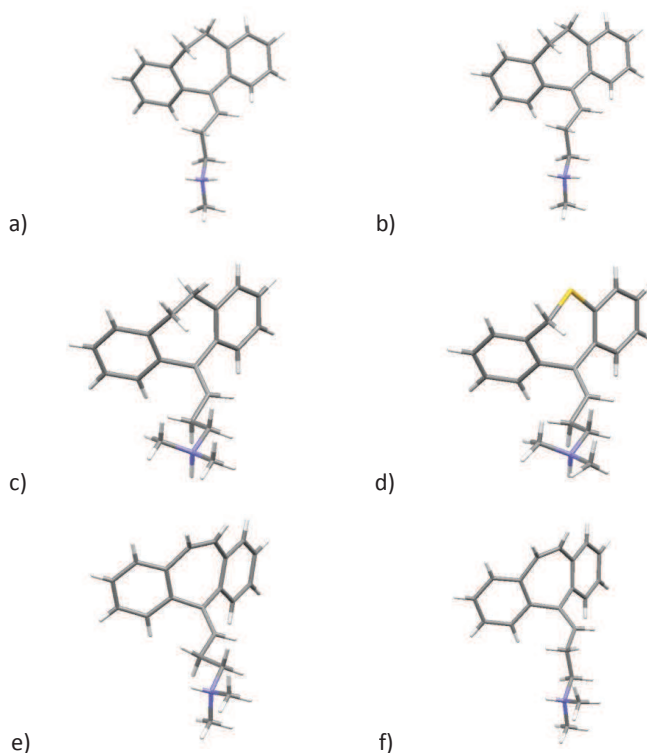
Table 4.4. Synoptic collection of the most relevant conformational features in **NOR*HCl$_\alpha$**, **NOR*HCl$_\beta$** and in three related crystal structures, amitriptyline hydrochloride, cyclobenzaprine hydrochloride and dothiepin hydrochloride.
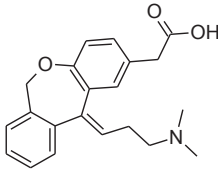
	NOR*HCl$_\beta$	NOR*HCl$_\alpha$	Amitriptyline HCl	Cyclobenzaprine HCl		Dothiepin HCl
ψ_1 [°]	1.4	3.0	8.3	-2.8	3.1	6.4
ψ_2 [°]	-113.0	-112.8	121.1	-134.8	-122.7	125.6
ψ_3 [°]	-155.9	-149.2	-173.0	-173.0	179.9	-171.5
ψ_4 [°]	-175.1	-177.5	-173.4	-163.0	-173.7	-174.5
ϕ_1 [°]	-7.7	-7.3	-8.5	31.1	30.4	-7.6
ϕ_2 [°]	-71.1	-70.5	-69.7	-30.0	-31.2	-76.0

As far as the packing arrangements are concerned, none of the other tricyclic antidepressants analyzed can give a hydrogen bond motif similar to those encountered in the two forms of nortriptyline, as the protonated forms (shown in Figure 4.6) of amitriptyline, dothiepin and cyclobenzaprine only have one hydrogen bond donor, the hydrogen on the ammonium group. This is due to the presence of a methyl group bonded to the nitrogen atom. Therefore, it is impossible for the molecules to form the long $C_4^2(4)$ chains found in **NOR*HCl$_\alpha$** and **NOR*HCl$_\beta$**. In all the other structures, amitriptyline, dothiepin and cyclobenzaprine hydrochloride, only discrete hydrogen bonds between the ammonium groups and the chlorine ion exist. No more complex hydrogen bond structures are present. In particular, amitriptyline and dothiepin were found to be isostructural, the only difference being the presence on the seven-membered ring of dothiepin of a sulphur atom instead of a methylene group. In the case of the tricyclic antidepressants analysed, therefore, the ability to form hydrogen bonds and the existence of different *anti* conformations are the driving force of crystal structure formation.

The fact that four different crystalline structures (**NOR*HCl$_\alpha$**, **NOR*HCl$_\beta$**, amitriptyline hydrochloride and dothiepin hydrochloride) all contain molecules in the *anti* conformation, suggests that the adoption of the *syn/anti* conformation in the solid-state is likely driven by intermolecular interactions,

rather than evident stereochemical (*intra*molecular) effects. The *anti* conformation stereochemical preference, however, is not ubiquitous in the solid state of related chemical structures, since a rare case of a *syn* disposition has been found in the crystal structure of an analogous species having antiallergic activity, the formula of which is reported in Scheme 4.5. [15] In this case, however, the structure is not directly comparable with the tricyclic antidepressants reported above for several reasons. First of all, the conformation of the side chain is influenced by the presence, on one of the aryls, of a -CH_2COO^- residue, involved in complex hydrogen bonding with the protonated amino group. Secondly, the single crystal structure solved is of the free base (in zwitterionic form) and not of the hydrochloride salt. Moreover, the phase is a trihydrate, not an anhydrous phase like the ones presented in the previous paragraphs.

Scheme 4.5. Molecular structure (shown in neutral form) and crystal data of a chemical analogue to tricyclic antidepressants (e.s.d.'s in parentheses).

Reference	[15]
Chemical Forumula	$C_{21}H_{23}NO_3 \cdot 3H_2O$
Crystal System	Monoclinic
Space Group	$P2_1$
a [Å]	12.4158 (9)
b [Å]	19.209 (2)
c [Å]	8.7081 (7)
β [°]	92.924 (6)
V [Å³] , Z	2074.1, 4

4.2 Thermal Analysis and Thermodynamic Considerations

As discussed in previous chapters, the knowledge of the thermodynamic relations between different polymorphic forms can be crucial to the understanding of polymorphic behavior. For this reason, the relationship between **NOR*HCl$_\alpha$** and **NOR*HCl$_\beta$** was investigated using thermal methods.

4.2.1 DSC Analysis

DSC analysis often gives precious information regarding thermodynamic relationships. However, in this case, it doesn't help much. Both polymorphs

NOR*HCl$_\alpha$ and **NOR*HCl$_\beta$** show only one thermal event, an endothermic peak having a nearly identical onset temperature of 216-217°C (see Figure 4.7). This was attributed to a melting event, as verified by visual observation with a melting point apparatus. However, the fusion enthalpy was found to be different for the two forms, higher for **NOR*HCl$_\alpha$** (34.3 kJ mol^{-1}) than for **NOR*HCl$_\beta$** (32.2 kJ mol^{-1}).

Figure 4.7. DSC characterization of **NOR*HCl$_\alpha$** (a) and **NOR*HCl$_\beta$** (b). The analyses were run between 30 and 220°C at 10°C/min under nitrogen flow.
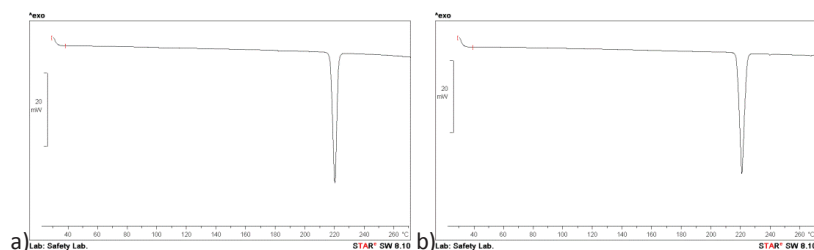
4.2.2 Thermodiffractometry

As DSC analyses alone could not unravel the thermodynamic relationships between the forms, thermodiffractometric analyses were also carried out on **NOR*HCl$_\alpha$** and **NOR*HCl$_\beta$**. Consistently with what observed in the DSC traces, both crystalline forms remained substantially unchanged up to the melting point, with minor peak shifts, attributed to thermal expansion. The linear thermal expansion coefficients, $\partial\ln x/\partial T$ ($x = a, b, c$), derived by the parametric approach described by Stinton and Evans, [16] are reported in Table 4.5, and show manifestly different trends, with very anisotropic inflation (or, for **NOR*HCl$_\beta$**, even shortening of the **b** axis). A closer look into the crystal packing did not reveal any specific (or evident to us) reason for these observations (particularly the shrinking of **b** in the **NOR*HCl$_\beta$** phase), which, however, speak for a rather different flexibility of the frameworks, *unrelated* to chain propagation axes.

Upon melting, form **NOR*HCl$_\beta$** converted into form **NOR*HCl$_\alpha$**. This was demonstrated by keeping a sample of **NOR*HCl$_\beta$** close to the melting point and

collecting several XRPD spectra in isothermal conditions and following the **NOR*HCl$_\beta$→NOR*HCl$_\alpha$** transition (see Figure 4.8). This event, not observed in the DSC trace, can be easily explained by the thermal gradients present in the sample positioned in diffractometer chamber, which, open to the air (see Chapter 2, section 2.1.5), induces melting and subsequent recrystallization near the (slightly colder) surface.

Table 4.5. Linear thermal expansion coefficients expressed in [10^{-6} K^{-1}] for **NOR*HCl$_\alpha$** and **NOR*HCl$_\beta$**. The order of the axes for **NOR*HCl$_\beta$** has been rearranged to reflect geometrical similarities between the axes of the two phases, as shown in Table 4.1.

	NOR*HCl$_\alpha$		**NOR*HCl$_\beta$**
∂ln$a$/∂T	17.1	∂ln$c$/∂T	50.8
∂ln$b$/∂T	28.8	∂ln$a$/∂T	123.6
∂ln$c$/∂T	82.3	∂ln$b$/∂T	-3.1

Figure 4.8. Thermodiffractometric plots for **NOR*HCl_α** (top) and **NOR*HCl_β** (bottom).
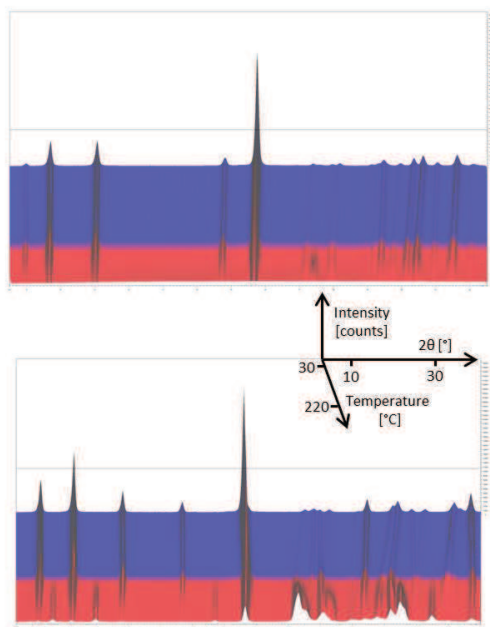
Horizontal scale: 10<2ϑ<30°; powder diffraction traces were recorded in isothermal conditions from room temperature, up to 220°C, in 20°C steps. Blue traces in the background are lower temperature scans, the red traces in the foreground are higher temperature scans

4.2.3 Thermodynamic Relationship between polymorphs

The higher fusion enthalpy of **NOR*HCl_α**, coupled with the fact that **NOR*HCl_β** converts into form **NOR*HCl_α** upon melting and recrystallization, suggest that the two crystalline forms are monotropically related to one another, with form **NOR*HCl_α** more stable than **NOR*HCl_β** *at every temperature*. This hypothesis is supported by the fact that the form that crystallizes out of the

131

melt, regardless of the cooling rate and of the starting polymorph, appears *always* to be **NOR*HCl$_\alpha$**. However, the similarities in melting points and fusion enthalpies, as well as the crystal structure analogies, suggest the two forms have only small differences in energy and stability. This is demonstrated by the fact that both polymorphs are indefinitely stable once isolated. Moreover, the supramolecular organization in infinitely-long hydrogen-bonded chains of the different conformers discussed above can help explain the lack of interconversion from **NOR*HCl$_\beta$** to **NOR*HCl$_\alpha$** unless melting occurs, as mentioned earlier, effectively severing the whole hydrogen bond system within the crystal.

References

1. U'Prichard, D.C., Greenberg, D.A., Sheehan, P.P., Snyder, S.H., *Science, 199* (**1978**), 197-198.

2. Zohar, J., Westenberg, H. G. M., *Acta Psychiatrica Scandinavica, 101* (**2000**), 39–49.

3. Amidon, G.L., Lennernas, H., Shah, V.P., Crison, J.R., *Pharmaceutical Research, 12* (**1995**), 413-420.

4. Yu, L.W., Amidon, G.L., Polli, J.E., Zhao, H., Mehta, M.U., Conner, D.P., Shah, V.P., Lesko, L.J., Chen, M.L., Lee, V.H., Hussain, A.S., *Pharmaceutical Research 19* (**2002**), 921-925.

5. Klein, C.L., Lear, J., O'Rourke, S., Williams, S., Liang, L*., Journal of Pharmaceutical Sciences, 83* (**1994**), 1253-1256.

6. Siddedowda, M.S., Jasinski, J.P., Golen, J.A., Yathirajan, H.S., Swamy, M.T., *Acta Crystallographica, E67* (**2011**), 1846.

7. Bandoli, G., Nicolini, M., Casellato, U., *Journal of Chemical Crystallography, 17* (**1987**), 281-293.

8. MacCalman, M.L., Roberts, K.J., Hendriksen, B.A*., Journal of Crystal Growth, 128* (**1993**), 1218-1224.

9. Klein, C.L., Banks, T.A., Rouselle, D., *Acta Crystallographica, C47* (**1991**) 1478-1480.

10. Vladiskovic, C., Masciocchi, N., *Journal of Pharmaceutical Sciences, 101* (**2012**), 4481–4489.

11. Marone, S., Rozas, I., Weaver, D.F., *Journal of Molecular Structure, 467* (**199**), 25-30.

12. Munro, S., Craik, D.J., Andrews, P., *Moleular Informatics, QSAR, 6* (**1987**), 104-110.

13. Casarotto, M.G., Craik, J., *Journal of Pharmaceutical Sciences, 90* (**2001**), 713-721.

14. Jablan S.V., 1995. Theory of Symmetry and Ornament. Mathematical Institute, Belgrade, Yugoslavia.

15. Ohshima, E., Otaki, S., Sato, K., Kumazawa, T., Obase, H., Ishii, A., Ishii, H., Ohmori, K., Hirayama, N., *Journal of Medicinal Chemistry, 35* (**1992**), 2074-2084.

16. Stinton, G.W., Evans, J.S.O*., Journal of Applied Crystallography, 40* (**2007**), 87-95.

5. Interconverting Polymorphs of Ibuprofen Lysinate

Solid-solid phase transitions between polymorphs can be induced by temperature, pressure, humidity, presence of solvents and other factors. The understanding of the characterisitics of a phase transition and the conditions in which it takes place, along with the knowledge of reversibility, can be very important. In particular, temperature-phase transitions are crucial in API polymophism. As many industrial processes, including drying, granulation and melt-extrusion, can involve heating, the detailed knowledge of the behavior of active pharmaceutical ingredients at temperatures above ambient conditions can be useful.

The most important types of phase transitions between polymorphs [1] are:

a) Displacive transformations of secondary coordination, where the crystal lattice is deformed but not broken.
b) Reconstructive transformations of secondary coordination, where the lattice framework is broken and reformed into a new arrangement.
c) Reorientation transformations of disorder, where some intermolecular bonds are broken and reformed to accommodate changes in conformation of the constituent molecules.

Generally, temperature-induced phase transitions of any kind are accompanied by change, typically – upon heating – increase, in symmetry. However, in some cases, symmetry is preserved. These kinds of transformations, more often induced by pressure but occasionally also by temperature, are called

isosymmetric and are relatively rare and difficult to study in organic molecules. [2] In isosymmetric transformations, not only does the space group remain the same before and after the transitions, but both phases are made up of the same atoms occupying the same Wyckoff positions. This implies that the transition is accompanied by an abrupt (but small) change in volume and lattice constants, but not of space group. Occasionally, these kinds of transitions are difficult to detect because the changes are often so small they can sometimes be misinterpreted as continuous lattice modifications due to temperature or pressure.

5.1 Thermal Behavior of Ibuprofen Lysinate

Ibuprofen, or (RS)-2-(4-(2-methylpropyl)phenyl)propanoic acid, is a well-known, over-the-counter analgesic belonging to the class of nonsteroidal anti-inflammatory drugs (NSAID). [3] Ibuprofen is a non-selective cyclooxygenase (COX) inhibitor, acting on both COX-1 and COX-2 forms. However, most of its effect is achieved through COX-2 inhibition. [4] It is widely used for pain relief, fever and inflammatory diseases. Known from the 1960's, it has been marketed in a great variety of forms and under numerous trade names. Although very effective as an anti-inflammatory drug, Ibuprofen in the free acid form has a low solubility which causes a slow onset of therapeutic efficacy. For this reason, different salts having better solubility characteristics have been studied, in particular the lysine [5] and sodium salts. [6] While the crystal structures and solid state characteristics of both ibuprofen free acid [7, 8] and ibuprofen sodium salt [9] have been studied, the lysine salt of ibuprofen, shown in Scheme 5.1, remains relatively absent from solid state literature. This is surprising, considering the widespread use made of ibuprofen lysine salt in solid formulations.

Scheme 5.1. Ibuprofen Lysine salt (represented in the neutral form).

136
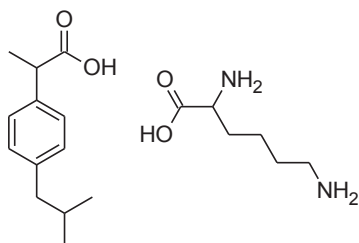
The only known characteristic of the lysine salt of ibuprofen is the existence of a reversible polymorphic conversion occurring upon heating. [10] Ibuprofen lysine salt therefore exists in two different polymorphic forms, one existing at lower temperatures and one existing at higher temperature. As no denomination has been previously used for the two forms of ibuprofen lysine salt, the crystal form which exists at room temperature will be referred to as **IBL-I**, while the high temperature crystal form will be referred to as **IBL-II**.

5.1.1 DSC Analysis

The DSC analysis of ibuprofen lysine salt, reported in Figure 5.1a, shows a small but sharp endothermic transition at about 70°C (onset temperature 69.5°C with a heating rate of 10°C min^{-1}, ΔH = +2.3 kJ mol^{-1}) and a melting event at 182.8°C (ΔH_{fus} = +58.4 kJ mol^{-1}). The endothermic event around 70°C is reported in the literature as being a fully reversible transition into another polymorph. [11] This was verified by using a custom-made temperature program, heating a sample of Ibuprofen lysine salt to 90°C and cooling back to room temperature to observe the reversibility of the transitions (as shown in Figure 5.1b). In order to determine the transition temperature at nearly equilibrium conditions (zero heating rate), DSC analyses were run at different heating rates (2, 5 and 10°C min^{-1}). The observed transition temperature (evaluated using the onset method, see Chapter 2) at each heating rate was plotted as a function of the heating rate (as shown in Figure 5.2) and the transition temperature at zero heating rate was extrapolated (R^2=0.9989), yielding the value 67.6°C.

Figure 5.1. DSC Analyses of Ibuprofen lysine salt, showing a) the endothermic transition from **IBL-I** to **IBL-II** followed by fusion and b) the fully reversible nature of the transition.
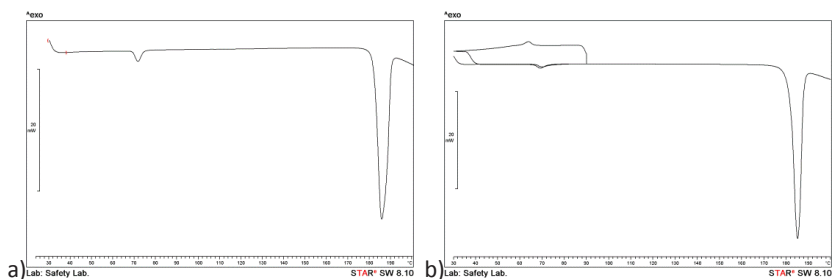
Figure 5.2. Extrapolation of the temperature of **IBL-I→IBL-II** at heating rate zero.
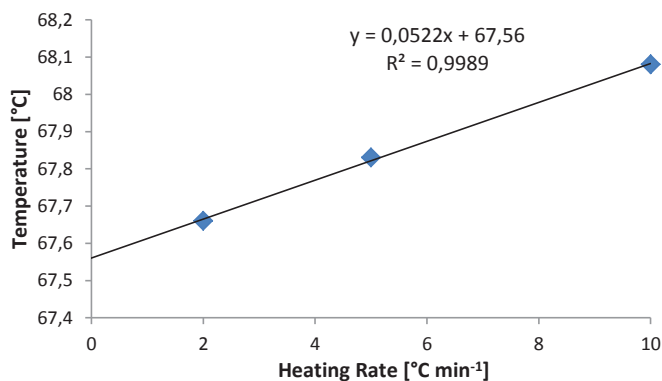
5.1.2 Thermodiffractometry

The sharp transition between **IBL-I** and **IBL-II** observed in the DSC analyses was followed using thermodiffractometric methods. An extract of the data collected is reported in Figure 5.3. The transition was found to be quite evident, even though the diffraction profile of the two forms shows many similarities. In particular, the XRPD traces of forms **IBL-I** and **IBL-II**, shown in the range 3-25° in 2θ in Figure 5.4, appear to differ only slightly in the more intense peaks at low

138

angles, suggesting similarities in the lattice constants. The phase transition was observed between 70 and 90°C similarly to what observed in DSC, but traces of **IBL-I** were visible up to about 110°C, when the conversion was complete. This can be attributed to the fact that the heated sample holder used is open to air. This can cause a temperature gradient in the sample, where the sample portion in contact with the sample holder is significantly warmer than the portion in contact with air at room temperature. The sample holder must therefore be heated to a higher temperature in order to ensure the whole sample is well above 70°C.

Figure 5.3. Thermodiffractometry (7-14° in 2θ portion) of **IBL-I** (blue area), showing the conversion into **IBL-II** (red area) at about 70°C.
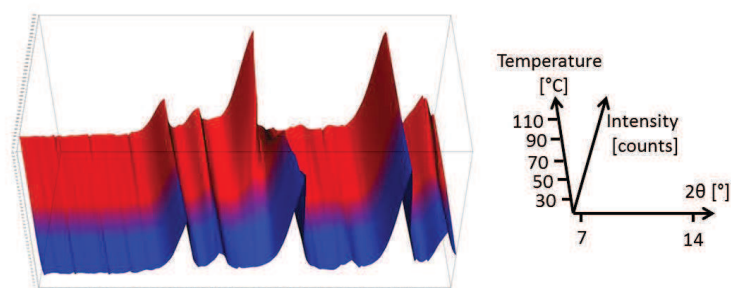
Figure 5.4. Overlaid powder diffractograms of **IBL-I** measured at room temperature (blue) and **IBL-II** measured at 110°C (red) in the 3-25° in 2θ range.
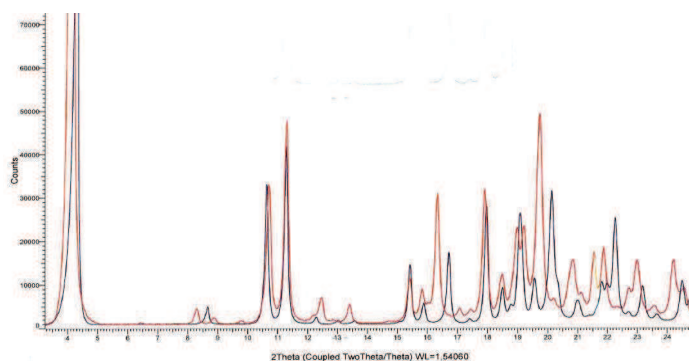
5.2 Structural Analysis

The structures of the two phases, **IBL-I** and **IBL-II**, were solved from powder diffraction data. Thermodiffractometric methods allowed to acquire powder diffraction data for **IBL-II** at 110°C, but it was not possible to explore the full range usually used for structure solution, because the aluminum heated sample holder did not allow the quality needed for structure solution at high angles. Moreover, keeping the sample overnight at 110°C (as a full range diffractogram usually requires about 15 hours of measurement to yield satisfactory results at high angles) might have degraded the sample. It was therefore unadvisable to collect such a wide range. For form **IBL-I,** an acquisition using transmission geometry on a cylindrical sample was preferred, due to marked preferred orientation effects. Indexing of **IBL-II** proved to be difficult, as no unique or sensible solution was found by the conventional methods described in Chapter 2 (probably because of uncontrolled instrumental effects and evident peak broadening and overlap). However, the reversibility of the phase transition and the already mentioned similarity of some of the low-angle diffraction features allowed to estimate the cell parameters of **IBL-II** using a "deformation" of the pristine cell, made accessible by the use of the CELL program. [12]

5.2.1 Crystal Data

The crystal data for both phases is reported in Table 5.1, while Figure 5.5 shows the final Rietveld refinement plots. The identity of the space group in the two phases and the analogies in the cell constants, explaining the similarities between the XRPD traces, suggest a strong structural correlation between the phases. As is to be expected, the higher temperature phase, **IBL-II**, appears to be less dense. However, the difference between **IBL-I** and **IBL-II,** though small, is too large to be attributable merely to thermal expansion. Moreover, the expansion is very anisotropic. In fact, while on the **b** axis there is a strong expansion (about 5 %), axis **a** exhibits only a very small contraction (about 0.2%). This thermally induced kind of strain cannot be attributed to vibrational effects only and must be attributed to structural reasons, *i.e.* an isosymmetric displacive phase transition.

Figure 5.5. Final Rietveld refinement plot for a) **IBL-I** and b) **IBL-II**. For **IBL-I**, the insert shows the high angle portion magnified 5x. For **IBL-II**, the high angle portion was not acquired, as explained in the text. The two peaks of the heated aluminum sample holder (visible) were modelled separately using the Fundamental Parameter Approach.

a)

b)
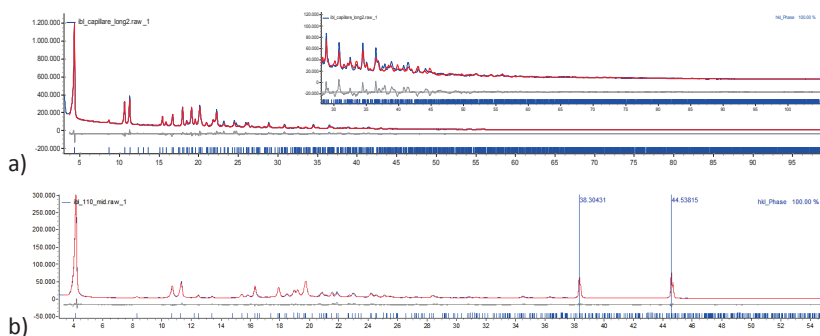
Table 5.1. Comparative crystal cell data of forms **IBL-I** and **IBL-II.** *(E.s.d.'s in parentheses).*

	IBL-I	IBL-II
Chemical Formula	$C_{19}H_{32}N_2O_4$	$C_{19}H_{32}N_2O_4$
Formula weight [g mol^{-1}]	352.47	352.47
Crystal System	Monoclinic	Monoclinic
Space Group	$P2_1/n$	$P2_1/n$
a [Å]	8.4664(6)	8.450(1)
b [Å]	40.619(3)	42.619(7)
c [Å]	5.7929(4)	5.8226(6)
β [°]	86.326(7)	85.72 (1)
V [Å^3] , Z	1988.1(2), 4	2091.1(5), 4
V/Z	497	523
T [K]	298	383
λ [Å]	1.5418	1.5418
ρ$_{(calc)}$ [g cm^{-1}]	1.178	1.120
μ [mm^{-1}]	0.665	0.632
R$_{Bragg}$	0.050	0.042

5.2.2 Structural Comparison

The conformation of the ibuprofen and lysine molecules was described by two separate set of dihedral angles, shown in Scheme 5.2.

Scheme 5.2. Torsion angles used to describe the molecular conformation for Ibuprofen and lysine.
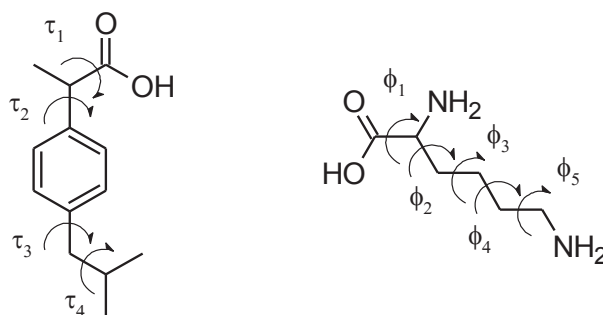
The conformation of the ibuprofen and lysine molecules in **IBL-I** and **IBL-II** was found to be rather similar, as is clearly shown in Figure 5.6. When comparing the dihedral angles used to describe molecular conformation, as is done in Table 5.2, the value which appears to change the most from one phase to the other for the ibuprofen molecule is τ_3, responsible for the orientation of the isopropyl group of ibuprofen, going from about 56° to about 67°. The other values have variations below 2°. This will be further explored and explained in the following paragraphs. The lysine molecule changes slightly from **IBL-I** to **IBL-II**, with three out of five dihedral angles varying of between 10 and 15°. This can be due to the fact that lysine has three functional groups involved in a complex hydrogen bonding structure, as described below. Therefore, even a small change in the positioning relative to the ibuprofen molecule, due to the phase transition, will cause the whole lysine molecule to slightly rearrange.

Table 5.2. Synoptic collection of the most relevant conformational features of the Ibuprofen and Lysine molecule (τ_{1-4} and φ_{1-5}, respectively, as defined in Scheme 5.2) for forms **IBL-I** and **IBL-II** *(E.s.d.'s in parentheses).*

	IBL-I	IBL-II
τ_1 [°]	103.6(5)	101.8(9)
τ_2 [°]	-16.7(8)	-18(1)
τ_3 [°]	56.3(2)	66.5(3)
τ_4 [°]	-161.2(4)	-160.2(7)
ϕ_1 [°]	177.3(4)	162.9(7)
ϕ_2 [°]	-93.9(2)	-98.7(3)
ϕ_3 [°]	-76.4(2)	-86.8(3)
ϕ_4 [°]	-79.7(3)	-74.4(5)
ϕ_5 [°]	133.9(5)	146.2(9)

Figure 5.6. Conformation of Ibuprofen and lysine molecules in a) **IBL-I** and b) **IBL-II.** The most different portions for each molecule are indicated by colored circles (see actual torsion angles collected in Table 5.2).

a)   b
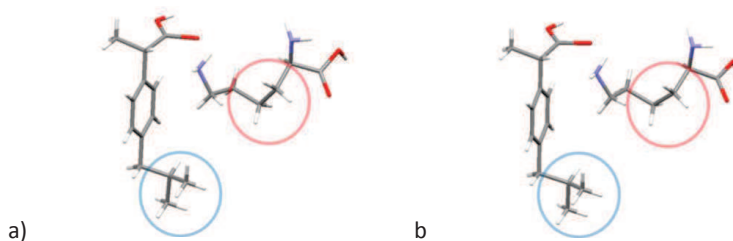
Interestingly, the hydrogen bonding scheme, identical in the two phases, is quite complex. Using the Graph set notation [13, 14] to analyze the hydrogen bonding scheme, five different kinds of discrete hydrogen bonds are identified (first order motifs), which then combine in several different second order patterns, including a $R_2^2(6)$ ring structure and several chain structures. The hydrogen bonding in **IBL-I** and **IBL-II** is depicted in Scheme 5.3. Worthy of note, as X-ray diffraction does not usually allow to determine hydrogen positions, much

less structure solution from powder data, the structures of Ibuprofen lysine salt here reported were solved using neutral ibuprofen and lysine molecules. As can be observed in the hydrogen bonding scheme depicted in Scheme 5.3, the carboxyl group of ibuprofen ($C_9O_1O_2H_6$) is involved in hydrogen bonding with the more basic amine group of lysine ($N_2H_{31}H_{32}$). The hydrogen, though positioned *by us* on the carboxyl group, could also be positioned on the amine group. Other techniques are necessary to determine the degree of proton transfer. Considering the significant difference between the pKa values of Ibuprofen [15] and lysine, the proton transfer should be considered complete and the proton should be positioned on the nitrogen atom of the lysine side chain.

Scheme 5.3**.** a) Hydrogen bonding present in both **IBL-I** and **IBL-II** and b) atom numbering for the ibuprofen and lysine molecules.

a)

b)
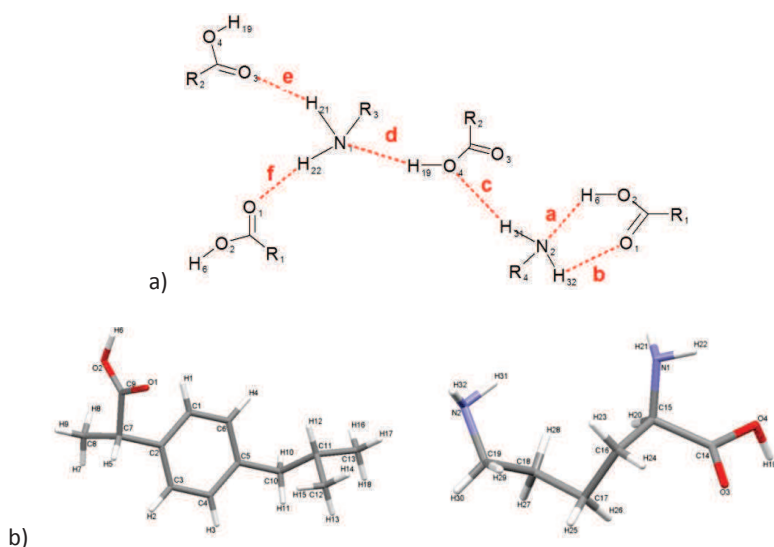
The analysis of the packing of ibuprofen and lysine molecules in forms **IBL-I** and **IBL-II** confirms the similarities already observed in lattice constants and molecular conformation, as can be seen in Figure 5.7. In both phases, the molecules are stacked so that the more hydrophilic groups (the whole lysine molecule and the carboxyl group of the ibuprofen molecule), responsible for the

144

hydrogen bonding, are organized in long and complex chains, while the more hydrophobic groups (the aromatic ring and isopropyl group of the ibuprofen molecules) are interacting with each other in long columns along the **a** axis, separately from the more polar groups.

Figure 5.7. Packing of Ibuprofen and lysine molecules in **IBL-I** and **IBL-II** viewed along the **c** axis. The red rectangles indicate the areas where the hydrogen bonding is located.

a)   b)
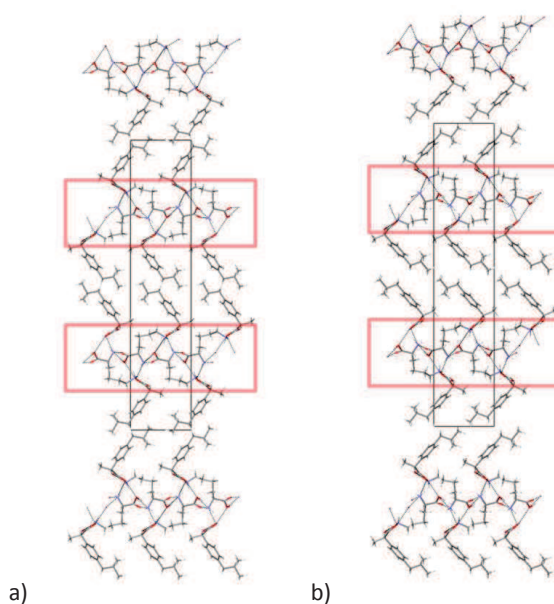
In order to understand the most significant differences between the structures of **IBL-I** and **IBL-II**, the thermal and structural strain tensors were calculated for comparable temperature differences. The thermal strain tensor was evaluated by refining cell parameters for **IBL-I** at 30 and 70°C and calculating the resulting strain tensor using a publicly available software tool [16, 17]. The structural strain tensor was evaluated using the cell of **IBL-I** refined at 70°C and the cell of **IBL-II** at 110°C. The tensors thus obtained were plotted using WinTensor[TM] [18] and compared (see Figure 5.8). The first obvious difference

between the thermal and structural strain tensors is the size, as the structural strain tensor is about an order of magnitude larger than the thermal tensor. This is particularly evident in Figure 5.8c, where the thermal strain tensor is plotted on a scale ten times smaller and is comparable in size with the structural strain tensor reported in Figure 5.8b. Secondly, even though the general shape is the same in both cases, the thermal strain is always positive (even though anisotropic), while the structural strain tensor has negative values (though small) in one direction (shown in Figure 5.8b as red areas). Thirdly, both the structural and the thermal strain tensors have the largest component in the same direction, in particular along the **b** axis. All together, these observations, together with the variation in dihedral angle τ_3 (responsible for the orientation of the isopropyl group of the ibuprofen molecule, as discussed previously) and the similarities of the hydrogen bonding scheme in the two phases, gave indication as to where to look to find the key differences between the structures of **IBL-I** and **IBL-II.**

Figure 5.8. Graphical representations of the a) structural and b) thermal strain tensors represented on the same scale and c) an expansion (10x) of the thermal strain tensor to show its shape. x, y and z are orthogonal coordinates, nearly, or exactly, aligned with **a**, **b** and **c**.
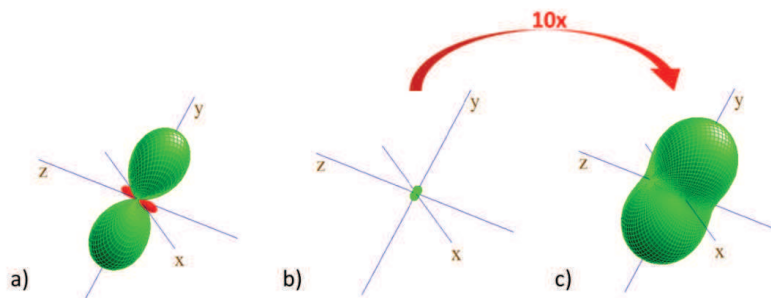
A closer inspection of the hydrophobic areas of the crystal structures allowed to understand not only the key differences between **IBL-I** and **IBL-II**, but especially the driving force of the phase transition. In fact, while in **IBL-I** the isopropyl groups are lodged into one another, in **IBL-II** they are "unfastened" and almost one next to the other. This is shown in Figure 5.9. The shape of the thermal strain tensor suggests that, upon heating, the structure of **IBL-I** expands

anisotropically in all directions, causing the isopropyl groups to move away from each other. When a critical distance is reached, the isopropyl groups disengage, causing the conversion from **IBL-I** to **IBL-II** to occur. Figure 5.10 schematically explains this transformation, which also explains the small shortening of the **a** axis: the disengaged isopropyl groups, having moved free of one another along the **b** axis, can now move closer along the **a** axis. The major difference between forms **IBL-I** and **IBL-II**, therefore, is the distance between neighboring ibuprofen molecules.

Figure 5.9. Closer view of **IBL-I** and **IBL-II** packing to show the differences in the relative positions of adjacent isopropyl groups (highlighted by blue circles).

a)   b)
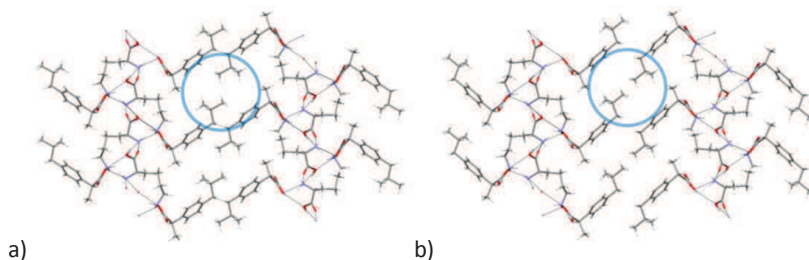
Figure 5.10. Schematic representation of a) thermal expansion and b) structural modification induced by the disengagement of the isopropyl groups of adjacent ibuprofen molecules.

a)   b)
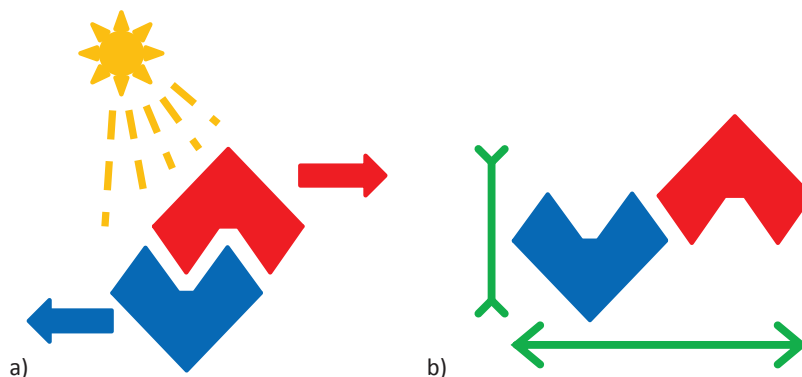
References

1. Brittain, H. G., Solid State Phase Transformations, in *Polymorphism of Pharmaceutical Solids, 2nd Edition*, Brittain, H. G. (ed), Informa Healthcare, New York (**2009**).

2. Ellena, J., de Paula, K., de Melo, C. C., da Silva, C. C. P., Bezerra, B. P., Venancio, T., Ayala, A. P., *Crystal Growth & Design, 14* (**2014**), 5700-5709.

3. Davies, N.M., *Clinical Pharmacokinetics, 34* (**1998**), 101-154.

4. Neupert, W., Brugger, R., Euchenhofer, C., Brune, K., Geisslinger, G., *British Journal of Pharmacology, 122* (**1997**), 487-492.

5. Geisslinger, G., Dietzel, K., Bezler, H., Nuernberg, B., Brune, K., *International Journal of Clinical Pharmacology, Therapy, and Toxicology, 27* (**1989**), 324-328.

6. Fini, A., Zecchi, V., Rodriguez, L., Tartarini, A., *Pharmaceutica Acta Helvetiae, 59* (**1984**), 106-108.

7. Shankland, N., Wilson, C. C., Florence, A. J., Cox, P. J., *Acta Crystallographica, C53* (**1997**), 951-954.

8. Goossens, D. J., Heerdegen, A. P., Welberry, T. R., Beasley, A. G., *International Journal of Pharmaceutics, 343* (**2007**), 59-68.

9. Zhang, Y., Grant, D. J. W., *Acta Crystallographica, 61* (**2005**), m435-m438.

10. Tung, H.-H., Paul, E. L., Midler, M., McCauley, J. A., Polymorphism, in *Crystallization of Organic Compounds – An Industrial Perspective*, John Wiley & Sons (**2009**), Hoboken, New Jersey, pp. 61-62.

11. McCauley, J.A., *American Institute of Chemical Engineers Symposium Series, 87* (**1991**), 58-63.

12. Huang, T.C., Masciocchi, N., Parrish, W., unpublished.

13. Etter, M.C., MacDonald, J.C., Bernstein, J., *Acta Cystallographica, B46* (**1990**), 256-262.

14. Bernstein, J., *Polymorphism in Molecular Crystals*, Clarendon Press, Oxford, (**2002**).

15. Melouna, M., Bordovska, S., Galla, L., *Journal of Pharmaceutical and Biomedical Analysis, 45* (**2007**), 552–564.

16. Ohashi, Y., STRAIN, http://www.cryst.ehu.es/cryst/strain.html.

17. Razen, R. M., Finger, L. W., *Comparative Crystal Chemistry: Temperature, Pressure, Composition and the Variation of Crystal Structure*, Wiley, (**1984**), New York, pp. 92-102.

18. Kaminsky, W., *Zeitschrift für Kristallographie Supplement, 17* (**2000**), 51.

6. Quantitation Methods: Venlafaxine Hydrochloride

6.1 Quantitation of Polymorphs

The importance of quantitation of different crystalline forms in a sample has already been discussed in previous Chapters. Many different techniques have been successfully employed for quantitative phase analysis of pharmaceutical solids, including infra-red spectroscopy (both mid- and near-IR), X-ray powder diffraction, thermal methods and SS-NMR. However, not all techniques are equally suited to all cases. For example, while infra-red spectroscopy can yield excellent results in cases where the hydrogen bonding scheme is very different in the phases to be analyzed, [1] it is not as successful in cases where there are similarities in the hydrogen bonding scheme of phases. In fact, infra-red spectroscopy is particularly sensitive to specific molecular features, like X-H bond overtones and combinations. [2] Different hydrogen bonding schemes will therefore generate very different IR spectra. Conversely, similar hydrogen-bonding schemes will often lead to similar IR spectra, as is the case with nortriptyline polymorphs **NOR*HCl$_\alpha$** and **NOR*HCl$_\beta$** discussed in Chapter 4 (the IR spectra for **NOR*HCl$_\alpha$** and **NOR*HCl$_\beta$** are reported in Figure 6.1).

Differential Scanning Calorimetry, on the other hand, can generally only be used for quantitative phase analysis when quantifying a solvate or a hydrate in an anhydrous form, like for example the quantitation of lactose monohydrate, done by using the well-defined dehydration peak. [3]

Figure 6.1. Infra-red spectra of a) **NOR*HCl$_\alpha$** and b) **NOR*HCl$_\beta$** collected in the range 4000-650 cm^{-1}.
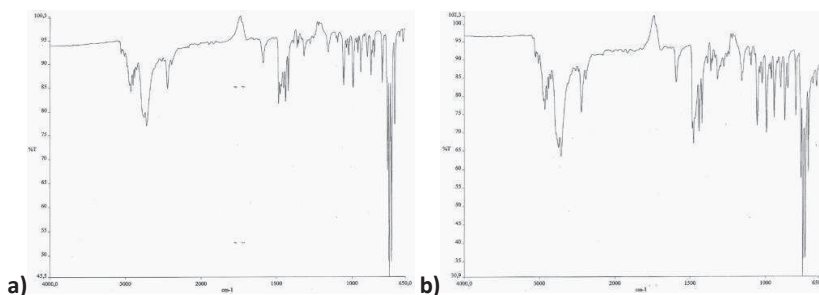
The only instrumental technique which always yields a unique response for each different crystalline form is X-ray diffraction. This is the main advantage of X-ray powder diffraction over other instrumental techniques used for quantification. [4] XRPD data, however, can be used in different ways to yield quantitative information. The most common quantitation methods used are the single peak method and the Rietveld method. [5] Both methods have advantages and disadvantages. The single peak method requires the identification of a well-defined, isolated and possibly intense peak for each phase analyzed. Subsequently, it requires the construction of a calibration curve, therefore monophasic samples of all the phases under examination must be available. [6] The Rietveld method, generally recognized as more precise and accurate than the single peak method, requires the knowledge of the crystal structures of all phases analyzed. [7] This can be difficult to obtain when dealing with polymorphs of API's.

In the Rietveld method, the ratio between the analyzed crystalline forms is obtained by simulating the powder diffraction profile of the various phases using the knowledge of the crystal structure and then varying the scale factor for each phase to fit the experimental data. No monophasic standard is required and there is no need to construct calibration curves. However, the main advantage of the Rietveld method over the single peak method is the fact that it uses the full diffraction profile and is therefore much less affected by preferred orientation

150

effects. Preferred orientation, rather common in crystalline forms of API's, is a major source of error for XPRD quantitation. [8]

One of the disadvantages of the Rietveld method is its complex nature. Calculations of the powder diffraction profiles from the crystal structure are necessary. Many software programs are available to carry out Rietveld calculations, including TOPAS-R [9] and QUANTO. [10]

6.1.2 Proposed Method

As the strongest advantage of the Rietveld method over other quantitation methods based on XRPD is the use of the full diffraction profile, while the main disadvantage is the requirement of the knowledge of the crystalline structures, a full-profile quantitation method using extracted intensities but does not require full structure characterization has been proposed, as described in Chapter 2, paragraph 2.2.4. [11] This method, which makes use of the Wilson plot to put experimental extracted intensities on the absolute scale in absence of a structural model, is implemented in the quantitative phase analysis (QPA) program QUANTO. Analogously to other XRPD quantitation methods, samples of the pure phases to be quantified are necessary for intensity extraction, but no calibration curve is needed. Worthy of note, the knowledge of the lattice parameters is necessary for correct indexing and intensity extraction, but lattice parameter determination is much easier than full structure determination and can be carried out reasonably quickly from powder data, as described in Chapter 2, paragraph 2.2.1.

As the structure-less full-profile method implemented in the software QUANTO has not been fully tested on API's, having been used only once, [12] it was decided to select a test API candidate and to compare the results obtainable from the structure-less method with the classical Rietveld approach.

6.2 Quantitative Phase Analysis on Venlafaxine Hydrochloride

Venlafaxine, or (RS)-1-[2-dimethylamino-1-(4-methoxyphenyl)-ethyl]cyclohexanol, shown in Scheme 6.1, is an antidepressant which acts as a

serotonin and norepinephrine reuptake inhibitor. Known since the 1990's, it is marketed as a hydrochloride salt.

Scheme 6.1. Venlafaxine Hydrochloride
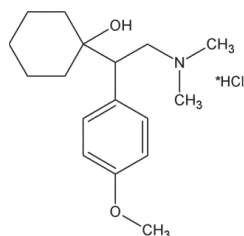
Venlafaxine hydrochloride is known to exhibit polymorphism, crystallizing in two anhydrous forms (forms I and II). The structures of both forms have been solved from single crystal X-ray diffraction and have been reported in the literature. [13, 14] The powder diffractograms for forms I and II, reported in Figure 6.2, show some overlapping but appear suitable for quantification using XRPD, as many intense peaks don't overlap. Interestingly, form II (red trace in Figure 6.2) has several intense peaks well isolated from peaks of form I, but the opposite is not true. This means small amounts of form II in form I might be easier to detect and quantify than the reverse.

Figure 6.2. Overlaid powder diffractograms of Venlafaxine hydrochloride form I (black line) and of Venlafaxine hydrochloride form II (red line)in the 5-35° in 2θ range.
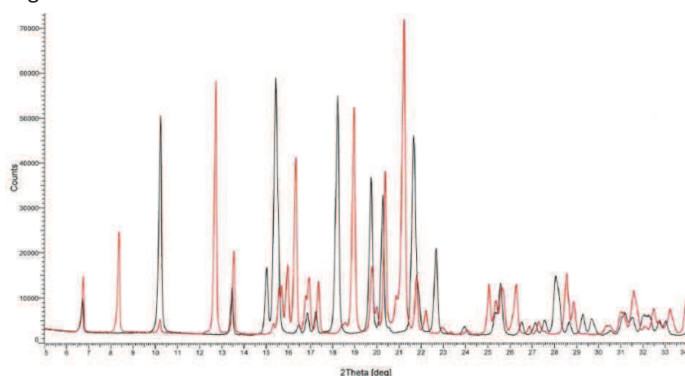
Venlafaxine hydrochloride was therefore chosen to test the structure-less full-profile quantitation method and compare the results with the classical Rietveld approach. Binary mixtures of Venlafaxine hydrochloride forms I and II were prepared in the range 5-95% w/w.

6.2.1 Preparation of Binary Mixtures

Venlafaxine hydrochloride form I was supplied by Dipharma Francis Srl. Form II was prepared by dissolving 13.5 g of Venlafaxine hydrochloride form I in 170 ml of refluxing isopropanol and cooling slowly back to room temperature. After filtration, the sample was dried under vacuum at 50°C overnight. In order to minimize preferred orientation and to make mixing more efficient, samples of both forms were ground in a mortar with a pestle and sieved using a 32 μm steel sieve. Karl Fischer analysis confirmed the samples to be anhydrous. Details of the preparation of the binary mixtures is reported in Table 6.1.

Table 6.1. Binary mixtures of Venlafaxine hydrochloride forms I and II.

Mixture	Venlafaxine hydrochloride form I [mg]	Venlafaxine hydrochloride form II [mg]	Nominal Composition [%form I: %form II]
A	190.66	190.73	50:50
B	239.18	82.10	75:25
C	95.46	284.36	25:75
D	455.97	23.96	95:5
E	22.18	419.26	5:95

Diffractograms of the pure phases and the five mixtures were collected in the range 5-105° in 2θ. Intensities were extracted from the diffractograms of the pure phases using the lattice parameters reported in the literature using the QUANTO program. The intensities thus obtained were stored in separate files which could subsequently be used by QUANTO for quantitation. During the quantitation calculations using extracted intensity files, the software automatically puts the extracted intensities on the absolute scale using the Wilson plot.

In order to test the capabilities of the method, calculations were performed in various ways. First of all, classical Rietveld calculations making use of the structural data were carried out to act as reference results. In order to verify the reference results, classical Rietveld calculations were also carried out using a different software, TOPAS-R.

The calculations were then carried out with QUANTO making use of the extracted intensities. To verify the scope of the method, mixed cases were also taken into account, simulating cases in which one of the structures is known, and extracted intensities have to be used for a single phase only.

6.2.2 Quantitation Results and Discussion

The results of the quantitation calculations are reported in Table 6.2, together with the profile agreement index R_{wp}, the goodness of fit (GoF) values and the absolute error (Err). The error was calculated based on the reference result (classical Rietveld calculation obtained with QUANTO) even if this value was not always perfectly aligned with the nominal concentration of the mixtures, as is the case with Mixture E. This was done because our aim was to verify if a structure-less method would lead to the same results as the classical Rietveld method using the same data set. The discrepancy between the nominal concentration and the reference result has not been investigated, but might be due to non-homogeneous sampling, incomplete mixing, weighing errors or other causes. Worthy of note, as discussed above, form I does not have many intense peaks well distinguishable from those of form II. This might also be a source of error for mixtures containing small amounts of form I in form II.

The results obtained both by using extracted intensities for the two phases and by simulating mixed cases are well aligned with the reference results, most errors having absolute values below 0.5% and none above 1%. Interestingly, also the values of R_{wp} and GoF are not far from the reference values, indicating that the extracted intensities placed on the absolute scale using the Wilson plot allow the calculation of a diffraction profile analogous to that obtainable from the structural data.

Figure 6.3 reports the results of the quantitation for each mixture using the classical Rietveld method plotted against the results obtained with the

extracted intensities for both phases and with extracted intensity for one phase and structure information for the other. The good agreement of the data confirms linearity comparable to that of the classical Rietveld method.

Figure 6.3. Plots of the results obtained with the classical Rietveld method against the results obtained using a) extracted intensities for form I, structure information for form II, b) structure information for form I, extracted intensities for form II and c) extracted intensities for both phases. The equation for the regression line is reported on the graphs.

Extracted intensities for form I, structure information for form II

$y = 1,0005x + 0,2231$

a)

Structure Information for form I, extracted intesities for form II

$y = 1,0225x - 1,409$

b)

Extracted Intensity for both phases

$y = 1,0036x - 0,5357$

c)
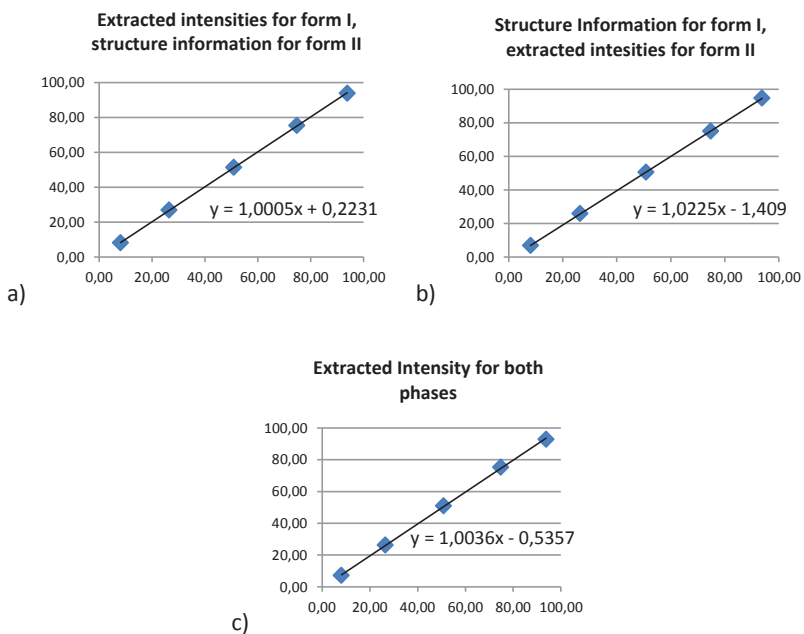
Table 6.2. Quantitation Results for Venalfaxine Hydrochloride binary mixtures of forms I and II.

Composition I:II % w/w	Mixture A 50:50	Mixture B 75:25	Mixture C 25:75	Mixture D 95:05	Mixture E 05:95
Classic Rietveld Method (Reference Result)	**50.87 : 49.13**	**74.80 : 25.20**	**26.45 : 73.55**	**93.79 : 6.21**	**8.11 : 91.89**
Rwp	5.60	5.77	5.90	6.21	7.84
Gof	2.75	2.77	3.12	3.03	4.15
Classic Rietveld Method calculated with TOPAS-R	(50.58 : 49.42)	(74.89 : 25.11)	(26.31 : 73.69)	(94.42 : 5.58)	(7.34 : 92.66)
Extracted Intensities for form I Structure for form II	51.29 : 48.71	75.24 : 24.76	26.84 : 73.15	93.80 : 6.20	8.09 : 91.91
Rwp	4.76	4.57	5.60	4.77	7.83
Gof	2.34	2.20	2.96	2.33	4.14
Err	**0.42**	**0.44**	**0.39**	**0.01**	**0.02**
Structure for form I Extracted Intensities for form II	50.46 : 49.54	74.93 : 25.07	25.79 : 74.21	94.65 : 5.35	6.87 : 93.13
Rwp	5.00	5.54	4.92	6.17	6.41
Gof	2.45	2.66	2.60	3.00	3.39
Err	**0.12**	**0.04**	**0.52**	**0.23**	**0.47**
Extracted Intensities for both phases	50.95 : 49.05	75.18 : 24.82	26.19 : 73.81	92.83 : 7.17	7.10 : 92.90
Rwp	4.31	4.40	4.69	5.08	6.38
Gof	2.11	2.11	2.48	2.47	3.37
Err	**0.34**	**0.06**	**0.65**	**0.97**	**0.99**

References

1. Bugay, D. E., Newman, A. W., Findlay, P., *Journal of Pharmaceutial and Biomedical Analysis, 15* (**1996**), 49-61.

2. Patel, A. D., Luner, P. E., Kemper, M. S., *Journal of Pharmaceutical Sciences, 90* (**2001**), 360-370.

3. Giron, D., *Thermochimica Acta, 248* (**1995**), 1-59.

4. Agatonovic-Kustrin, S., Wu, V., Rades, T., Saville, D., Tucker, I. G., *International Journal of Pharmaceutics, 184* (**1999**), 107-114.

5. Rietveld, H. M., *Journal of Applied Crystallography, 2* (**1969**), 65-71.

6. Tiwari, M., Chawla, G., Bansal, A. K., *Journal of Pharmaceutical and Biomedical Analysis, 43* (**2007**), 865-872.

7. Yamamura, S., Momose, Y., *International Journal of Pharmaceutics, 212* (**2001**), 203-212.

8. Campbell Roberts, S. N., Wlliams, A. C., Grimsey, I. M., Booth, S. W., *Journal of Pharmaceutical and Biomedical Analysis, 28* (**2002**), 1149-1159.

9. Coelho, A.A., TOPAS-R, v3.0. (**2005**) Bruker AXS, Karlsruhe, Germany.

10. Altomare, A., Burla, M. C., Giacovazzo, C., Guagliardi, A., Moliterni, A. G. G., Polidori, G., Rizzi, R., *Journal of Applied Crystallography, 34* (**2001**), 392-397.

11. Giannini, C., Guagliardi, A., Millini, R., *Journal of Applied Crystallography, 35* (**2002**), 481-490.

12. Giannini, C., Guagliardi, A., Tedesco, E., *Newsletter of Commision on Powder Diffraction, IUCr, 29* (**2003**), 42-43.

13. Vega, D., Fernández, D., Echeverría, G., *Acta Crystallographica, C56* (**2000**), 1009-1010.

14. Sivalakshmidevi, A., Vyas, K., Mahender Rao, S., Om Reddy, G., *Acta Crystallographica, E58* (**2002**), o1072-o1074.

7. Technology Transfer and Knowledge Sharing

Solid state of active pharmaceutical ingredients is a field in which different disciplines, environments and interests meet: industrial, scientific and legal issues all have important roles to play in almost every aspect of API polymorphism.

Obviously, API's are produced, formulated and sold not only to offer the population a longer lifespan and a better quality of life, but also to allow the companies which produce and sell API's enough profit to sustain the industry and be able to research and market new products. Therefore, a strong commercial interest surrounds API's. Industry needs to focus on what is necessary and not employ resources on purely scientific issues.

Conversely, the scientific aspect also needs to be addressed. Advancements in knowledge and understanding of solid-state issues, cutting-edge research and excellence are necessary to all parties involved. This is mostly the interest of academia, where more resources can be employed on purely scientific issues or on the devising of new techniques for the preparation and characterization of crystalline forms. This can lead to better, safer and more effective products. Also, scientific publications strongly contribute to the sharing and promulgation of knowledge.

Finally, legal and intellectual property issues come into play for industry but also for academia, protecting the interests mostly of companies but also of academic organizations. Moreover, the essence of intellectual property is to offer a protection which is limited in time, in exchange for the divulgation of an

invention. The subject matter of an invention must be publicly available at the end of the protection period, ideally contributing to knowledge promulgation.

These three aspects are strongly entwined. In the world of API's, all are necessary to successful problem solving in the quest for better medicinal products. The roles of each must necessarily be separate and different, and it is the synergy between industry and academia that can lead to the best results. Industry needs academia to offer scientific excellence, and academia needs industry to offer directions and pose questions which need answering. This is demonstrated by the growing number of joint ventures and collaborations which exist between pharmaceutical companies and universities, or by the many events organized by academia and industry alike as occasions of meeting and discussion.

During this thesis work, which lies on the boundary between industry and academia, these issues have been met and addressed over and over again. As a consequence, some of the contributions which have emerged in these years have not been purely scientific or purely industrial in nature, but have trod on the boundary, addressing the need to share knowledge and information.

7.1 Written Contributions

7.1.1 Structural Analysis by Powder Diffraction Methods

In occasion of the 2012 International Insubria Summer School dedicated to crystallography, having title "Crystallography for Health and Biosciences", a volume was published, summarizing the issues addressed. The purpose of the school was to explore multiple aspects of crystallography, regarding both crystallization techniques and characterization methods. A focus was placed on applications to health and bio-science issues. As the main focus of this thesis work was structural analysis from powder diffraction data and knowledge sharing also played an important part, as discussed in the previous paragraphs, the chapter dedicated to structural analysis from powder diffraction finds place here. [1]

7.1.2 API Polymorphism: Uses and Abuses of Intellectual Property Protection

It is a well-known fact that polymorphism has been gaining importance in the pharmaceutical industry over the past years. The importance of solid-state

issues has been discussed extensively in this work. However, there are many instances in which polymorphism and solid-state issues are used not to address serious scientific issues, but, opportunely employing intellectual property protection, to hinder or disincentive competition. A brief discussion about this was published in a journal specifically designed to scientifically address industrial issues, effectively linking industry and academia. [2]

7.2 Oral Presentations

7.2.1 Use of XPRD for Fingerprinting

A presentation was given in April 2011, having title "Utilizzo di XRPD per l'identificazione di fasi cristalline di principi attivi farmaceutici: esempi di casi non ovvi", during a workshop organized by Bruker AXS on non-destructive techniques used on solid API's, "XRD e non solo: tecniche analitiche non distruttive per il mondo farmaceutico". The main technique discussed during the workshop was XRPD, but SS-NMR and IR were also mentioned. The workshop was intended as a meeting occasion between industry and academia.

My presentation was centered on the use of X-ray powder diffraction as a fingerprinting technique, therefore meant only to identify the crystalline form under examination by comparing the experimental measurement with a reference XRPD trace. The aim of this presentation was to illustrate, with numerous examples, the unexpected complexity which can await behind the apparently simple task of overlapping two diffractograms.

Obviously, overlapping two diffractograms can give any range of results from perfect correspondence to no correspondence at all. [3] However, the more complex and interesting cases arise when there is some correspondence, but is not total. Extra, missing or shifted peaks can all suggest different problems. In these cases, a great deal of information can be inferred from the XRPD data.

What this presentation meant to highlight is that XRPD, even when used as a fingerprinting technique, can offer a lot more information to the attentive (and prepared!) observer. For example, positioning, shape and number of the peaks which do not match the reference can give insight into where and how to search for an answer. To give a couple of examples, few sharp peaks at high angles can

suggest an inorganic contaminant, while several low intensity peaks at lower angles can suggest the presence of small amounts of a different crystalline form. Very different peak intensities, which can sometimes make two diffractograms appear not to overlap at first glance, can be due to preferred orientation effects, as is the case with crystals of very different shapes of Ibuprofen lysine salt reported in Figure 7.1.

Figure 7.1. Crystals of Ibuprofen lysine salt in a) needle and b) prism shape obtained by crystallization from different solvent systems, giving rise to c) very different XPRD traces (shown overlapped). The picture were taken with a light microscope at 100x.

a)

b)

c)
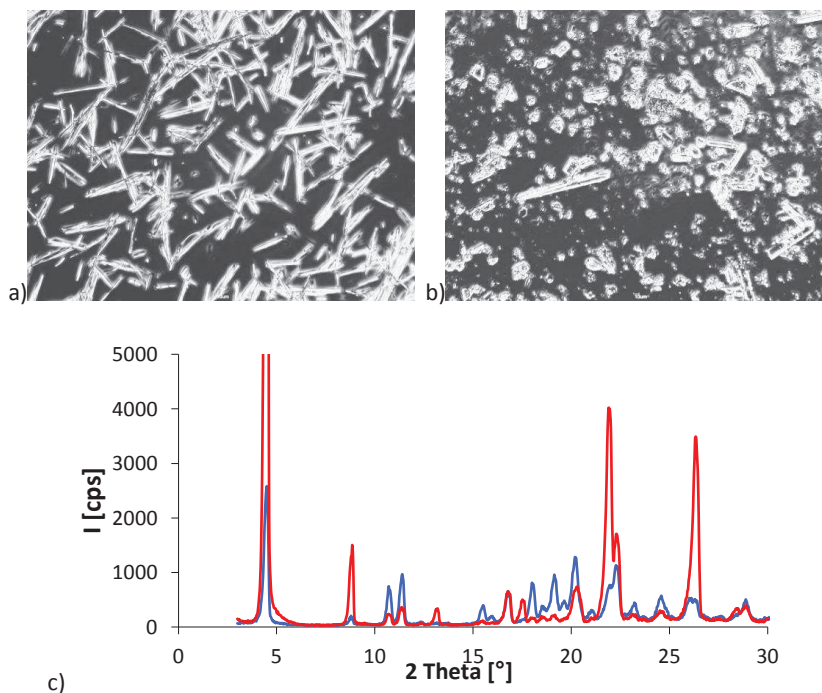
A different meeting point between industry and academia revolving around API's was the workshop organized by the University of Florence in May 2014, having title "SIMPLy CRIST: SoluzIoni per Materiali PoLicristallini". The aim of my presentation, having title "Principi Attivi Farmaceutici: a cosa serve la diffrazione da Polveri" was to explore the aspects of powder diffraction, and of the information that can be obtained from the technique, which hold particular industrial interest.

While most of the issues discussed have already been addressed in this work, one aspect which has not been mentioned is the use of XRPD as process control during the synthesis of a specific target crystalline form. In some cases, a specific crystalline form may be obtainable only from desolvation of a specific solvate or from crystallization from a specific starting form. This implies that even small amounts of a crystalline contaminant at any step can cause problems on the polymorphic purity of the finished product. A general example of an industrial procedure used to obtain two different crystalline forms of the same product is reported in Figure 7.2.

Figure 7.2. Synthetic Scheme for two different crystal forms of an API.

Each red rectangle represents a solid form which is isolated and analyzed via XRPD. If one of the intermediates is not monophasic, problems will arise on the subsequent steps.
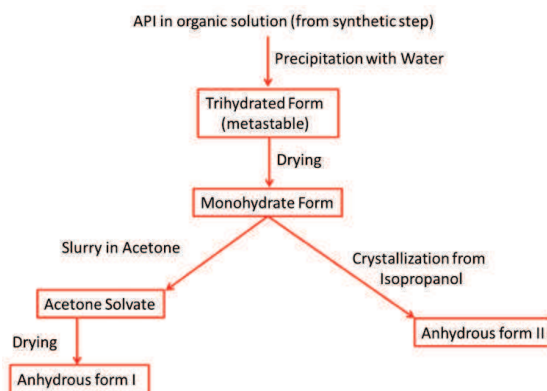
References

1. Masciocchi N., Vladiskovic, C., Structural Analysis by Powder Diffraction Methods, in *Crystallography for Health and Biosciences*, Guagliardi A., Masciocchi, N. (ed.), Insubria University Press, Varese, **2012**.

2. Allegrini, P., Vladiskovic, C., *Chemistry Today*, *3*(15) (**2012**), 30-33.

3. Byrn, S. R., Pfeiffer, R. R., Stowell, J. G., The X-ray Powder Diffraction Method, in *Solid State Chemistry of Drugs, 2nd Edition*, SSCI, Inc. (**1999**), West Lafayette, Indiana.

8. Conclusions and future perspectives

This thesis work, focusing on structural analysis of active pharmaceutical ingredients using mainly X-ray powder diffraction, has highlighted and demonstrated the usefulness of solving structures from powder data and the richness of information that can be obtained from structural analysis. Even though it is undoubtedly true that crystallography is a mature science, it is still growing and is still a mining field for novelty, innovation and scientific excellence. Many of these aspects have been brought to public attention during the numerous events organized this year to celebrate the International Year of Crystallography declared by the United Nations.

8.1 Conslusions

8.1.1 Bupropion Hydrohalides

We have presented the complete structural analysis of six new bupropion hydrohalide crystal unsolvated phases and three new bupropion hydrobromide solvates, performed with the aid of state-of-the art *ab-initio* powder diffraction methods. A full comparative crystallo-chemical analysis, including structural results of six additional crystal phases appeared in the literature (two hydrochloride and two hydrobromide unsolvated salts, one solvate of bupropion hydrochloride and one solvate of bupropion hydrobromide), has been performed, showing the persistency of a two-fold embrace, in which halides are

systematically hidden in a dimeric (centrosymmetric) moiety, interacting with two secondary ammonium sites. More relevantly, the large diversity of different crystal packing motifs (8 for 15 different crystal phases, several of which are isomorphous) shows that even in the presence of simple molecules with limited conformational freedom, subtle modifications on the preparation conditions may selectively drive the formation of distinct phases.

Even though Bupropion hydrochloride and hydrobromide salts are both in BCS (Biopharmaceutics Classification System) Class I and is therefore highly unlikely that polymorphism will affect overall therapeutic efficacy, structural analysis yielded information that can still be precious and useful at the industrial level. For example, it allowed to explain the relative stability of the solvate phases and their desolvation behavior. Moreover, desolvation studies led to the discovery of new bupropion hydrochloride phases. Comparative structural analysis and structure solution from X-ray powder diffraction data proved to be a powerful tool to study API polymorphism.

8.1.2 Nortriptyline Hydrochloride

A polymorphic form of nortriptyline hydrochloride, **NOR*HCl$_\alpha$**, has been characterized by structural and variable temperature powder diffraction methods and differential scanning calorimetry, revealing it to be monotropically related to **NOR*HCl$_\beta$**, previously characterized by single crystal analysis. **NOR*HCl$_\alpha$** represents the thermodynamically stable phase, as demonstrated by the higher fusion enthalpy and the conversion of **NOR*HCl$_\beta$** into **NOR*HCl$_\alpha$** upon melting. The structure determination from synchrotron radiation powder diffraction data of **NOR*HCl$_\alpha$** allowed to perform a comparative stereochemical analysis between the two crystal phases, revealing a distinct pattern in the sequence of the hydrogen bonds. Both polymorphs present a $C_4^2(4)$ hydrogen bond motif, constituted of alternating protonated nortriptyline molecules and μ_2-chlorine ions. As the conformation of the nortriptyline molecules is nearly identical in the two polymorphs, the major difference between the two crystal phases was found to reside in the presence of homochiral hydrogen-bonded chains in **NOR*HCl$_\alpha$** and of racemic ones in **NOR*HCl$_\beta$**. The supramolecular arrangement of the two polymorphs allowed to explain the lack of solid-solid interconversion between the forms upon heating.

8.1.3 Ibuprofen Lysine Salt

The structure of two polymorphs of Ibuprofen lysine salt, one existing at lower temperatures and one existing at higher temperatures, were solved using powder diffraction methods. Structural analysis was then carried out to understand and explain the transition between the two forms and its full reversibility.

Fully reversible thermally induced phase transitions occurring at relatively low temperature are normally associated to minor "packing" rearrangements. In these cases, an enthalpy change limited to a few kJ mol^{-1} and relative atomic positions only marginally affected by the phase transformation suggest the occurrence of a displacive transformation, not requiring significant bond breaking. In the transition between the two forms, the integrity of the molecular skeletons, as well as that of the primary supramolecular network (the extensive hydrogen-bond interactions occurring among the polar carboxyl and amino groups of ibuprofen and lysine) together with the symmetry preservation, indicate a displacive isosymmetric phase transition. Isosymmetric reversible phase transitions are rare for organic compounds, and often, but not uniquely, associated to pressure-driven processes.

Since structural similarities between interconverting phases are not always easy to study, as conventional single crystal structure determination of these kinds of systems can present unavoidable experimental difficulties (for example, sample polyfragmentation). In such cases, state-of-the-art structural powder diffraction methods may become the only viable tool, as here demonstrated by our variable-temperature XRPD study, which allowed the molecular details and changes at the heart of the phase transformation to be "easily" tracked.

8.1.4 Structure-less Full-Profile Quantitation Method

A method has been tested to extend the application of QPA (Quantitative Phase Analysis) making use of the full diffraction profile (Rietveld-like) to API's of which no structural information is known, providing that the pure phases are available for XRPD analysis and intensity extraction. The method makes use of the full diffraction profile, using the Wilson plot to place extracted experimental intensities on an absolute scale. Moreover, mixed cases in which one structure is

known have been simulated to test the method further. A test candidate, venlafaxine hydrochloride, has been chosen to verify the applicability of the method to binary mixtures of API polymorphs.

The quantitation results obtained have shown good correspondence with the reference results (obtained by classical Rietveld calculation methods) and demonstrate the applicability of the structure-less full-profile method to API's. The software QUANTO was moreover demonstrated to allow intensity extraction and quantitation calculations to be performed simply and rapidly.

8.2 Future Perspectives

This work has demonstrated how useful structural analysis can be when studying API polymorphism. However, the work is by no means finished, and represents more of a starting point than a finish line. The world of polymorphism of pharmaceuticals is wide and rich, raising more and more questions and issues to be addressed with growing scientific knowledge.

8.2.1 Structural Analysis

As the quest for new crystalline form in search of better characteristics and bulk properties plays an important role in solid-state studies of API's, one of the future issues what will be addressed is the possibility of coupling structure solution from powder diffraction data with molecular modelling, in order to verify the possibility of "forcing" crystallization of a different stable molecular conformation. This can be done for example by adding a specifically chosen solvent for complexation or chelation. As demonstrated in this work, tailored desolvations may then lead to discovery of new crystalline forms.

In order to test the hypothesis proposed, the *syn/anti* conformations of nortriptyline hydrochloride seem a good starting point. As described in Chapter 4, solution NMR studies have demonstrated the existence of different conformations in solution which do not (yet) exist in the solid state. Molecular modelling on the nortriptyline molecule might suggest a co-former to be used in the quest of a solvated crystal structure containing molecules having *syn*

conformation. If this were possible, tailored desolvations might lead to a new nortriptyline form.

8.2.2 Quantitation Methods

As the structure-less full-profile quantitation method has given good results when applied to API's, the scope and potential of the method should be explored further. First of all, binary mixtures containing smaller amounts of a crystalline "contaminant" will be prepared to verify the limit of detection (LOD) and limit of quantitation (LOQ) of the method. Mixtures of Venlafaxine hydrochloride forms I and II of 98:2 and 99:1 composition will be prepared and tested for this investigation.

In order to test the method further, a candidate has been selected to try quantitation of ternary mixtures. Piroxicam, a non-steroidal anti-inflammatory drug (NSAID), is known to exist in two anhydrous and one hydrated form, all of which have been characterized by single crystal. As the three crystalline structures are known and available, piroxicam is a good test candidate for future work on ternary mixtures.

Appendix A. Atomic Coordinates

A.1 Atomic Coordinates of Bupropion Hydrohalides

A.1.1 Bupropion Hydrochloride

Bupropion Hydrochloride Form III

```
Crystal System: triclinic
Space Group: P-1
a[Å]:   7.7478(2)
b[Å]:   8.1124(2)
c[Å]:   13.1768(3)
alpha[°]: 117.03(2)
beta[°]:  81.34(2)
gamma[°]: 89.00(2)
volume[Å³]:  725.9(3)
```

Atom Name	Fractional Coordinates (x,y,z)			Occupancy	B
Cl2	-0.22765	-0.03739	0.09541	1	2.5(1)
Cl1	0.35454	-0.24922	0.58215	1	2.5(1)
O1	0.05931	-0.09149	0.30175	1	2.5(1)
N1	0.13947	0.06048	0.15605	1	2.5(1)
C1	0.42036	-0.24192	0.45215	1	2.5(1)
C2	0.59458	-0.28242	0.40198	1	2.5(1)
C3	0.64788	-0.26704	0.30153	1	2.5(1)
C4	0.52654	-0.21245	0.25281	1	2.5(1)
C5	0.35105	-0.17653	0.30326	1	2.5(1)
C6	0.29758	-0.19196	0.40431	1	2.5(1)
C7	0.21200	-0.11774	0.25626	1	2.5(1)
C8	0.26217	-0.09168	0.14764	1	2.5(1)
C9	0.24406	-0.27246	0.04233	1	2.5(1)
C10	0.17366	0.26103	0.22872	1	2.5(1)

```
C11      0.15680      0.30608      0.35548   1   2.5(1)
C12      0.35932      0.28706      0.18215   1   2.5(1)
C13      0.03656      0.37933      0.21200   1   2.5(1)
H1       0.02354      0.05399      0.18120   1   2.5(1)
H2       0.13480      0.03965      0.08361   1   2.5(1)
H3       0.67558     -0.31957      0.43482   1   2.5(1)
H4       0.76553     -0.29337      0.26684   1   2.5(1)
H5       0.56307     -0.19980      0.18634   1   2.5(1)
H6       0.17986     -0.16876      0.43856   1   2.5(1)
H7       0.38332     -0.05947      0.14139   1   2.5(1)
H8       0.27510     -0.25828     -0.02637   1   2.5(1)
H9       0.12502     -0.30250      0.04889   1   2.5(1)
H10      0.32067     -0.37054      0.03812   1   2.5(1)
H11      0.24444      0.22978      0.36351   1   2.5(1)
H12      0.04236      0.28207      0.38225   1   2.5(1)
H13      0.17280      0.43470      0.40078   1   2.5(1)
H14      0.36807      0.25825      0.10228   1   2.5(1)
H15      0.44302      0.20565      0.18891   1   2.5(1)
H16      0.38294      0.41357      0.22605   1   2.5(1)
H17      0.05022      0.34811      0.13145   1   2.5(1)
H18      0.05184      0.50850      0.25619   1   2.5(1)
H19     -0.07870      0.35588      0.23767   1   2.5(1)
```

Bupropion Hydrochloride Form III

```
Crystal System: triclinic
Space Group: P-1
a[Å]:   7.5154(3)
b[Å]:   7.8712(3)
c[Å]:  13.7033(6)
alpha[°]: 88.12(3)
beta[°]:  86.41(2)
gamma[°]: 67.78(2)
volume[Å³]:  748.9(5)

Atom Name, Fractional Coordinates (x,y,z), Occupancy, B
Cl1     0.19880      0.57302      0.40324   1   7.8(2)
Cl2    -0.44868      0.80935      0.86472   1   7.8(2)
C1     -0.50948      0.76574      0.98346   1   7.8(2)
C2     -0.69400      0.77371      1.00829   1   7.8(2)
C3     -0.74319      0.73731      1.10363   1   7.8(2)
C4     -0.60782      0.69269      1.17410   1   7.8(2)
C5     -0.42335      0.68533      1.14938   1   7.8(2)
C6     -0.37427      0.72172      1.05400   1   7.8(2)
C7     -0.27804      0.63785      1.22372   1   7.8(2)
C8     -0.32145      0.58555      1.32683   1   7.8(2)
C9     -0.39990      0.75673      1.39080   1   7.8(2)
O1     -0.12038      0.63955      1.20162   1   7.8(2)
```

172

```
N1    -0.14334    0.45321    1.36605    1    7.8(2)
C10   -0.08525    0.25861    1.33980    1    7.8(2)
C11   -0.23928    0.18439    1.37536    1    7.8(2)
C12   -0.05132    0.23516    1.22887    1    7.8(2)
C13    0.10261    0.14848    1.38790    1    7.8(2)
H1    -0.15495    0.46215    1.43993    1    7.8(2)
H2    -0.03575    0.49297    1.34072    1    7.8(2)
H3    -0.80221    0.80842    0.95161    1    7.8(2)
H4    -0.89109    0.74340    1.12333    1    7.8(2)
H5    -0.64717    0.66257    1.25021    1    7.8(2)
H6    -0.22624    0.71494    1.03401    1    7.8(2)
H7    -0.43107    0.52238    1.32645    1    7.8(2)
H8    -0.55975    0.81592    1.39173    1    7.8(2)
H9    -0.35456    0.71897    1.46681    1    7.8(2)
H10   -0.34505    0.86211    1.36144    1    7.8(2)
H11   -0.22413    0.06150    1.33282    1    7.8(2)
H12   -0.22131    0.14529    1.45381    1    7.8(2)
H13   -0.38560    0.28976    1.36629    1    7.8(2)
H14    0.04226    0.30757    1.19974    1    7.8(2)
H15    0.01961    0.08646    1.21273    1    7.8(2)
H16   -0.18973    0.29161    1.19238    1    7.8(2)
H17    0.16203    0.00462    1.36163    1    7.8(2)
H18    0.20789    0.21430    1.36897    1    7.8(2)
H19    0.07712    0.14717    1.46861    1    7.8(2)
```

A.1.2 Bupropione Hydrobromide

Bupropion Hydrbromide Form I

```
Crystal System: triclinic
Space Group: P-1
a[Å]:   7.69386(22)
b[Å]:   7.93659(19)
c[Å]:   13.84976(25)
alpha[°]: 94.0622(17)
beta[°]:  94.4074(17)
gamma[°]: 65.9613(19)
volume[Å³]:  769.350(34)

Atom Name, Fractional Coordinates (x,y,z), Occupancy, B
Br   0.28974(57)   -0.06438(49)    0.39847(21)   1   4.34(12)
Cl   0.9772411     -0.2999097      0.8621458     1   4.34(12)
C1   1.025362      -0.2637468      0.9834176     1   4.34(12)
C2   1.208781      -0.2897566      1.016353      1   4.34(12)
C3   1.247905      -0.2594234      1.1138        1   4.34(12)
C4   1.103592      -0.2028305      1.178288      1   4.34(12)
C5   0.9201546     -0.1774028      1.145437      1   4.34(12)
C6   0.8811589     -0.2077422      1.04795       1   4.34(12)
```

```
C7    0.7653945     -0.117064     1.213361     1   4.34(12)
C8    0.7999572     -0.07554804   1.31938      1   4.34(12)
C9    0.8637006     -0.2519713    1.375573     1   4.34(12)
O1    0.6071797     -0.09917726   1.183562     1   4.34(12)
N1    0.6223041      0.06403734   1.357223     1   4.34(12)
C10   0.5777745      0.259738     1.341923     1   4.34(12)
C11   0.3951987      0.3867591    1.390685     1   4.34(12)
C12   0.7416494      0.3104417    1.382819     1   4.34(12)
C13   0.5510707      0.2885281    1.233013     1   4.34(12)
H1    0.6240198      0.04826715   1.429288     1   4.34(12)
H2    0.5146737      0.03629749   1.324008     1   4.34(12)
H3    1.32427       -0.3340714    0.9645039    1   4.34(12)
H4    1.394971      -0.2799866    1.140017     1   4.34(12)
H5    1.13498       -0.1775989    1.256133     1   4.34(12)
H6    0.7340416     -0.186502     1.021482     1   4.34(12)
H7    0.9134509     -0.02197218   1.327855     1   4.34(12)
H8    1.021882      -0.3213815    1.380474     1   4.34(12)
H9    0.8112097     -0.2164854    1.450066     1   4.34(12)
H10   0.8067773     -0.3488556    1.338076     1   4.34(12)
H11   0.3918802      0.5277308    1.403679     1   4.34(12)
H12   0.2702862      0.3944678    1.342398     1   4.34(12)
H13   0.3870432      0.3334005    1.461427     1   4.34(12)
H14   0.879493       0.2065532    1.35743      1   4.34(12)
H15   0.7171631      0.448342     1.357437     1   4.34(12)
H16   0.7482169      0.3161241    1.463215     1   4.34(12)
H17   0.5373481      0.429222     1.217917     1   4.34(12)
H18   0.6771089      0.1836287    1.197191     1   4.34(12)
H19   0.4205049      0.2716926    1.203328     1   4.34(12)
```

Bupropion Hydrobromide Form II

```
Crystal System: orthorhombic
Space Group: Pbca
a[Å]:   8.63283(63)
b[Å]:   12.40924(93)
c[Å]:   27.70399(84)
alpha[°]: 90
beta[°]:  90
gamma[°]: 90
volume[Å³]:  2967.84(32)

Atom Name, Fractional Coordinates (x,y,z), Occupancy, B
Br    0.47147(77)    0.34316(67)   0.04484(14)  1 3.03(16)
Cl    0.8382352     -0.6521145     0.3138388    1 5.03(16)
C1    0.9183345     -0.7781465     0.3067078    1 5.03(16)
C2    0.8696037     -0.8435112     0.2691206    1 5.03(16)
C3    0.9346095     -0.9447092     0.2630084    1 5.03(16)
C4    1.048489      -0.9804866     0.2944334    1 5.03(16)
```

```
C5      1.096922     -0.9152712    0.3321557    1  5.03(16)
C6      1.031852     -0.8140545    0.3382326    1  5.03(16)
C7      1.218102     -0.9524348    0.3658009    1  5.03(16)
C8      1.217859     -0.9188644    0.4181657    1  5.03(16)
C9      1.15114      -0.8050813    0.4229624    1  5.03(16)
O1      1.31924      -1.011595     0.3513043    1  5.03(16)
N1      1.377801     -0.9206876    0.4364798    1  5.03(16)
C10     1.49368      -0.8537202    0.4113337    1  5.03(16)
C11     1.658391     -0.8872685    0.4251291    1  5.03(16)
C12     1.474924     -0.8635501    0.3565601    1  5.03(16)
C13     1.467892     -0.7363053    0.4257763    1  5.03(16)
H1      1.41565      -0.9979643    0.4364676    1  5.03(16)
H2      1.373402     -0.8943618    0.4709752    1  5.03(16)
H3      0.7789174    -0.8145229    0.2437433    1  5.03(16)
H4      0.8956005    -0.9968918    0.2327902    1  5.03(16)
H5      1.100987     -1.061234     0.2893078    1  5.03(16)
H6      1.071137     -0.7615313    0.3682963    1  5.03(16)
H7      1.145233     -0.9757415    0.4393826    1  5.03(16)
H8      1.024531     -0.8094684    0.43         1  5.03(16)
H9      1.208227     -0.762826     0.4535742    1  5.03(16)
H10     1.170132     -0.7588739    0.389103     1  5.03(16)
H11     1.741817     -0.860628     0.3970357    1  5.03(16)
H12     1.689479     -0.8488918    0.4600303    1  5.03(16)
H13     1.666685     -0.9762185    0.4286632    1  5.03(16)
H14     1.35172      -0.8522654    0.346273     1  5.03(16)
H15     1.546853     -0.8005936    0.3389757    1  5.03(16)
H16     1.513722     -0.9439329    0.3438841    1  5.03(16)
H17     1.541927     -0.6819674    0.403755     1  5.03(16)
H18     1.343889     -0.7158527    0.4198528    1  5.03(16)
H19     1.496905     -0.7247088    0.4644959    1  5.03(16)
```

A.1.3 Bupropion Hydroiodide

Bupropion Hydroiodide Form I

```
Crystal System: monoclinic
Space Group: C2/c
a[Å]:   8.5910(2)
b[Å]:   14.6100(3)
c[Å]:   25.6710(6)
alpha[°]: 90
beta[°]:  92.626(2)
gamma[°]: 90
volume[Å³]:  3218.3(1)

Atom Name, Fractional Coordinates (x,y,z), Occupancy, B
I       0.09367      -0.16116      -0.56341     1  6.53(8)
Cl      0.38944      -0.01048      0.34224      1  6.53(8)
```

```
C1    0.30231    -0.03145    0.28169    1   6.53(8)
C2    0.23861    -0.11677    0.27065    1   6.53(8)
C3    0.16727    -0.13376    0.22210    1   6.53(8)
C4    0.15941    -0.06541    0.18462    1   6.53(8)
C5    0.22361     0.01988    0.19558    1   6.53(8)
C6    0.29492     0.03681    0.24416    1   6.53(8)
C7    0.21585     0.09317    0.15603    1   6.53(8)
C8    0.15198     0.07541    0.10121    1   6.53(8)
C9    0.28088     0.03738    0.06811    1   6.53(8)
O1    0.26052     0.16925    0.16775    1   6.53(8)
N1    0.09279     0.16182    0.07851    1   6.53(8)
C10  -0.06546     0.19092    0.09125    1   6.53(8)
C11  -0.09495     0.29064    0.07548    1   6.53(8)
C12  -0.18825     0.13033    0.06325    1   6.53(8)
C13  -0.08096     0.18113    0.15002    1   6.53(8)
H1    0.09723     0.15785    0.03921    1   6.53(8)
H2    0.16656     0.21154    0.09152    1   6.53(8)
H3    0.24410    -0.17141    0.30084    1   6.53(8)
H4    0.11599    -0.20214    0.21337    1   6.53(8)
H5    0.10147    -0.07898    0.14591    1   6.53(8)
H6    0.34569     0.10527    0.25307    1   6.53(8)
H7    0.05571     0.02463    0.10214    1   6.53(8)
H8    0.27913    -0.03868    0.06904    1   6.53(8)
H9    0.26159     0.06070    0.02708    1   6.53(8)
H10   0.39684     0.06122    0.08359    1   6.53(8)
H11  -0.22209     0.30403    0.07077    1   6.53(8)
H12  -0.04401     0.33613    0.10646    1   6.53(8)
H13  -0.04120     0.30607    0.03795    1   6.53(8)
H14  -0.15850     0.05699    0.06904    1   6.53(8)
H15  -0.30323     0.14463    0.07958    1   6.53(8)
H16  -0.19526     0.14512    0.02082    1   6.53(8)
H17  -0.20339     0.19306    0.16052    1   6.53(8)
H18  -0.04489     0.11071    0.16180    1   6.53(8)
H19  -0.00462     0.23156    0.17113    1   6.53(8)
```

Bupropion Hydroiodide Form II

```
Crystal System: monoclinic
Space Group: C2/c
a[Å]:   14.6084(3)
b[Å]:    8.0869(2)
c[Å]:   27.0461(4)
alpha[°]: 90
beta[°]:  92.760(1)
gamma[°]: 90
volume[Å³]:  3191.4(1)
```

Atom Name, Fractional Coordinates (x,y,z), Occupancy, B

```
I1      0.60703       0.856391     -0.94383     1   5.5(1)
Cl      0.27906      -0.90676      0.33710      1   5.5(1)
C1      0.24995      -0.89209      0.27482      1   5.5(1)
C2      0.16135      -0.84908      0.25934      1   5.5(1)
C3      0.13778      -0.83586      0.20925      1   5.5(1)
C4      0.20282      -0.86540      0.17464      1   5.5(1)
C5      0.29140      -0.90901      0.19010      1   5.5(1)
C6      0.31492      -0.92218      0.24021      1   5.5(1)
C7      0.36122      -0.94062      0.15362      1   5.5(1)
C8      0.34367      -0.89998      0.09952      1   5.5(1)
C9      0.30801      -0.05351      0.07166      1   5.5(1)
O1      0.43428      -0.99923      0.16729      1   5.5(1)
N1      0.42982      -0.84453      0.07887      1   5.5(1)
C10     0.46046      -0.67406      0.08989      1   5.5(1)
C11     0.39198      -0.54774      0.06788      1   5.5(1)
C12     0.47152      -0.64668      0.14587      1   5.5(1)
C13     0.55330      -0.64806      0.06742      1   5.5(1)
H1      0.42451      -0.85867      0.04163      1   5.5(1)
H2      0.47952      -0.92080      0.09271      1   5.5(1)
H3      0.10934      -0.82441      0.28712      1   5.5(1)
H4      0.06676      -0.80102      0.19692      1   5.5(1)
H5      0.18394      -0.85381      0.13458      1   5.5(1)
H6      0.38599      -0.95629      0.25264      1   5.5(1)
H7      0.29153      -0.80006      0.09563      1   5.5(1)
H8      0.23184      -0.05451      0.07017      1   5.5(1)
H9      0.33191      -0.05165      0.03323      1   5.5(1)
H10     0.33314      -0.16760      0.09080      1   5.5(1)
H11     0.40001      -0.42754      0.08748      1   5.5(1)
H12     0.40514      -0.52940      0.02814      1   5.5(1)
H13     0.32057      -0.59157      0.07145      1   5.5(1)
H14     0.51208      -0.74873      0.16349      1   5.5(1)
H15     0.50752      -0.52739      0.15282      1   5.5(1)
H16     0.40367      -0.64171      0.16255      1   5.5(1)
H17     0.58332      -0.52734      0.07932      1   5.5(1)
H18     0.59999      -0.74990      0.08002      1   5.5(1)
H19     0.54533      -0.64983      0.02637      1   5.5(1)
```

Bupropion Hydroiodide Form III

```
Crystal System: triclinic
Space Group: P-1
a[Å]:   7.9819(4)
b[Å]:   8.2163(5)
c[Å]:   13.7557(8)
alpha[°]: 84.51(4)
beta[°]:  84.75(4)
gamma[°]: 63.07(4)
```

volume[Å^3]: 799.42(9)

```
Atom Name, Fractional Coordinates (x,y,z), Occupancy, B
I      0.04972    0.22615   -0.61361   1   4.6(2)
Cl    -0.27339    0.47408   -0.85454   1   4.6(2)
C1    -0.26140    0.51394   -0.97953   1   4.6(2)
C2    -0.31897    0.69111   -1.01948   1   4.6(2)
C3    -0.30822    0.72374   -1.12004   1   4.6(2)
C4    -0.23964    0.57922   -1.18063   1   4.6(2)
C5    -0.18262    0.40197   -1.14071   1   4.6(2)
C6    -0.19340    0.36947   -1.04013   1   4.6(2)
C7    -0.10927    0.24707   -1.20445   1   4.6(2)
C8    -0.07578    0.27362   -1.31330   1   4.6(2)
C9    -0.25228    0.31162   -1.36557   1   4.6(2)
O1    -0.07393    0.09538   -1.16886   1   4.6(2)
N1     0.08356    0.10680   -1.34838   1   4.6(2)
C10    0.27433    0.07138   -1.32504   1   4.6(2)
C11    0.32518    0.21974   -1.37373   1   4.6(2)
C12    0.28835    0.06464   -1.21434   1   4.6(2)
C13    0.41419   -0.11381   -1.36247   1   4.6(2)
H1     0.08010    0.10881   -1.42194   1   4.6(2)
H2     0.06254    0.00023   -1.31779   1   4.6(2)
H3    -0.37290    0.80690   -0.97083   1   4.6(2)
H4    -0.35408    0.86585   -1.15190   1   4.6(2)
H5    -0.23013    0.60554   -1.26104   1   4.6(2)
H6    -0.14686    0.22741   -1.00806   1   4.6(2)
H7    -0.04301    0.39179   -1.32882   1   4.6(2)
H8    -0.34249    0.46155   -1.37489   1   4.6(2)
H9    -0.21079    0.25426   -1.43887   1   4.6(2)
H10   -0.33467    0.24869   -1.32199   1   4.6(2)
H11    0.43912    0.22412   -1.33502   1   4.6(2)
H12    0.37473    0.18797   -1.45088   1   4.6(2)
H13    0.20111    0.35615   -1.37181   1   4.6(2)
H14    0.23059   -0.02600   -1.17642   1   4.6(2)
H15    0.43876    0.01082   -1.19843   1   4.6(2)
H16    0.20865    0.20328   -1.18658   1   4.6(2)
H17    0.55696   -0.15454   -1.33727   1   4.6(2)
H18    0.36575   -0.21759   -1.33396   1   4.6(2)
H19    0.42133   -0.10666   -1.44370   1   4.6(2)
```

Bupropion Hydroiodide Form IV

```
Crystal System: monoclinic
Space Group: P21/n
a[Å]: 8.2635(5)
b[Å]:  9.7799(3)
c[Å]:  20.2113(6)
alpha[°]: 90
```

```
beta[°]:  99.98(3)
gamma[°]: 90
volume[Å³]:  1608.6(1)

Atom Name, Fractional Coordinates (x,y,z), Occupancy, B
I        0.20410    -0.13743    -0.04442   1   6.1(1)
Cl      -0.88165     0.58142     0.76669   1   6.1(1)
C1      -0.67373     0.55078     0.77646   1   6.1(1)
C2      -0.61274     0.46825     0.73078   1   6.1(1)
C3      -0.44530     0.44414     0.73814   1   6.1(1)
C4      -0.33884     0.50271     0.79110   1   6.1(1)
C5      -0.39986     0.58492     0.83697   1   6.1(1)
C6      -0.56734     0.60899     0.82956   1   6.1(1)
C7      -0.28776     0.64789     0.89350   1   6.1(1)
C8      -0.33990     0.76940     0.93078   1   6.1(1)
C9      -0.35311     0.89623     0.88578   1   6.1(1)
O1      -0.15163     0.60083     0.91073   1   6.1(1)
N1      -0.21709     0.79304     0.99166   1   6.1(1)
C10     -0.22160     0.70315     0.04993   1   6.1(1)
C11     -0.23235     0.55271     0.02885   1   6.1(1)
C12     -0.06787     0.72380     0.10333   1   6.1(1)
C13     -0.37251     0.74042     0.08037   1   6.1(1)
H1      -0.22689     0.89120     0.00647   1   6.1(1)
H2      -0.10569     0.78035     0.97833   1   6.1(1)
H3      -0.69807     0.42195     0.68806   1   6.1(1)
H4      -0.39663     0.37818     0.70138   1   6.1(1)
H5      -0.20483     0.48394     0.79667   1   6.1(1)
H6      -0.61625     0.67540     0.86608   1   6.1(1)
H7      -0.46169     0.74853     0.94497   1   6.1(1)
H8      -0.48110     0.90734     0.85827   1   6.1(1)
H9      -0.31998     0.98873     0.91723   1   6.1(1)
H10     -0.26947     0.88679     0.84847   1   6.1(1)
H11     -0.18846     0.48605     0.07280   1   6.1(1)
H12     -0.36241     0.52717     0.00845   1   6.1(1)
H13     -0.15540     0.53287     0.98996   1   6.1(1)
H14     -0.04647     0.83444     0.11355   1   6.1(1)
H15     -0.08631     0.67115     0.15013   1   6.1(1)
H16     -9.95819     0.68003     0.08633   1   6.1(1)
H17     -0.37105     0.68518     0.12853   1   6.1(1)
H18     -0.37142     0.85257     0.08960   1   6.1(1)
H19     -0.48640     0.71264     0.04515   1   6.1(1)
```

A.1.4 Bupropion Solvates

Bupropion Hydrobromide 1-Propanol solvate

Crystal System: triclinic
Space Group: P-1
a[Å]: 7.827(6)
b[Å]: 9.392(6)
c[Å]: 11.838(9)
alpha[°]: 85.70(6)
beta[°]: 101.75(7)
gamma[°]: 90.37(6)
volume[Å^3]: 849.6(11)

Atom Name, Fractional Coordinates (x,y,z), Occupancy, B

Atom	x	y	z	Occ	B
Br	0.19594	0.36417	0.58242	1	0.0541
Cl	0.4949	0.31127	0.03314	1	0.0874
O1	0.1573	-0.1177	0.2890	1	0.0664
N1	0.2027	-0.3005	0.4684	1	0.0351
H1A	0.1975	-0.3934	0.4939	1	0.042
H1B	0.1017	-0.2797	0.4459	1	0.042
C1	0.5472	0.1457	0.0936	1	0.0553
C2	0.7166	0.1015	0.0749	1	0.0710
H2	0.8037	0.1572	0.0267	1	0.085
C3	0.7574	-0.0254	0.1278	1	0.0683
H3	0.8727	-0.0555	0.1157	1	0.082
C4	0.6283	-0.1091	0.1990	1	0.0545
H4	0.6573	-0.1939	0.2361	1	0.065
C5	0.4553	-0.0662	0.2150	1	0.0421
C6	0.4142	0.0635	0.1609	1	0.0488
H6	0.2991	0.0936	0.1702	1	0.059
C7	0.3080	-0.1498	0.2877	1	0.0446
C8	0.3474	-0.2821	0.3635	1	0.0387
H8	0.4593	-0.2697	0.3866	1	0.046
C9	0.3527	-0.4130	0.2936	1	0.0543
H9A	0.3776	-0.4963	0.3394	1	0.081
H9B	0.4421	-0.3999	0.2248	1	0.081
H9C	0.2418	-0.4250	0.2726	1	0.081
C10	0.2117	-0.2135	0.5702	1	0.0425
C11	0.3619	-0.2679	0.6248	1	0.0565
H11A	0.4702	-0.2498	0.5708	1	0.085
H11B	0.3478	-0.3688	0.6447	1	0.085
H11C	0.3625	-0.2196	0.6934	1	0.085
C12	0.2371	-0.0547	0.5302	1	0.0606
H12A	0.1411	-0.0222	0.4962	1	0.091
H12B	0.3441	-0.0414	0.4741	1	0.091
H12C	0.2419	-0.0011	0.5955	1	0.091
C13	0.0373	-0.2397	0.6537	1	0.0566

```
H13A   -0.0552  -0.2038   0.6177    1     0.085
H13B    0.0367  -0.1915   0.7225    1     0.085
H13C    0.0205  -0.3403   0.6737    1     0.085
O1S     0.0028   0.3283)  0.8731    0.50  0.098
C1S     0.113    0.449    0.9168    0.50  0.127
C2S    -0.003    0.546    0.9589    0.50  0.129
C3S    -0.026    0.567    1.0908    0.50  0.104
```

Bupropion Hydrobromide Ethanol solvate

```
Crystal System: triclinic
Space Group: P-1
a[Å]:  7.7746(2)
b[Å]:  9.3626(3)
c[Å]:  11.6801(2)
alpha[°]: 85.99)1)
beta[°]: 101.39(2)
gamma[°]: 90.18(3)
volume[Å³]:  828.3
```

```
Atom Name, Fractional Coordinates (x,y,z), Occupancy, B
Br    0.3103042 -0.1270082   0.08699004  1   2.935038
Cl    1.013941   1.192782    0.4710263   1   4.935038
C1    1.060798   1.355913    0.407934    1   4.935038
C2    1.234078   1.399375    0.4217168   1   4.935038
C3    1.272556   1.530124    0.3703215   1   4.935038
C4    1.13781    1.617316    0.3050089   1   4.935038
C5    0.9643347  1.574116    0.2915248   1   4.935038
C6    0.9259879  1.443306    0.3429463   1   4.935038
C7    0.8198532  1.665933    0.2221454   1   4.935038
C8    0.8551471  1.789782    0.1408219   1   4.935038
C9    0.8757175  1.927459    0.2055996   1   4.935038
O1    0.6698367  1.641116    0.2298114   1   4.935038
N1    0.706651   1.805881    0.03867177  1   4.935038
C10   0.7101437  1.718682   -0.06125601  1   4.935038
C11   0.7231039  1.558944   -0.02218842  1   4.935038
C12   0.5439662  1.746205   -0.1577915   1   4.935038
C13   0.8704005  1.761454   -0.1113833   1   4.935038
H1    0.695916   1.910315    0.008616808 1   4.935038
H2    0.5971444  1.778519    0.06818159  1   4.935038
H3    1.342217   1.329014    0.4735201   1   4.935038
H4    1.411595   1.564627    0.3812783   1   4.935038
H5    1.168971   1.721514    0.2633906   1   4.935038
H6    0.7871169  1.40828     0.3316951   1   4.935038
H7    0.9785917  1.768423    0.1110022   1   4.935038
H8    1.016965   1.944146    0.2452161   1   4.935038
H9    0.8258297  2.020207    0.142557    1   4.935038
H10   0.8010829  1.920259    0.2769723   1   4.935038
```

```
H11   0.6751579   1.494275   -0.0986056   1   4.935038
H12   0.8629649   1.530107    0.0165323   1   4.935038
H13   0.6421222   1.533542    0.04401515  1   4.935038
H14   0.5201705   1.863036   -0.1776432   1   4.935038
H15   0.5625194   1.69662    -0.2380001   1   4.935038
H16   0.4274303   1.698267   -0.1300428   1   4.935038
H17   0.867638    1.709294   -0.194354    1   4.935038
H18   0.868344    1.879791   -0.1290608   1   4.935038
H19   0.9934486   1.728521   -0.04721448  1   4.935038
C01   0.5606401   0.01456266  0.5592663   1   6.935038
O03   0.4852087   0.1285083   0.6114834   0.5 6.935038
HO    0.5560867   0.1455296   0.6807557   1   6.935038
H011  0.6732903   0.04224282  0.5469298   1   6.935038
H012  0.5722964  -0.0699107   0.6104637   1   6.935038
```

Bupropion Hydrobromide Trifluoroethanol solvate

```
Crystal System: triclinic
Space Group: P-1
a[Å]:  7.9000(2)
b[Å]:  9.3673(2)
c[Å]:  11.7354(3)
alpha[°]: 86.425(1)
beta[°]: 102.501(2)
gamma[°]: 91.033(2)
volume[Å³]:  846.2
```

```
Atom Name, Fractional Coordinates (x,y,z), Occupancy, B
Br    0.31096(45) -0.13460(39) 0.08417(28)  1   5.17(12)
Cl    1.008971    1.200165    0.4674276    1   7.17(12)
C1    1.054052    1.3632      0.4042038    1   7.17(12)
C2    1.223972    1.41125     0.4203316    1   7.17(12)
C3    1.261049    1.541928    0.3688563    1   7.17(12)
C4    1.128268    1.624462    0.3011221    1   7.17(12)
C5    0.958137    1.576676    0.2852836    1   7.17(12)
C6    0.9211904   1.445939    0.3367877    1   7.17(12)
C7    0.8157756   1.663511    0.2133173    1   7.17(12)
C8    0.8515592   1.792338    0.1381068    1   7.17(12)
C9    0.8625349   1.926902    0.2070096    1   7.17(12)
O1    0.6672303   1.630478    0.2138143    1   7.17(12)
N1    0.710368    1.807294    0.0334035    1   7.17(12)
C10   0.7171293   1.717695    0.06452996   1   7.17(12)
C11   0.8618003   1.767718    0.1259802    1   7.17(12)
C12   0.747972    1.560936    0.02079875   1   7.17(12)
C13   0.5430705   1.728989    0.1517775    1   7.17(12)
H1    0.704086    1.911114    0.003003533  1   7.17(12)
H2    0.5994141   1.781567    0.05966505   1   7.17(12)
H3    1.330565    1.344615    0.4740893    1   7.17(12)
```

182

```
H4    1.397404     1.580109     0.3816996   1   7.17(12)
H5    1.158332     1.728604     0.2594563   1   7.17(12)
H6    0.7850246    1.407233     0.3236615   1   7.17(12)
H7    0.9768315    1.777786     0.111716    1   7.17(12)
H8    0.9994514    1.947433     0.2508575   1   7.17(12)
H9    0.8137406    2.02028      0.1462842   1   7.17(12)
H10   0.7840124    1.912986     0.2749426   1   7.17(12)
H11   0.8996249    1.679783     0.1745437   1   7.17(12)
H12   0.8142586    1.859408     0.1887067   1   7.17(12)
H13   0.9779851    1.801144     0.0613914   1   7.17(12)
H14   0.6572275    1.527197     0.03608087  1   7.17(12)
H15   0.7261993    1.494026     0.09755458  1   7.17(12)
H16   0.8828243    1.545258     0.02985694  1   7.17(12)
H17   0.5361222    1.651439     0.2205884   1   7.17(12)
H18   0.4377193    1.705544     0.1038866   1   7.17(12)
H19   0.5259008    1.838712     0.1941442   1   7.17(12)
C01   0.5889      -0.90631      0.5658      0.5 7.17(12)
O03   0.4922      -0.83445      0.6371      0.5 7.17(12)
HO    0.5539      -0.83514      0.7112      0.5 7.17(12)
H011  0.6277      -0.83808      0.5137      0.5 7.17(12)
H012  0.6862      -0.95314      0.6148      0.5 7.17(12)
C02   0.4715      -0.01746      0.4952      0.5 7.17(12)
F021  0.5623      -0.08486      0.4284      0.5 7.17(12)
F022  0.3323      -0.95054      0.425       0.5 7.17(12)
F023  0.416       -0.11526      0.5698      0.5 7.17(12)
```

Bupropion Hydrobromide Ethylene Glycol solvate

```
Crystal System: triclinic
Space Group: P-1
a[Å]:  7.8338(2)
b[Å]:  9.3544(2)
c[Å]:  11.5267(2)
alpha[°]: 87.05(1)
beta[°]: 103.42(2)
gamma[°]: 90.29(3)
volume[Å³]:  820.5

Atom Name, Fractional Coordinates (x,y,z), Occupancy, B
Br   0.3127971   -0.1332383   0.09396218  1 3.081075
Cl   0.9832017    1.189821    0.4644801   1 5.081075
C1   1.041808     1.350736    0.4060156   1 5.081075
C2   1.217243     1.387958    0.4261823   1 5.081075
C3   1.26517      1.516894    0.3785187   1 5.081075
C4   1.137717     1.608511    0.3105526   1 5.081075
C5   0.9620901    1.57156     0.2906868   1 5.081075
C6   0.9142902    1.442557    0.3383794   1 5.081075
C7   0.8253081    1.668127    0.2184296   1 5.081075
```

```
C8     0.8705636   1.789346    0.1395325    1 5.081075
C9     0.9080893   1.924816    0.2099762    1 5.081075
O1     0.6735871   1.649435    0.2216836    1 5.081075
N1     0.721795    1.815425    0.03622332   1 5.081075
C10    0.7057222   1.722307   -0.06519688   1 5.081075
C11    0.7262233   1.564497   -0.02216265   1 5.081075
C12    0.5271415   1.74434    -0.1527278    1 5.081075
C13    0.849633    1.762278   -0.1302573    1 5.081075
H1     0.7263685   1.918415    0.0053622    1 5.081075
H2     0.6115635   1.802193    0.0668388    1 5.081075
H3     1.319529    1.314044    0.480102     1 5.081075
H4     1.405921    1.54639     0.3945887    1 5.081075
H5     1.176432    1.711244    0.2719189    1 5.081075
H6     0.7736885   1.412532    0.3220063    1 5.081075
H7     0.989187    1.760102    0.1082457    1 5.081075
H8     1.050942    1.932048    0.2506461    1 5.081075
H9     0.8664687   2.020599    0.1488392    1 5.081075
H10    0.8361505   1.922305    0.2825918    1 5.081075
H11    0.6653299   1.495307   -0.09587725   1 5.081075
H12    0.8681807   1.537824    0.0077313    1 5.081075
H13    0.6615418   1.542852    0.05300039   1 5.081075
H14    0.5001154   1.860263   -0.1740974    1 5.081075
H15    0.5293129   1.690044   -0.235817     1 5.081075
H16    0.4208224   1.697906   -0.1140129    1 5.081075
H17    0.8308026   1.705244   -0.2145002    1 5.081075
H18    0.8439022   1.879834   -0.1510878    1 5.081075
H19    0.9804583   1.732965   -0.07270268   1 5.081075
C01    0.5644148  -0.0068766   0.5663485    1 7.081075
O03    0.4977957   0.1187918   0.6103808    1 7.081075
HO     0.5273261   0.197872    0.5718682    1 7.081075
H011   0.6885766  -0.0015907   0.5800193    1 7.081075
H012   0.5332439  -0.0903501   0.6070008    1 7.081075
```

A.2 Atomic Coordinates of Nortriptyline Hydrochloride

Nortriptyline Hydrochloride Form Alpha

```
Crystal System: Monoclinic
Space Group: P2/c
a[Å]:    9.991260(7)
b[Å]:    5.100210(3)
c[Å]:    34.16361(2)
alpha[°]: 90
beta[°]:  98.68405(8)
gamma[°]: 90
volume[Å³]:  1720.935(2)
```

```
Atom Name, Fractional Coordinates (x,y,z), Occupancy, B
Cl1    0           -0.2339        -0.25           1    8.313(87)
Cl2    0.5         -0.2737(11)    -0.25           1    8.313(87)
N1     0.2532397    0.08456877    -0.2572618      1    8.313(87)
C1     0.6150856    0.2527944     -0.06534552     1    8.313(87)
C2     0.6973394    0.3895128     -0.08680149     1    8.313(87)
C3     0.6417282    0.5316338     -0.1196434      1    8.313(87)
C4     0.5032649    0.5279877     -0.1309304      1    8.313(87)
C5     0.4194916    0.388086      -0.110082       1    8.313(87)
C6     0.4748363    0.2512259     -0.07643295     1    8.313(87)
C7     0.382237     0.1115614     -0.05287344     1    8.313(87)
C8     0.3019544    0.2997837     -0.03057117     1    8.313(87)
C9     0.2021039    0.4824833     -0.05408921     1    8.313(87)
C10    0.1140634    0.6239649     -0.0336185      1    8.313(87)
C11    0.01906927   0.7926235     -0.05047435     1    8.313(87)
C12    0.004967236  0.8306192     -0.09023033     1    8.313(87)
C13    0.08652479   0.6924958     -0.11192        1    8.313(87)
C14    0.1853392    0.5190847     -0.09516029     1    8.313(87)
C15    0.2697953    0.385679      -0.1212835      1    8.313(87)
C16    0.2099027    0.273918      -0.1547652      1    8.313(87)
C17    0.2750598    0.1235582     -0.1842588      1    8.313(87)
C18    0.2607912    0.267577      -0.223284       1    8.313(87)
C19    0.2455693    0.2201625     -0.2955984      1    8.313(87)
H1     0.3242807   -0.02096691    -0.2531184      1    8.313(87)
H2     0.1674347   -0.02697227    -0.2591366      1    8.313(87)
H3     0.6523016    0.1474456     -0.04351914     1    8.313(87)
H4     0.7943359    0.3968716     -0.07960605     1    8.313(87)
H5     0.7014485    0.6423524     -0.1341738      1    8.313(87)
H6     0.4678218    0.6185278     -0.1518482      1    8.313(87)
H7     0.3201532    0.001951403   -0.06921087     1    8.313(87)
H8     0.4372245   -0.005734197   -0.03072126     1    8.313(87)
H9     0.3710803    0.4033882     -0.01765408     1    8.313(87)
H10    0.2536023    0.1980258     -0.01077908     1    8.313(87)
H11    0.1285381    0.595017      -0.007578621    1    8.313(87)
H12   -0.04454056   0.8826547     -0.0333042      1    8.313(87)
H13   -0.06103766   0.951671      -0.102916       1    8.313(87)
H14    0.08017943   0.7070498     -0.1353278      1    8.313(87)
H15    0.1062486    0.288817      -0.1619472      1    8.313(87)
H16    0.3721433    0.08047892    -0.1736326      1    8.313(87)
H17    0.2244574   -0.02403209    -0.190264       1    8.313(87)
H18    0.1753032    0.377335      -0.2286228      1    8.313(87)
H19    0.3412545    0.3835846     -0.2257086      1    8.313(87)
H20    0.3312234    0.3340013     -0.2995984      1    8.313(87)
H21    0.2372183    0.1177676     -0.3183534      1    8.313(87)
H22    0.1556602    0.317134      -0.3041755      1    8.313(87)
```

A.3 Atomic Coordinates of Ibuprofen Lysine Salts

A.3.1 IBL-I

Ibuprofen Lysine Salt Form I

```
Crystal System: Monoclinic
Space Group: P21/n
a[Å]:   8.46665(53)
b[Å]:   40.6211(25)
c[Å]:   5.79317(33)
alpha[°]: 90
beta[°]:  86.3382(63)
gamma[°]: 90
volume[Å³]:  1988.35(21)

Atom Name, Fractional Coordinates (x,y,z), Occupancy, B
O1    0.0909802   -0.1756606   -0.7513078 1 3.92(24)
O2    0.301643    -0.1510493   -0.9984207 1 3.92(24)
C1    0.123069    -0.09389852  -0.6685384 1 3.92(24)
C2    0.2277418   -0.1077672   -0.520824  1 3.92(24)
C3    0.2470521   -0.093626    -0.3059527 1 3.92(24)
C4    0.1616895   -0.06561603  -0.2387958 1 3.92(24)
C5    0.05701672  -0.0517473   -0.3865102 1 3.92(24)
C6    0.03770645  -0.06588854  -0.6013815 1 3.92(24)
C7    0.3198597   -0.1379938   -0.5932955 1 3.92(24)
C8    0.4913282   -0.1280203   -0.6662459 1 3.92(24)
C9    0.2424214   -0.1541655   -0.7983112 1 3.92(24)
C10  -0.03510114  -0.0215207   -0.3140387 1 3.92(24)
C11  -0.2130012   -0.02864304  -0.3265951 1 3.92(24)
C12  -0.2721943   -0.04824097  -0.1110664 1 3.92(24)
C13  -0.3024253    0.004535733 -0.3332947 1 3.92(24)
H1    0.1098713   -0.1035634   -0.8153929 1 3.92(24)
H2    0.3185911   -0.1031046   -0.2049968 1 3.92(24)
H3    0.1748872   -0.05595115  -0.0919412 1 3.92(24)
H4   -0.03383252  -0.05640992  -0.7023374 1 3.92(24)
H5    0.3188362   -0.1528679   -0.4666523 1 3.92(24)
H6    0.2303417   -0.159501    -1.103981  1 3.92(24)
H7    0.537187    -0.1178929   -0.5387164 1 3.92(24)
H8    0.4904401   -0.1129949   -0.7918303 1 3.92(24)
H9    0.5496695   -0.1471638   -0.7121445 1 3.92(24)
H10  -0.00447153  -0.003945766 -0.4154546 1 3.92(24)
H11  -0.01296945  -0.01600444  -0.1600474 1 3.92(24)
H12  -0.2290482   -0.04076804  -0.4623732 1 3.92(24)
H13  -0.254634    -0.03573215   0.0234685 1 3.92(24)
H14  -0.3820552   -0.05251629  -0.1186795 1 3.92(24)
H15  -0.2154439   -0.06839807  -0.1082592 1 3.92(24)
```

```
H16  -0.2641066   0.01655648  -0.4659796 1 3.92(24)
H17  -0.4122862   0.000260422 -0.3409078 1 3.92(24)
H18  -0.2846477   0.01666534  -0.197163  1 3.92(24)
O3    0.1486683   0.2660886    0.7475858 1 3.92(24)
N1   -0.2211726   0.2322047    0.8149658 1 3.92(24)
N2   -0.5753757   0.3198268    0.7134542 1 3.92(24)
C14   0.04427517  0.2548184    0.8882575 1 3.92(24)
C15  -0.131112    0.2630611    0.8611418 1 3.92(24)
C16  -0.1429048   0.2867651    0.6554839 1 3.92(24)
C17  -0.1461914   0.3224262    0.7459197 1 3.92(24)
C18  -0.3118645   0.3298605    0.859243  1 3.92(24)
C19  -0.4254845   0.337551     0.6711881 1 3.92(24)
O4    0.09135375  0.2325471    1.089982  1 3.92(24)
H19   0.1691636   0.2434757    1.172288  1 3.92(24)
H20  -0.1751617   0.2734062    0.9975707 1 3.92(24)
H21  -0.2827671   0.2261875    0.9516118 1 3.92(24)
H22  -0.1482093   0.2151449    0.7728221 1 3.92(24)
H23  -0.2373201   0.2821783    0.5812797 1 3.92(24)
H24  -0.05356722  0.283635     0.5499884 1 3.92(24)
H25  -0.1233059   0.3369835    0.6198386 1 3.92(24)
H26  -0.06885634  0.324769     0.8565824 1 3.92(24)
H27  -0.3051719   0.3477962    0.9621574 1 3.92(24)
H28  -0.3480521   0.3106693    0.9450346 1 3.92(24)
H29  -0.3729649   0.331034     0.5225283 1 3.92(24)
H30  -0.4401661   0.3608624    0.6658537 1 3.92(24)
H31  -0.5570913   0.301693     0.8025881 1 3.92(24)
H32  -0.6168257   0.3139162    0.5690299 1 3.92(24)
```

A.3.2 IBL-II

Ibuprofen Lysine Salt Form II

```
Crystal System: Monoclinic
Space Group: P21/n
a[Å]:   8.4507(8)
b[Å]:   42.631(5)
c[Å]:   5.8229(5)
alpha[°]: 90
beta[°]:  85.721(9)
gamma[°]: 90
volume[Å³]:  2091.9(4)

Atom Name, Fractional Coordinates (x,y,z), Occupancy, B
O1    0.1265316   -0.176482    -0.7148897 1 0.99(57)
O2    0.3247713   -0.1475704   -0.9531673 1 0.99(57)
C1    0.1046568   -0.09680342  -0.647389  1 0.99(57)
C2    0.2081302   -0.107164    -0.4888483 1 0.99(57)
C3    0.2078312   -0.09293053  -0.2740257 1 0.99(57)
```

```
C4    0.1040588   -0.06833648   -0.2177438    1 0.99(57)
C5    0.0005853   -0.0579759    -0.3762846    1 0.99(57)
C6    0.0008843   -0.07220936   -0.5911072    1 0.99(57)
C7    0.3201148   -0.1337043    -0.5495841    1 0.99(57)
C8    0.4870675   -0.1202726    -0.6113478    1 0.99(57)
C9    0.2619711   -0.1515844    -0.7571666    1 0.99(57)
C10  -0.1113992   -0.03143556   -0.3155488    1 0.99(57)
C11  -0.2828005   -0.04395902   -0.3013374    1 0.99(57)
C12  -0.3188755   -0.06014672   -0.0669579    1 0.99(57)
C13  -0.397424    -0.01618768   -0.3252167    1 0.99(57)
H1    0.1048611   -0.1065313    -0.7942103    1 0.99(57)
H2    0.2785505   -0.1000115    -0.1656705    1 0.99(57)
H3    0.1038545   -0.05860857   -0.07092264   1 0.99(57)
H4   -0.0698349   -0.06512839   -0.6994624    1 0.99(57)
H5    0.3222638   -0.1473776    -0.4209989    1 0.99(57)
H6    0.2637044   -0.1579838    -1.061205     1 0.99(57)
H7    0.5209096   -0.1091434    -0.4824018    1 0.99(57)
H8    0.4828927   -0.1065       -0.7390411    1 0.99(57)
H9    0.5579911   -0.1370815    -0.6498138    1 0.99(57)
H10  -0.098342    -0.0157482    -0.4313241    1 0.99(57)
H11  -0.08799334  -0.02298009   -0.1709704    1 0.99(57)
H12  -0.2933861   -0.05850164   -0.4225593    1 0.99(57)
H13  -0.306897    -0.04534538    0.0525023    1 0.99(57)
H14  -0.4246704   -0.06783989   -0.05817598   1 0.99(57)
H15  -0.2467358   -0.07703975   -0.05399825   1 0.99(57)
H16  -0.3731751   -0.006278984  -0.4697168    1 0.99(57)
H17  -0.5032189   -0.02388085   -0.3164347    1 0.99(57)
H18  -0.3848811   -0.001702202  -0.2039008    1 0.99(57)
O3    0.1239177    0.2556122     0.7174117    1 0.99(57)
N1   -0.246947     0.2304387     0.7983181    1 0.99(57)
N2   -0.60014      0.320129      0.6592564    1 0.99(57)
C14   0.02253727   0.2491984     0.8779117    1 0.99(57)
C15  -0.1521533    0.2585547     0.8601244    1 0.99(57)
C16  -0.1610282    0.2835642     0.6706186    1 0.99(57)
C17  -0.1734853    0.3162382     0.783464     1 0.99(57)
C18  -0.3493308    0.323563      0.8506174    1 0.99(57)
C19  -0.4331535    0.3314642     0.6332268    1 0.99(57)
O4    0.07265047   0.2318283     1.094835     1 0.99(57)
H19   0.1586507    0.2429262     1.154459     1 0.99(57)
H20  -0.1945337    0.2670646     1.002475     1 0.99(57)
H21  -0.3092908    0.2235341     0.9312836    1 0.99(57)
H22  -0.1763091    0.2142566     0.7444141    1 0.99(57)
H23  -0.2519237    0.2796777     0.5882303    1 0.99(57)
H24  -0.06779527   0.2823632     0.5692148    1 0.99(57)
H25  -0.1307164    0.3314131     0.6765987    1 0.99(57)
H26  -0.1152837    0.3162312     0.9168943    1 0.99(57)
H27  -0.3560975    0.3405744     0.9552164    1 0.99(57)
```

```
H28  -0.3971935    0.3053247    0.9237617    1 0.99(57)
H29  -0.3769829    0.3215287    0.5037669    1 0.99(57)
H30  -0.4299023    0.3536174    0.6113065    1 0.99(57)
H31  -0.6067891    0.301603     0.7323569    1 0.99(57)
H32  -0.640956     0.3193949    0.5080416    1 0.99(57)
```

ERRATA CORRIGE

Structural Studies of Active Pharmaceutical Ingredients:

Polymorphism and Solid-State Reactivity

By Chiara Vladiskovic

On pages 27, 121 (several times), 127 and 166, the term $C_4^2(4)$ is incorrect and should be replaced with $C_2^1(4)$.

On page 89, the fifth row of the sixth column of Table 3.4 contains the number 3.5(2). This is incorrect and should be replaced with 179.7(2).